Natural disasters mitigation by using construction methods with geosynthetics (earthquakes)

F. Tatsuoka
Tokyo University of Science, Chiba, Japan

J. Koseki
University of Tokyo, Tokyo, Japan

J. Kuwano
Saitama University, Saitama, Japan

ABSTRACT: Properly designed, constructed and maintained geosynthetic-reinforced soil (GRS) structures are much more cost-effective being much more seismic-resistant than conventional type embankments and retaining walls (RWs). These features of GRS structures are achieved by proper geosynthetic-reinforcing of the backfill with structural integration of the components (i.e. backfill, reinforcement and facing, and also a bridge girder with GRS integral bridges). The advantages of GRS structures become more significant by better compaction, better drainage, better facing structure etc. as requested by relevant seismic design. The construction of GRS structures in place of conventional type soil structures is promoted by performing seismic design. On the other hand, some design codes allow no seismic stability analysis under some broad conditions (referred as the no-seismic-design policy) based on such experiences as "*seismic performance better than expected*" of soil structure under some limited conditions. These experiences are due principally to redundancy (i.e. implicit safety margin) that is not specified in design. Although the no-seismic-design policy relies on redundancy in design, redundancy decreases in an uncontrolled and random manner by poor design, poor construction and poor maintenance. Redundancy also decreases by a decrease in apparent cohesion due to wetting of the backfill by heavy/prolonged rains, scoring/excavation in the ground in front of wall, too fast deterioration of reinforcement etc. As a result, the no-seismic-design policy does not contribute to a reduction of the number of failure/collapse but it increases the possibility of failure/collapse by earthquakes as well as heavy/prolonged rains and floods. The no-seismic-design policy tends to increase the residual deformation associated with a decrease in the stability. To realize actually sufficiently stable GRS structures, it is necessary to perform properly seismic design while manifesting and controlling some relevant components of redundancy. An increase in the cost by conducting relevant seismic design can be smaller but more valuable than the cost of failure/collapse. The total cost for construction and lifespan maintenance (i.e. the life cycle cost, LCC) of properly seismic-designed GRS structure can be much lower than that of non-seismic-designed conventional type soil structure. To explain the above, the latest seismic design code for railway soil structures in Japan is described. Some recent typical case histories showing high seismic performance of GRS structures and efficient restoration of soil structures that collapsed by earthquakes to GRS structures are also presented. After all, safety is not free but the cost of disaster is more significant, and GRS technology can contribute to safety cost-effectively.

Keywords: GRS integral bridge, GRS retaining wall, Redundancy, Safety margin, Seismic design

1 INTRODUCTION

Our experiences, particular those since the 1995 Great Kobe Earthquake (i.e. the 1995 Hyogo-ken Nanbu Earthquake), showed that properly designed, constructed and maintained geosynthetic-reinforced soil (GRS) structures, in particular GRS retaining walls (RWs), are much more cost-effective while being much more seismic-resistant than conventional soil structures (e.g. Tatsuoka et al., 1997a&b, 1998, 2007, 2014a; Koseki, 2012; Koseki, et al., 2006, 2007, 2008, 2009; Kuwano et al., 2012, 2014). It was learned that relevant seismic design leads to better structure, better compaction, better drainage etc. then, it promotes the use of GRS structures in place of conventional type soil structures. "Better structure" implies

not only proper geosynthetic-reinforcing of the backfill but also structural integration of the components (i.e. backfill, reinforcement and facing, and also a bridge girder with GRS integral bridges).

On the other hand, many soil structures, including GRS RWs, "*performed better than expected based on the seismic stability evaluated in design*", or just "*performed better than expected*", during many previous earthquakes. Based on such experiences as above, some design codes employ "no-seismic-design policy" not requiring seismic analysis under some broad conditions. However, "*performance better than expected*" of soil structures is due principally to the redundancy included in design (i.e. implicit safety margin) (Leshchinsky & Tatsuoka, 2013). With GRS RWs, this redundancy is usually created by: 1) ignoring apparent cohesion due to matric suction of soil; 2) under-estimating the angle of internal friction of soil; 3) ignoring toe resistance at the facing bottom; 4) underestimating the rupture strength of geosynthetic reinforcement; and 5) others. However, the redundancy components 1) – 3) in particular are not specified in design codes, therefore they are not controlled and are random to be taken into account in design. Poor design, poor construction and poor maintenance largely reduce redundancy. In that case, the total safety margin may have become very small even under ordinary static conditions. Furthermore, this redundancy also decreases by heavy/prolong rains, unexpected scouring/excavation in the ground in front of wall and so on. As a result, even "*seismic performance worse than expected based on the no-seismic design policy*" and "*seismic performance worse than expected based on a calculated safety factor*" may be observed. That is, the no-seismic design policy relying on redundancy is not reliable. As the no-seismic-design policy reduces the calculated safety factor (i.e. explicit safety margin), it reduces the actual safety factor when compared with the values when relevant seismic design is performed. As a result, the number of such failure/collapse as have been observed during many previous earthquakes will increase. Besides, this policy increases the residual deformation associated with a decrease in the stability. In any case, this policy does not promote the use of GRS structures (including GRS RWs) as more cost-effective and more seismic-resistant soil structures than conventional type soil structures.

An increase in the cost by relevant seismic design can be smaller but more valuable than the cost of failure/collapse. The total cost for construction and maintenance for lifespan (i.e. the life cycle cost, LCC) of properly seismic-designed GRS structures can be much lower than that of non-seismic-designed conventional type soil structures. An increase in the design load by employing relevant seismic design can be compensated by explicitly taking into account some relevant redundancy components in seismic design. As a result, actually stable GRS structures are realized cost-effectively, although this procedure reduces the redundancy.

These issues are discussed based on recent case histories and some stability analysis in this report.

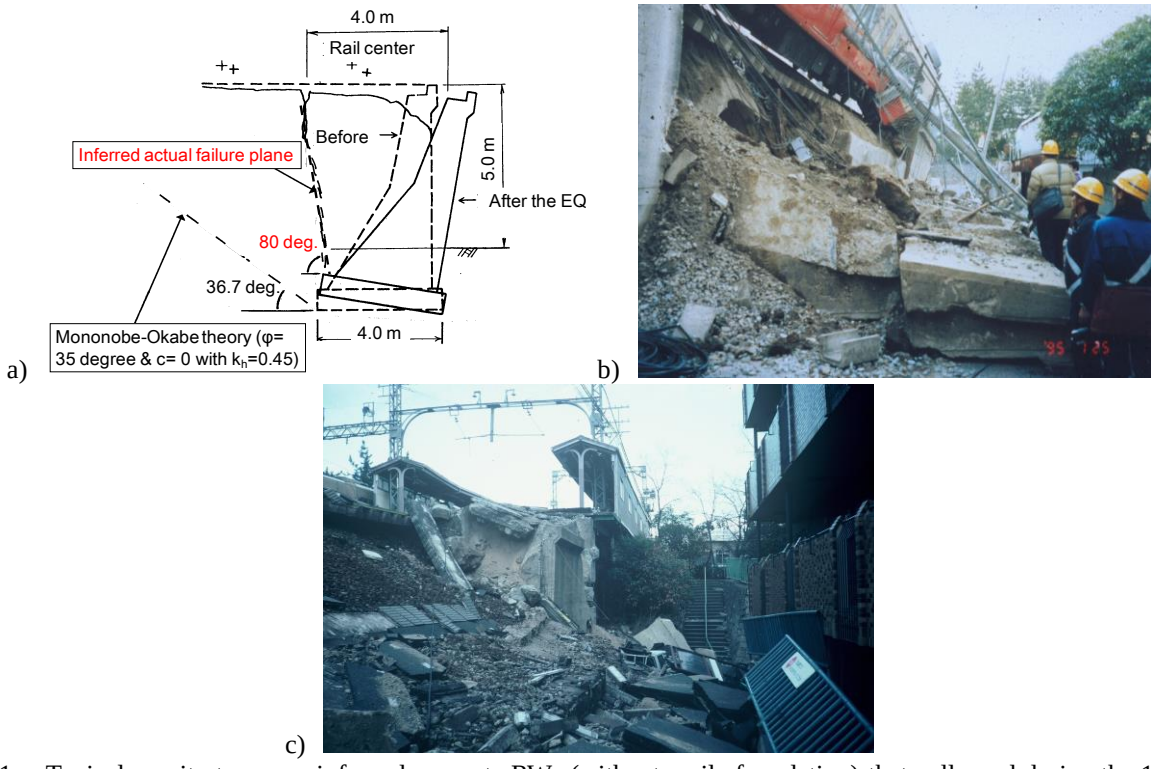

Figure 2-1. Typical gravity type unreinforced concrete RWs (without a pile foundation) that collapsed during the 1995 Great Kobe Earthquake, Ishiyagawa Station, Hanshin Railway (Tatsuoka et al., 1996, 1997a & b, 1998): a) a sketch of typical section; and b) & c) typical damaged sections on the opposite sides of the embankment.

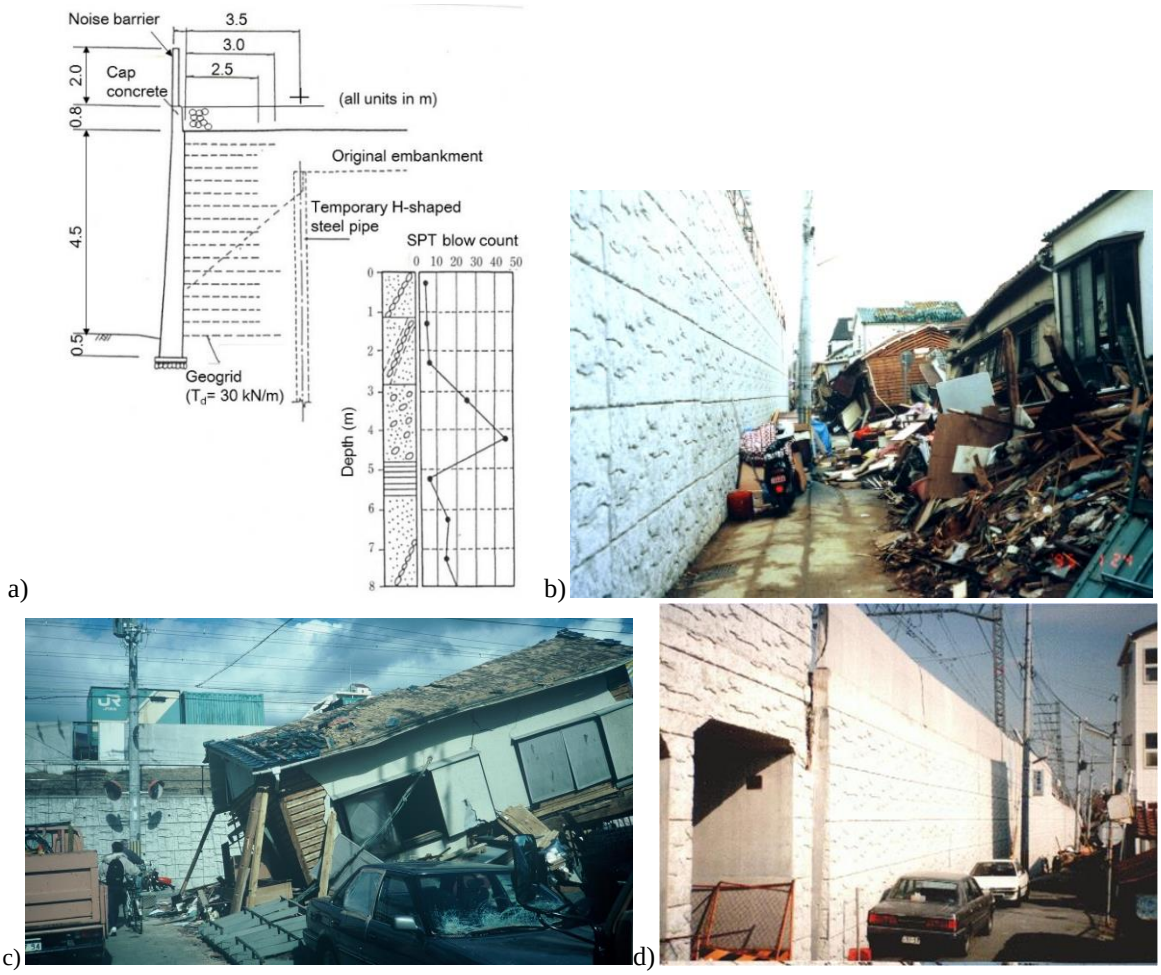

Figure 2-2. A GRS RW having FHR facing at Tanata, Kobe city (Tatsuoka et al., 1996, 1997a & b, 1998): a) a typical cross-section (H= 4.5 m + 0.8 m= 5.3 m); and b), c) & d) views of the wall one week after the earthquake.

2 DIFFERENT SEISMIC PERFORMANCES OF DIFFERENT SOIL STRUCTURE TYPES

2.1 *High Seismic Performance of GRS RWs*

It has been observed during recent earthquakes, in particular those in Japan, that the seismic performance of GRS structures are generally better than conventional type soil structures. For example, a number of conventional type RWs collapsed during the 1995 Great Kobe Earthquake. Fig. 2-1 shows a typical collapsed gravity type RW. The wall was seismic-designed and constructed about 85 years ago. Pseudo-static seismic analysis using a design horizontal seismic coefficient, $(k_h)_d$, equal to 0.2 was performed with a required minimum safety factor equal to 1.5. This and other many similar walls collapsed by seismic loads much higher than the design value, as expected based on the stability analysis. In contrast, several GRS RWs with full-height rigid (FHR) facing performed very well during this earthquake. With the GRS RW at Tanata (Fig. 2-2), the wall height is varying along a total length of 305 m with a largest height equal to 6 m. This wall was constructed in 1992, so it was designed before the 1995 Great Kobe Earthquake based on the pseudo-static limit equilibrium stability analysis using $(k_h)_d$= 0.2 (Horii et al., 1994). The required minimum overall safety factor, $(F_s)_{c.s}$, was equal to 1.5, thus the required minimum yield k_h value at which $(F_s)_{c.s}$ became unity was equal to 0.2×1.5= 0.3. This safety factor comprised a safety factor equal to 1.25 for the global structural equilibrium times a safety factor for the tensile rupture failure of geogrid equal to 1.25 (i.e. 1.25 × 1.25= 1.5). At Higashi Nada located only about 2 km west from the site, the peak horizontal ground acceleration, α_{max}, estimated from recorded velocities was as high as more than 775 cm/sec^2 in EW and 421 cm/sec^2 in NS, which are considerably higher than the yield k_h value required in design (= 0.3)“ times g (= 980 gal). Damage to the wooden houses in front of the wall was extremely serious (Figs. 2-2b &c). Despite the above, Tanata wall did not collapse. The tallest section of the wall with a height of 6 m, in contact with a box culvert structure, exhibited lateral outwards displacements of 26 cm at the top and 10 cm at the bottom (Fig. 2-2d). Associated with this wall movement/deformation, the railway track located above the reinforced backfill zone settled down with a

maximum of about 15 cm, which is close to the allowable limit of settlement equal to 20 cm required for this RW (supporting ballasted tracks of an important railway): i.e. rank II performance) according to the current seismic design code (explained later). Immediately after the earthquake, the tallest section of the wall for a length of about 8.5 m was reinforced by installing several anchors at the top. With no increase in the deformation/displacement afterwards, the wall has been used without any problem until today. This "*seismic performance better than expected*" for seismic loads much higher than assumed in design is due likely to a sufficient amount of redundancy (i.e. implicit safety margin) included in the original seismic design.

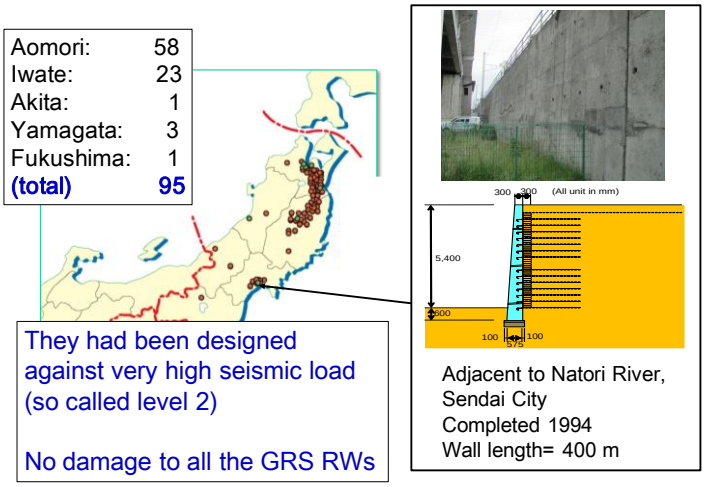

Figure 2-3. High performance of GRS RWs with FHR facing for railways, including those for high-speed trains, constructed before the 2011 Great East Japan Earthquake (Tatsuoka et al., 2012a&b, 2014a).

Largely different seismic performances of these two types of RW designed based on the same stability analysis method using the same $(k_h)_d$ (= 0.2) and the same minimum required overall safety factor (= 1.5) shown above and other similar cases reported in Tatsuoka et al. (1998) indicate that the redundancy is different among different RW types, larger with GRS RW having FHR facing than with the conventional cantilever RWs. A high seismic stability of GRS RWs of this type was re-confirmed by their high performance during the 2011 Great East Japan Earthquake (i.e. the 2011 off Pacific Coast of Tohoku Earthquake) (Fig. 2-3).

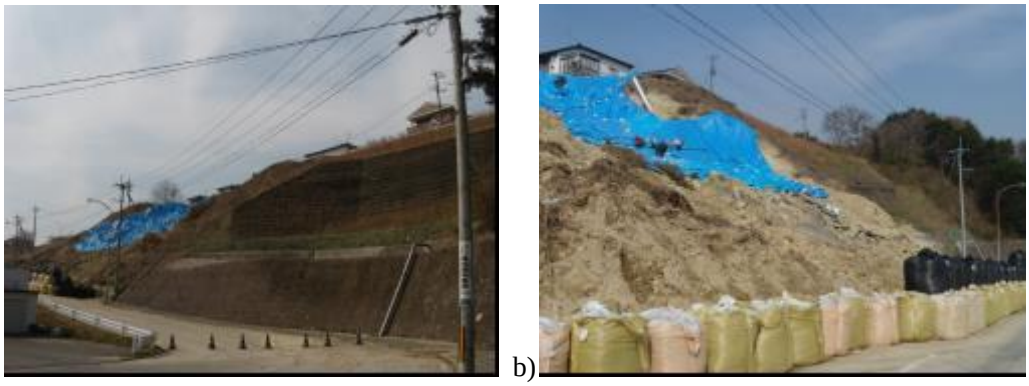

Figure 2-4. a) No damage to a GRS RW; and b) collapse of embankment, Yamamoto-cho, Miyagi Prefecture, the 2011 Great East Japan Earthquake (Miyata, 2014).

Fig. 2-4a shows another example of high seismic performance of GRS RW during this earthquake. A 5.4 m-high GRS RW with wire mesh facing exhibited no damage. This wall was constructed to repair residential embankment that had previously failed due to heavy rain. On the other hand, conventional embankment (without reinforcement) adjacent to the GRS RW collapsed (Fig. 2-4b). Essentially the same strong seismic motion having the JMA (Japan Meteorological Agency) seismic intensity of 6 lower seemed to have been acted on these soil structures (Miyata, 2014).

Based on these and other similar experiences, a number of conventional type RWs and embankments that collapsed during the 1995 Great Kobe Earthquake, the 2011 Great East Japan Earthquake and others in between them, as well as those that collapsed by heavy rains, floods and ocean wave actions during a

typhoon, were reconstructed to GRS RWs, including those having FHR facing (Tatsuoka et al., 2007, 2012a & b; Tatsuoka, 2008).

2.2 *Performance Better than Expected*

During the 1995 Great Kobe Earthquake, the GRS RWs having FHR facing at Tanata and other places survived seismic loads significantly higher than the one used in their original design. This good performance is due to the safety margin consisting of: 1) explicit safety margin equal to "the calculated overall safety factor against Level 1 seismic load, $(F_s)_{c.s}$" – 1.0, where the required minimum value of $(F_s)_{c.s}$ was 1.5; and 2) implicit safety margin (i.e. redundancy ignored in their design). The "*seismic performance better than expected based on a calculated safety factor*" of these walls can be attributed to the following redundancy components among others (Tatsuoka et al., 1998):

1) The design friction angle ϕ for the backfill (a well-graded sandy soil) was a default value, equal to 35°. As seen from Fig. 2-5c, this ϕ value corresponds approximately to a degree of compaction D_c (standard Proctor) equal to 90 %, which was the allowable lower limit for all measured values in field compaction control with these GRS RWs. The average of actual D_c values of the backfill should have been higher, at least by about 5 % (Tatsuoka, 2011). Tatsuoka et al. (1998) inferred ϕ= 42° with c= 0 as a more realistic peak value in this case.

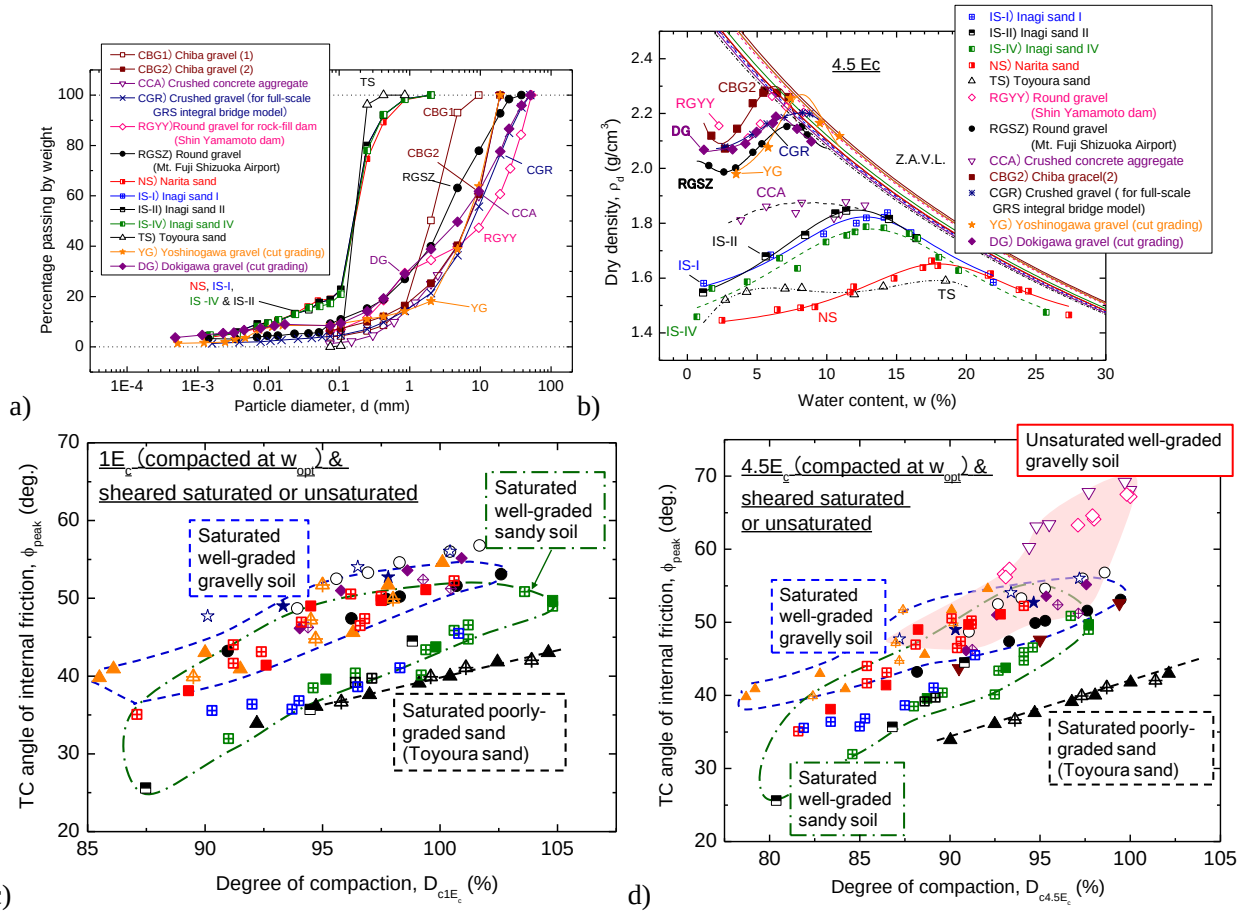

Figure 2-5. a) Grading curves; b) compaction curves; and c) peak friction angle ϕ_{peak} =arcsin{$(\sigma_1-\sigma_3)/(\sigma_1+\sigma_3)$}$_{peak}$ from drained triaxial compression tests at σ_3= 50 kPa of sandy and gravelly soils compacted at the optimum water content, plotted against the degree of compaction defined for standard Proctor (1Ec) (saturated specimens); and d) modified Proctor (4.5Ec) (saturated & moist specimens) (Tatsuoka, 2011).

2) As seen from Fig. 2-5d, the drained ϕ_{peak} value of gravelly soils moist as when compacted during shearing becomes higher than the one of saturated soils with an increase in D_c. This difference is due to an apparent cohesion by matric suction. The effect of apparent cohesion on the stability of Tanata wall during the 1995 Great Kobe Earthquake may not be negligible, because there had been no major rainfall at the site for a long period by the time of the earthquake, while the backfill was a well-graded sandy soil with a fines content of about 9 %. In the design of Tanata wall, however, the apparent cohesion was ignored following the standard practice.

3) Toe resistance was ignored in the design considering that the ground in front of the toe could be excavated in the future. Actually, it was the case with Tanata wall (see Fig. 2-2b): i.e. it is likely that, sometime before the earthquake, the pavement in front of the wall was cut along two lines in parallel to the wall to excavate the ground for some underground work.

Not only with these walls, but also generally, these redundancy components are not documented in design codes, therefore their implications are not well recognized. As a result, they are not controlled in design and construction, therefore their contribution is random.

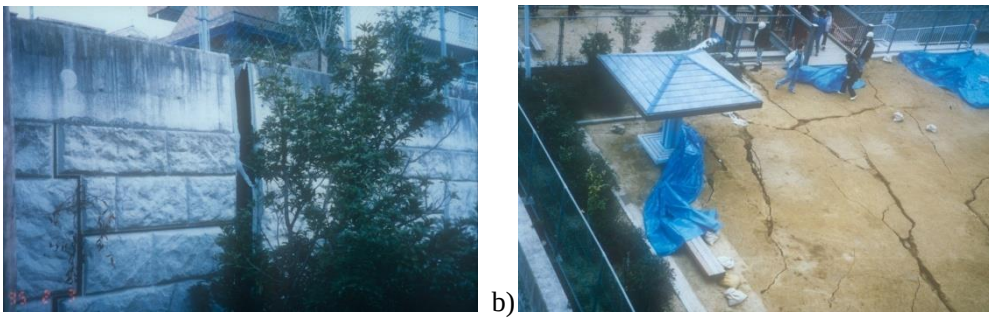

a) b)

Figure 2-6. Large opening at a vertical construction joint; and b) cracks on the crest of backfill of a Terre Armée wall for Hoshiga-oka Park, Kobe City, during the 1995 Great Kobe Earthquake (JTAA, 1995; Tatsuoka et al., 1997b).

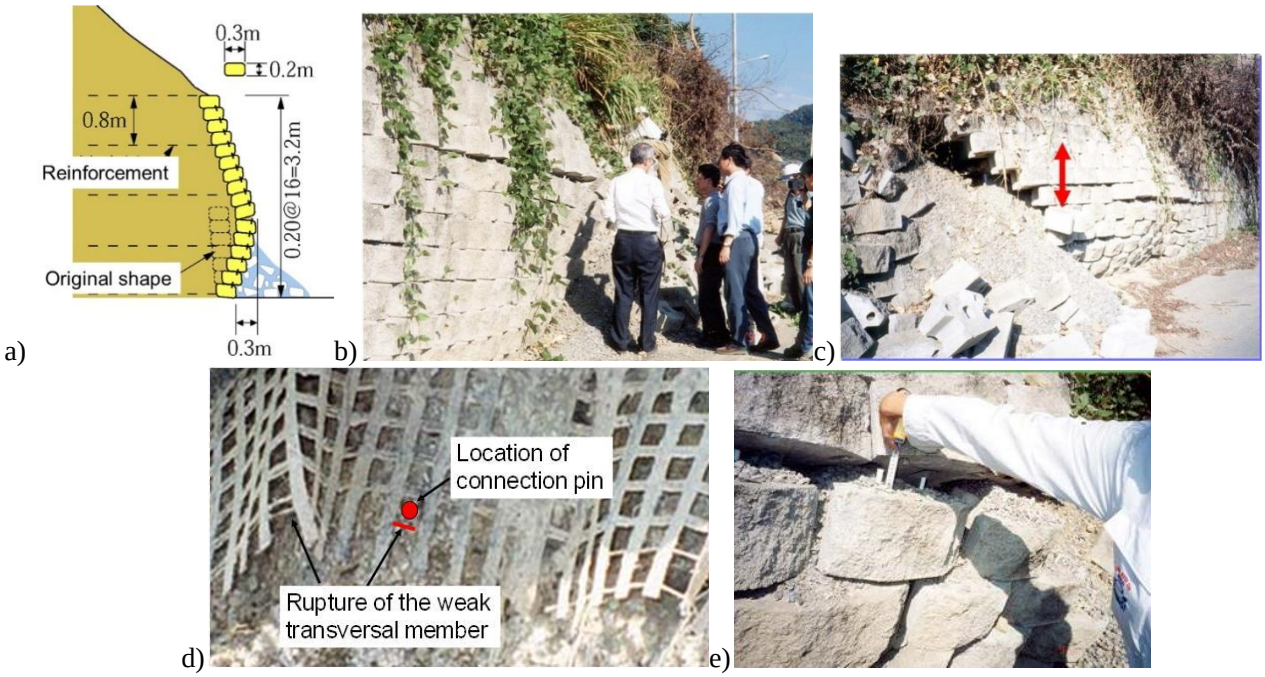

a) b) c) d) e)

Figure 2-7. Collapse of a modular block GRS RW in Taiwan during the 1999 ChiChi Earthquake: a) typical cross-section; b) overview; c) a large vertical spacing between geogrid layers; d) weak connection strength; and e) short connection pins.

2.3 *Failure and Collapse of MSE RWs by Earthquakes*

Many conventional type RWs and mechanically stabilized earth (MSE) RWs including GRS RWs did not fail/collapse, like Tanata wall, did not fail/collapse having "*performed better than expected*" during many previous earthquakes. Based on such experiences as above obtained under some limited conditions, some design codes do not require stability analysis of RW under some broad conditions: i.e. with RWs with a height equal to, or smaller than, 8 m (Japan Road Association, 2012); and with RWs at sites where the site-adjusted peak horizontal ground acceleration, α_{max}, is less than, or equal to, 0.4 g (AASHTO, 2010 & 2012). Of course, these codes do not expect that RWs designed following this policy fail/collapse by seismic loading. Road Embankment Design Guideline (Japan Road Association, 2010) does not require seismic stability analysis with road embankments carefully designed under static conditions and properly constructed (in particular in terms of drainage and backfill compaction) if effects of failure/collapse are judged to be not very serious. It is also specified that, in case seismic stability analysis is required, the stability against Level 2 design seismic load, which is severe as experienced during the 1995 Great Kobe

Earthquake) is not required if the stability against Level 1 seismic load (which is the same level as have been used in the conventional seismic design) is ensured.

However, not only many embankments and conventional type RWs (as typically shown in Fig. 2-1) but also many mechanically stabilized earth (MSE) RWs, including GRS RWs, failed/collapsed during recent major earthquakes as described below. Such a no-seismic-design policy as described above do not contribute to a reduction of such failure/collapse of RWs, while it is questionable whether the cost saving by not carrying out seismic design is larger than the cost of failure/collapse in terms of not only restoration but also negative social impact.

Fig. 2-6 shows one of the several Terre Armée walls that exhibited large deformation during the 1995 Great Kobe Earthquake. Although the walls did not collapse, it is likely that if the facing had been FHR facing as Tanata wall, this type of failure would not have taken place. Fig. 2-7 shows collapse of a GRS RW having modular block facing during the 1999 Chi-Chi Earthquake in Taiwan. It is likely that this collapse was triggered by collapse of the facing caused by a too large vertical spacing between the vertically adjacent geogrid layers (i.e. 80 cm) with too many (i.e. four) modulus blocks in between, too short connection pins between the blocks and too small connection strength of geogrid, as a result of design not taking into account the earth pressure acting on the facing that increases by seismic loads. Koseki and Hayano (2000) reported that the damage level of similar type GRS RWs in Taiwan during this earthquake decreased with a decrease in the vertical spacing between geogrid layers (i.e. with a decrease in the number of modular blocks between the vertically adjacent geogrid layers).

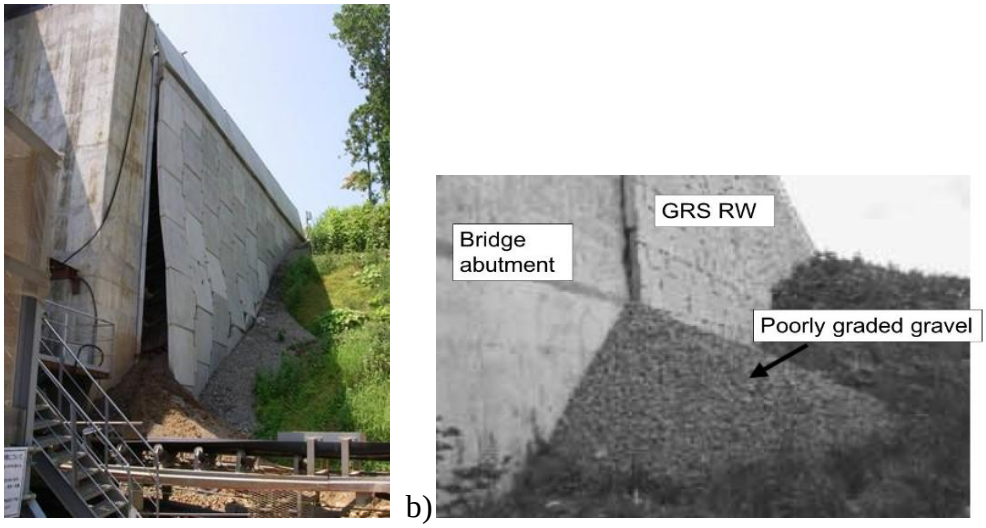

Figure 2-8. Large deformation of discrete panel facing, Iwate Prefecture during the 2008 Iwate-Miyagi Nairiku Earth quake; a) Terre Armée RW, Isawa, Iwate Prefecture; and b) GRS RW (Wang et al. 2011).

Fig. 2-8a shows large deformation/displacement of the discrete panel facing of a temporary Terre Armée RW with a maximum height of 14 m constructed as part of a sieving plant of the fill material for construction of a rockfill dam. The backfill was gravelly soil (D_{max} < 150 mm) and the length of metal strip reinforcement was 7 – 10.5 m. The wall was seismic-designed using $(k_h)_d$= 0.15 and ϕ= 30°. The maximum horizontal acceleration on the ground at sites around the dam far exceeded 1,000 gal (cm/sec^2). An adjacent RC cantilever RW displaced laterally by sliding for a distance of 80 – 100 cm, while the Terre Armée wall displaced more by about 50 cm. An opening was developed between the facing of the Terre Armée wall and the RC cantilever RW likely associated with pull-out of metal strips at lower levels of the wall. The backfill flowed out from the opening. It seems that the redundancy in design by using a low ϕ value and others is not sufficient to resist seismic loads far exceeding the design value. It is likely that the damage would have been severer if seismic design had not been carried out.

Fig. 2-8b also shows large deformation/displacement of the discrete panel facing of a GRS RW during the same earthquake (Wang et al., 2011). The wall was constructed as an approach to a bridge abutment with a maximum height of 10.6 m and a total length of 47.5 m at a distance of only about 4.5 km northeast from the epicenter. According to its design and construction manual (Committee for Double-Facing GRS RW, 2010), the external discrete panel facing is not a structural component contributing to the stability of the wall. So, the facing and its connection to the geogrid reinforcement were not designed to resist the earth pressure acting on the main body of the GRS RW having internal expanded metal facing. Despite that the main body was rather stable, the discrete panel facing exhibited relatively large lateral

outward displacements of 17 cm at a maximum being separated from the main body of GRS RW. Poorly graded gravel that was filling the space between the discrete panel facing and the main body as a drainage layer flowed out from an opening that developed between the facing and the RC abutment. Although the main body *"performed better than expected*", the discrete panel facing did not behave so, showing that the redundancy was not sufficient in this case. Wang et al. (2011) considered that this level of damage was acceptable, as the restoration of the facing was easier than the case where the facing is integrated to the main body of GRS RW. However, it is arguable whether the cost saving by adopting this facing structure is larger than the cost of such damage as above. This type of damage would not have taken place if the facing had been designed to resist the seismic earth pressure and firmly connected to the reinforcement layers. Besides, it is likely that the additional cost by adopting such a facing structure as above is smaller and more valuable than the cost of such damage as above.

a)  b) 

Figure 2-9. Performance at ultimate limit state during the 2011 Great East Japan Earthquake: a) GRS RW (Kaneko & Kumagai, 2011); and b) Terre Armée RW (Japan Terre Armée Association, 2011).

During the 2011 Great East Japan Earthquake, MSE RWs performed generally very well. However, several failed/collapsed at different levels. Fig. 2-9a shows collapse of a 5 m-high GRS RW with expanded metal mesh facing. Not only internal slip but also connection failure was observed. This damage state was classified into the "ultimate limit state" (Kuwano et al., 2012, 2014). The estimated seismic JMA intensity at this site was 6 lower and the equivalent ground acceleration estimated for a period of 0.5 sec was 300 gal (i.e. cm/sec^2). This α_{max} value is lower than 0.4g, below which no seismic stability analysis is required according to AASHTO (2010 & 2012). The site investigation indicated that this collapse was caused by a high ground water level in the backfill, which is due likely to the lack of a proper drainage system. Such a GRS RW wall as above would not have been designed and constructed if serious seismic design had been performed.

Fig. 2-9b shows collapse of a 10 m-high Terre Armée RW, triggered by horizontal sliding for a distance of 7 m in the foundation slope of soft soil caused by seismic motion. The estimated JMA seismic intensity at this site was 6 lower and the equivalent peak horizontal ground acceleration, α_{max}, was about 300 gal (cm/sec^2) (Kuwano et al., 2012, 2014). The site investigation revealed that this slip failure in the subsoil layer occurred due to insufficiently improvement. Adequate ground improvement would have been carried out if the wall had been properly seismic-designed.

At the time of the earthquake, a new expressway was just under construction near the Pacific coastline in Fukushima Prefecture. Several GRS RWs with wire mesh facing had been completed as wing RWs for approach embankments to bridge abutments. Fig. 2-10a shows damage to a 5.4-m high GRS RW. Considerable deformation/displacement of the wall produced a large gap between the wall and a RC bridge abutment. This damage was classified into the "restorability limit state" damage, although the deformation of the facing was more than the allowable serviceability limit (Kuwano et al., 2012, 2014). The estimated JMA seismic intensity was 6 lower at this location and the equivalent peak ground acceleration was 300 gal (cm/sec^2). The site investigation revealed that this damage could be attributed to a high fines content of the fill material and a very high water level in the backfill. Fig. 2-10b shows a similar case as above. As the deformation of the facing was at its allowable serviceability limit, the damage of the wall was ranked as the "serviceability limit state" and the wall was repaired by using nailing, soil cement and vegetation. Fig. 2-10c shows typical buckling type deformation of the wire mesh facing, which may have been induced by an increase in the vertical force in the facing and/or vertical compression of the backfill

immediately behind the wall face by seismic effects. It seems that the damage described above would have not taken place if a more stable facing system firmly connected to the reinforcement layers had been used ensuring its sufficient seismic stability.

The GRS RWs having FHR rigid facing that performed very well during severe earthquakes as described in Section 2.1 had been seriously seismic-designed. Most MSE RWs also performed satisfactorily. It seems therefore that most of such failure/collapse of MSE RWs as described above would not have taken place if better facing structure, better drainage, better backfill compaction and other relevant measures had been employed. These measures are required by proper seismic design more seriously than when following the no-seismic design policy. Additional cost of these measures is usually lower and more valuable than the cost of failure/collapse.

Figure 2-10. Performance of GRS RW with wire mesh facing at: a) restorability limit state; b) serviceability limit state; and; c) overall picture and d) zoom-up of buckling deformation of metal mesh facing of GRS RW for a wing of a bridge abutment of an expressway (under construction) in Minami-Soma, Fukushima Prefecture (Kuwano et al., 2014).

3 SEISMIC DESIGN OF RETAINING WALLS

3.1 *Opposite Directions*

Since the 1955 Great Kobe Earthquake, different policies in two opposite directions, "leveling up of design seismic load" versus "no change in the design seismic load or maintaining of no-seismic-design policy", in the design of soil structures including MRE/GRS RWs have been employed by different sectors. It seems that, after the 2011 Great East Japan Earthquake, the implications of this separation have become more significant.

3.1.1 *Leveling up of Design Seismic Load*

The design seismic load for civil engineering RC/metal structures has been leveled up to such a high level as experienced during the 1955 Great Kobe Earthquake (i.e. Level 2 design seismic load). This trend has been much slower with soil structures although steady. With railway soil structures, this policy was taken ahead of others and its execution promoted the use of GRS structures in place of conventional type soil structures. This is because the advantage of higher cost-effectiveness (i.e. higher performance at a lower LCC) of GRS structures over conventional type soil structures becomes more obvious with an increase in the design seismic load. That is, GRS structures can be designed against Level 2 seismic load at a lower construction cost than conventional type soil structure, while the maintenance cost decreases due to a substantial decrease in the residual deformation (in particular bumps immediately behind bridge abutments

and box culverts) as a result of an increase in the stability by seismic design (e.g. Tatsuoka et al., 2014a, b; Yonezawa et al., 2014). This leveling up policy with soil structures has been enhanced by serious damage to numerous soil structures in a wide area giving a strong negative impact to the society during the 2011 Great East Japan Earthquake (e.g. a serious delay in rescuing and evacuation) and after.

3.1.2 *No-Seismic-Design Policy*

The opinion supporting the traditional no-seismic-design policy not requiring seismic stability analysis under rather broad conditions with soil structures, or the weak-seismic-design policy not increasing the design seismic load from a traditional lower value to a more realistic higher value, has been strong. The following is typical justifications for this policy:

a) Effects of failure/collapse of soil structures by seismic loading is generally not serious and restoration of failed/collapsed soil structures is relatively easy in terms of cost and time when compared with RC/steel structures.
b) There are too many soil structures to deal with, so the seismic design of all soil structures is financially not affordable.
c) Seismic design by stability analysis is too complicated with soil structures and soil properties are very complicated and very difficult to identify due to a large variety and variation.

Based on these justifications, some civil engineers still support the no-seismic-design-policy that allows failure/collapse of soil structures by seismic loading while not relying on redundancy and not expecting "*performance better than expected based on the seismic stability evaluated in design*". They consider that the total cost of failure/collapse in terms of negative impact to the society and restoration of failed/collapsed soil structures is lower than the total cost of seismic design. However, such a policy as this is not recommended nor specified in any design code, as far as the authors know. Besides, these justifications are now not always relevant, in particular with important large-scale soil structures. Therefore, this policy is not discussed anymore in this report. If failure/collapse of soil structures by seismic loading is to be avoided as much as possible, the no-seismic-design policy is difficult to be justified and perplexing, in particular to practicing engineers, as argued below:

Firstly, this policy is a sort of 'empiricism'. In the design codes adopting this policy, it is often mentioned that there are some experiences of "*no failure/collapse of soil structures that were not seismic-designed*". However, these experiences were obtained under limited conditions, therefore they cannot be generalized to other broader conditions (in terms of ground conditions, wall dimensions, backfill conditions, construction details and so on) than those under which the "*performance better than expected*" was observed. Despite the above, this empirical no-seismic-design policy tends to expel rational design by stability analysis based on statics and dynamics that can be applicable to general conditions. Besides, this policy is inconsistent with the ordinary design of RC/metal civil engineering structures. Then, civil engineers in charge of a given construction project, typically structure engineers, tend to adopt RC/metal structures avoiding soil structures (e.g. embankments with RWs).

Secondly, logical justifications of the no-seismic-design policy for soil structures aiming at ultimately reducing their failure/collapse by seismic loading are usually not provided. In this respect, a calculated safety factor is introduced in static design to accommodate uncertainties in the design factors other than seismic loads (i.e. soil strength, dimensions, static loads, boundary conditions …). This safety margin is not prepared for seismic loading. Rather, the experiences of "*performance better than expected based on a calculated safety factor*" should be attributed to implicit safety margin by redundancy. However, this redundancy is not controlled and is random, therefore it is not reliable. In addition, the no-seismic-design policy decreases the safety margin directly by reducing the explicit safety margin (i.e. calculated safety factor) and indirectly by reducing the implicit safety margin (i.e. a reduction of redundancy) associated with less serious design and construction than when seismic-designed. This results in a global decrease in the stability of soil structures, which generally increases failure/collapse by seismic loading. In fact, a number of soil structures, including MSE RWs, failed/collapsed during many previous earthquakes, due likely to a low level of seismic stability resulting from no seismic design or no serious seismic design (e.g. Tatsuoka et al., 1997b; 1998; Koseki et al., 2006, 2007, 2008, 2009; Koseki, 2012; Kuwano et al., 2012, 2014).

Thirdly, the no-seismic-design policy tends to introduce an unnatural discontinuity in design: e.g. no seismic design for a/g= 0.39 versus seismic design for a/g= 0.41; and no seismic design for H= 7.9 m versus seismic design for H= 8.1 m.

Fourthly, the seismic design of soil structure is much more complicated and difficult to validate than that of industrial products. This is because, although design conditions of extreme events (i.e. severe earthquakes, heavy/prolonged rainfalls, floods etc.) tend to determine structural design, their occurrence

is rare or very rare during a long design lifespan, typically 100 years. Moreover, the stress-strain and hydraulic properties of soil could be largely different due to different degrees of saturation and drainage among compaction conditions, ordinary conditions and extreme conditions, particularly with soils including a large fines content. It is feasible to evaluate the soil properties immediately after compaction and under ordinary conditions. On the other hand, those under extreme conditions are very difficult to evaluate. Typically, the apparent cohesion, c, which has significant effects on the stability of soil structure, may decrease to an uncertain extent or disappear by heavy/prolonged rains. So, usually c= 0 is assumed in both static and seismic design. Actual situations of several other factors, such as compaction efforts and changes in the boundary conditions by, for example, erosion or excavation in the ground in front of the wall, in the future are also quite uncertain, so they are assumed conservatively. Despite these difficulties, relevant seismic design aiming at reducing failure/collapse of soil structures by seismic loading, as well as by heavy/prolonged rains and floods, is necessary and quite feasible, as shown below.

3.2 *Redundancy as Implicit Safety Margin*

3.2.1 *Implications of Redundancy in Design for Actual Performance*

"*Performance better than expected*" exhibited by not only GRS RWs (typically Tanata wall), but also many conventional type embankments and RWs should be explained by implicit safety margin (i.e. redundancy in design). As analyzed below, the redundancy in design can contribute significantly to the actual stability of RWs if it is actually available. In Chapter 4, it is argued that the actual seismic stability of soil structure can be improved cost-effectively by increasing the seismic design load to a more realistic higher value (e.g. from zero to a certain value in the case of previous no-seismic design; or from an under-estimated value to a more realistic higher value), while manifesting (i.e. explicitly specifying) some redundancy components (not all) in design.

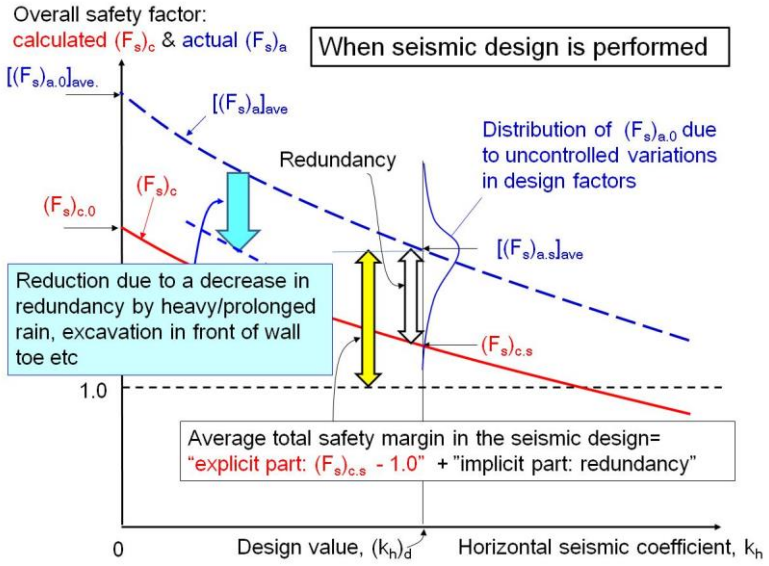

Figure 3-1. Implications of redundancy when seismic design is carried out.

Fig. 3-1 illustrates the implications of redundancy for actual performance of soil structures including GRS RWs when seismic design is carried out. It is considered that the approach using the safety factor in terms of the allowable limit state design, as shown in this figure, is more straightforward and tangible than dealing with load and resistance factors. In this figure, the design seismic load is expressed by the horizontal seismic coefficient, $(k_h)_d$. $(F_s)_{c.s}$ denotes the calculated overall safety factor in the seismic design. The value "$(F_s)_{c.s} - 1.0$" is the nominal explicit safety margin in this seismic design. $(F_s)_{a.s}$ is the actual overall safety factor for the seismic load, $(k_h)_d$. $(F_s)_{a.s}$ is unknown, unlike $(F_s)_{c.s}$, and it scatters for the same value of $(F_s)_{c.s}$ among different soil structures. This is because the difference between $(F_s)_{a.s}$ and $(F_s)_{c.s}$ is due to redundancy, which is usually uncontrolled and unknown.

As indicated by a solid curve, the calculated overall safety factor, $(F_s)_c$, for a given value of $(F_s)_{c.s}$ increases with a decrease in k_h and becomes $(F_s)_{c.0}$ when k_h= 0 (i.e. static conditions). The redundancy defined as "$(F_s)_a$ - $(F_s)_c$" may vary with k_h and becomes "$(F_s)_{a.0}$ - $(F_s)_{c.0}$ when k_h= 0". The redundancy with GRS RWs that results from several conservatisms are discussed below. The broken curve in Fig. 3-1 denotes the $[(F_s)_a]_{ave}$ versus k_h relation, where $[(F_s)_a]_{ave}$ is the average of $(F_s)_a$. The average total safety mar-

gin is equal to "$[(F_s)_a]_{ave} - 1.0$", which comprises: 1) the explicit part "$(F_s)_c - 1.0$"; and 2) the implicit part "$[(F_s)_a]_{ave} - (F_s)_c$". Due to the total safety margin, $(F_s)_a - 1.0$, Tanata wall survived Level 2 seismic load despite that the wall was designed against Level 1 seismic load.

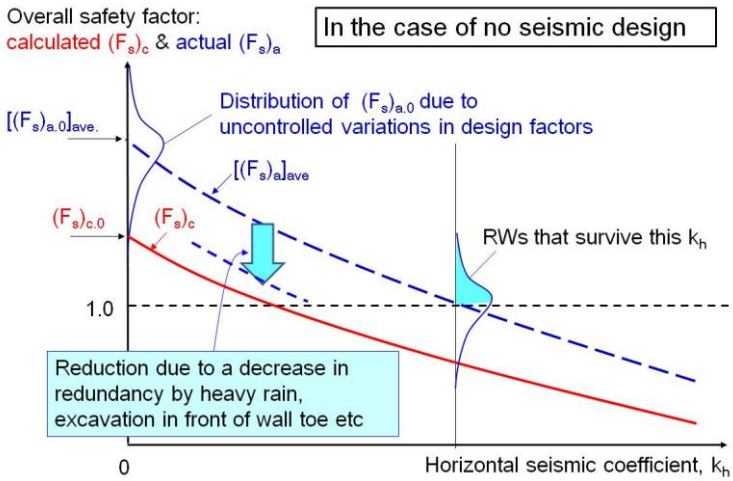

Figure 3-2. Implications of no-seismic-design policy.

Fig. 3-2 illustrates the implications of no-seismic-design policy. Although the actual safety factor, $(F_s)_a$, decreases with an increase in k_h, due to the safety margin in static design, $(F_s)_{a.0}$ -1.0, the value of $(F_s)_{a.s}$ is maintained higher than unity and some non-seismic-designed soil structures (including GRS RWs) can survive until k_h becomes a certain value. However, this approach cannot be recommended, in particular with important soil structures, as this is not reliable for the following reasons. Firstly, when following this policy, the explicit safety margin by calculated safety factor, $(F_s)_c$, becomes definitely smaller than when performing seismic design (Fig. 3-1). Then, under otherwise the same conditions, the value of k_h at which $(F_s)_a$ becomes unity becomes smaller than when seismic-designed. Secondly, due to positive redundancy included in design, the actual overall safety factor under static conditions, $(F_s)_{a.0}$, becomes larger than the calculated overall safety factor in static design, $(F_s)_{c.0}$. The no-seismic-design policy relies on the redundancy, $(F_s)_a$ - $(F_s)_c$. However, this redundancy is not controlled and is random among different soil structures. Inadequate or improper design and construction (i.e. poor drainage, poor compaction, poor facing structure with poor connection, poor treatment of weak supporting ground, inadequate arrangement of reinforcement etc.) may have decreased substantially the redundancy. Besides, the actual safety factor, $(F_s)_a$, may also drop by a drop in the redundancy during extreme events other than earthquakes (i.e. heavy/prolonged rains, unexpected souring/excavation & loading etc.) sometime during its lifespan. Then, failure/collapse may take place under not only seismic conditions but also non-seismic conditions, as seen from the examples presented below.

Fig. 3-3 shows a collapse in August 2001 of a Terre Armée wall constructed to retain embankment in a valley for an approach road to an irrigation dam. The wall was completed in February 2001, a half year before the collapse. The wall was supported by a relatively stiff subsoil with the foundation of the facing on a rock layer. Although the backfill was on-site clayey soil including gravel particles and the wall was constructed in a water-collecting place, no drainage was provided. After a rainy season in June and July, excessive deformation of the wall face with cracks in many panels (finally 50 panels) was noticed. After the crest of the backfill immediately behind the facing had settled down about 50 cm and the facing had been pushed out about 10 cm at a maximum, the wall collapsed during rehabilitation works. It seems that pull-out failure of some metal reinforcement strips took place, which developed an active wedge (Fig. 3-3c). Downward displacements of the active wedge relative to the facing sheared off the connection between the reinforcement and the facing at a limited number of panels (Fig. 3-3d). The falling-off of several panels due to this connection failure destabilized many panels located above, which ultimately resulted in a large-scaled collapse of the wall. This failure/collapse mechanism is similar to the one observed with four Terre Armée walls in eastern Tennessee reported by Lee et al. (1994). It is likely that the degree of saturation in the backfill had been high by the time of collapse due to preceding prolonged raining, a low permeability of the backfill and no internal drainage despite construction in a water-collecting place. Upon excavation after the collapse, the backfill could stand for a large height without support, due likely to apparent cohesion that developed by drying associated with excavation (Fig. 3-3c).

Figure 3-3. Collapse of a Terre Armée RW for an approach road to an irrigation dam in Aomori Prefecture, August 2001 (constructed February 2001): a) overview; b) front view; c) excavated cross-section; and d) typical sheared-off connection.

Fig.3-4 shows a more drastic collapse of Terre Armée wall caused by heavy rainfall associated with typhoon No. 23 in October 2004. The wall was completed in 2000, four years before the collapse. The wall was double-tiered with a total height of 23 m. There was no adequate internal drainage in the fine-grained backfill, in particular no drainage crossing the backfill to collect and drain surface water from behind and both sides of the wall. Redundancy due to apparent cohesion disguised the lack of proper drainage for four years holding the wall system stable. When heavy rainfall occurred as should have been expected during the lifespan of this wall, it is likely that the apparent cohesion vanished and positive pore water pressure developed resulting in collapse. A high degree of saturation of the backfill at the time of collapse can be seen from flow failure for a long distance of the backfill (Fig. 3-4b).

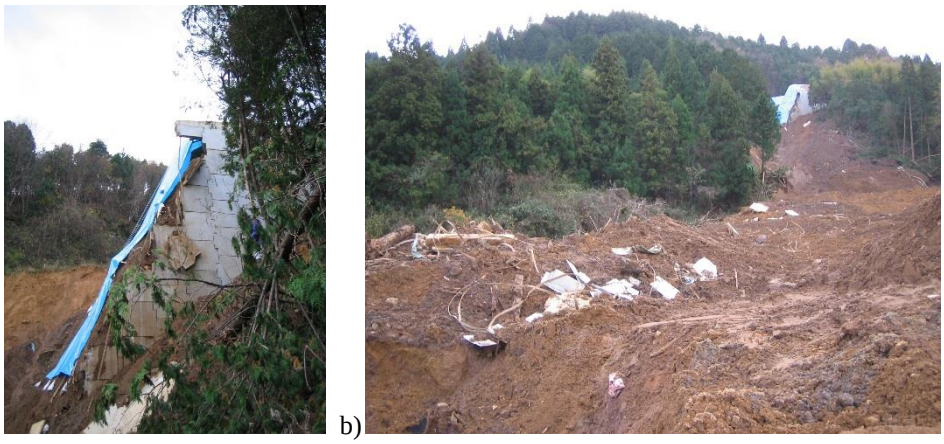

Figure 3-4. Collapse by heavy rainfall in 2004 of Terre Armée wall for a local road lacking proper drainage, Yabu City, Hyogo Prefecture (Shibuya, et al., 2007): a) remaining part of the lower tier: and b) a view from downstream.

Koerner et al. (2013) reported 171 collapse cases of GRS RWs since 1987. 134 cases were in North America. The largest number of failures 71 (42 %) were from 1 to 2 years after construction. The major failure mode is excessive deformation of wall face, many associated with the connection failure. They felt the primary causes of the failures to be inadequate or improper design and/or construction (i.e. poor drainage and poor compaction of fine grained soil). Interestingly, there are no cases involving inadequate or improper manufactured geotextile or geogrid products. Valentine (2013) also reported 45 GRS struc-

tures that performed poorly to the point that it no longer satisfied the requirements of the owner. Consistent with Koerner et al. (2013), the two major causes of failure he found are poor drainage and the use of fine grained soil that was poorly compacted.

In these and other failure/collapse cases of GRS structures, the redundancy under ordinary static conditions should have been insufficient, not prepared for extreme events of not only earthquakes but also heavy/prolonged rains, unexpected excavation and external loading etc. These cases indicate that the no-seismic-design-policy relying on redundancy is not reliable, because redundancy is not reliable as it is not controlled and is random.

3.2.2 *Components of Redundancy (Summary)*

The major redundancy components with GRS RWs (or more generally, with soil structures) that are usually implicitly included in design and can explain "*seismic performance better than expected based on a calculated safety factor*" are summarized below:

1) Under-estimation of soil shear strength by:
   1a) ignoring apparent cohesion due to matric suction, c, prepared for insufficient drainage during heavy/prolonged rainfalls and/or abundant ground and surface water supply; and
   1b) under-estimating the friction angle ϕ (with c= 0), prepared for insufficient compaction.
2) Under-estimating the rupture strength of geosynthetic reinforcement by:
   2a) the use of creep reduction factor to obtain the design tensile strength assuming that creep takes place by design sustained load that is substantially higher than actual sustained load; and
   2b) the use of multiple correction factors, assuming conservatively that all negative phenomena take place consecutively at any places;
3) Ignoring toe resistance, prepared for unexpected ground excavation and scoring in front of the wall.
4) Under-estimating positive dynamic effects due to ductility in pseudo-static analysis (if relevant).
5) Under-estimating the contribution of facing rigidity to wall stability (if relevant).
6) Positive 3D effects against 2D approximation in stability analysis.
7) Others.

Significant redundancy is created by ignoring some or all of these components in design if they are actually available as a result of, in particular good drainage, the use of drainable backfill, good compaction, a sufficient toe depth, the use of rigid facing etc. However, most of these redundancy components is usually not well recognized and, as a result, the importance of these good practices to achieve sufficient wall stability is often overlooked. In the following, these redundancy components are discussed separately.

3.3 *Soil Shear Strength*

3.3.1 *Apparent Cohesion*

Apparent cohesion resulting from the intercept produced by fitting a linear Mohr-Coulomb failure envelope to a curved failure envelope is herein out of the scope. In some previous earthquakes, typically the 1968 Tokachi-Oki Earthquake (e.g. Ikehara, 1970; Yoshimi, 1970); and the 2004 Niigata-ken Chuetsu Earthquake (e.g. Tatsuoka et al., 2006), the damage to soil structures was amplified likely by a loss of apparent cohesion due to a heavy rain immediately before the respective earthquakes. Another example is collapse of embankment at a water collecting place between Yoshida and Sagara-Makinogahara for one of the busiest highways in Japan (Tomei), opened in 1968. The collapse took place on 11 August 2009 by a small-scaled earthquake in Shizuoka Prefecture. It is likely that the backfill of crushed sedimentary softrock had been deteriorated by slaking due to effects of ground water for a long period since its construction (Express Highway Research Foundation, 2014). Besides, the precipitation one day before the collapse was 55 mm by an effect of a typhoon, while the precipitation on the day of collapse was 13 mm. The lane toward Tokyo was closed for five days, giving a serious social impact.

The use of c= 0 and $\gamma = \gamma_{sat}$ in seismic design is particularly relevant with walls of which the degree of saturation in the backfill is always kept high due to insufficient drainage despite construction in a water collecting place. Fig. 3-5 shows one extreme case, in which a Terre Armée wall largely deformed during the 2004 Niigata-ken Chuetsu Earthquake. A large amount of liquefied sand spouted from a narrow opening between two vertically adjacent panels near the wall bottom that developed by large deformation of the facing due to seismic loads (Figs. 3-5c & d). This unusual event should be attributed to nearly saturated conditions of sand backfill at the time of the earthquake, which is due to not only heavy rainfall immediately before the earthquake but also poor drainage despite abundant supply of water from the back hill. There were no drain holes in the facing (as with all Terre Armée walls) and the base drain pipes crossing

the wall were not functioning as their outlets in front of the wall were closed for an unknown reason. A high degree of saturation under ordinary conditions could be inferred from a plenty of vegetation on the wall face and at the footing toe which would have not been so if the backfill had been well drained (Figs. 3-5a & b). Fig. 2-8a shows another collapse case of poorly drained GRS RW by seismic loads.

Figure 3-5. Terre Armée wall (5 – 9 m-high & 100 m-long, constructed 1997) along a ramp at Horinouchi interchange, Kan-etsu expressway, damaged during the 2004 Niigata-ken Chutsu Earthquake (Kitamura et al., 2006): a) & b) views of the wall; and c) opening between panels from which a large amount of liquefied sand spouted; and c) sedimentation of sand in front of the wall.

Based on lessons from many failures/collapses of soil structures including MSE RWs due to heavy/prolonged rains, as described in Section 2.3 and this section, historically many design guidelines (e.g. Japan Road Association, 2012; Railway Technical Research Institute, 2007a; AASHTO 2010) recommend excluding apparent cohesion from both static and seismic designs of RWs including GRS RWs and the use of $\gamma = \gamma_{sat}$. Some investigators (e.g. Leshchinsky, 2010; Ling et al., 2012; Leshchinsky & Tatsuoka, 2013) support this design policy. However, the recent edition of AASHTO LRFD bridge design specifications (AASHTO, 2012) allows the use of apparent cohesion, c, in seismic analysis, without showing how to determine the value of c under various different conditions, while prohibiting it in static analysis dealing with the external stability of GRS structures. This may yield perplexing results in that a wall becomes more stable under certain seismic conditions than under static conditions (Vahedifard et al., 2014).

To show implications of the redundancy gained by ignoring apparent cohesion, c, in static and seismic design, Fig. 3-6b was produced for the simplest wall structure (i.e. vertical smooth wall with zero back slope, Fig. 3-6a) from the data presented in Vahedifard et al. (2014) and those provided by them. They chose a soil friction angle $\phi = 34^o$ as a typical default value used in ordinary practical design in North America. The results obtained by using two extreme wall friction angles, $\delta = 0$ and ϕ, are similar. It is to be noted that c=10 kPa is not a large value. For example, with c= 10 kPa, the free standing height of unsupported vertical wall height is only of the order of 1 m. The safety factor for sliding is defined as: $F_s = P_{available}/P_{applied}$, where:

- $P_{applied}$ is the total earth pressure activated on the RW determined by using c= 0 and c > 0, which increases with an increase in k_h; and
- $P_{available}$ is the fixed total earth pressure that can be resisted by the RW equal to "$P_{applied}$ when $k_h = 0$ and c= 0" times an assumed safety factor under static conditions, $(F_s)_{c.0}$, equal to 1.5.

The seismic inertia effect of RW structure is ignored. If it is included, the F_s values when $k_h > 0.0$ become smaller than those presented in Fig. 3-6b and the other similar figures that appear below. This result is equally relevant to any RW types (including GRS RWs) having the same $P_{available}$ value. The sliding failure mode is selected to demonstrate the implications of redundancy. The same conclusion is obtained for the overturning failure mode. In Fig. 3-6b, the difference in F_s between two curves for c > 0 and c= 0

denotes the implicit safety margin (i.e. redundancy) with RWs designed assuming that c= 0 whereas c> 0 is actually available.

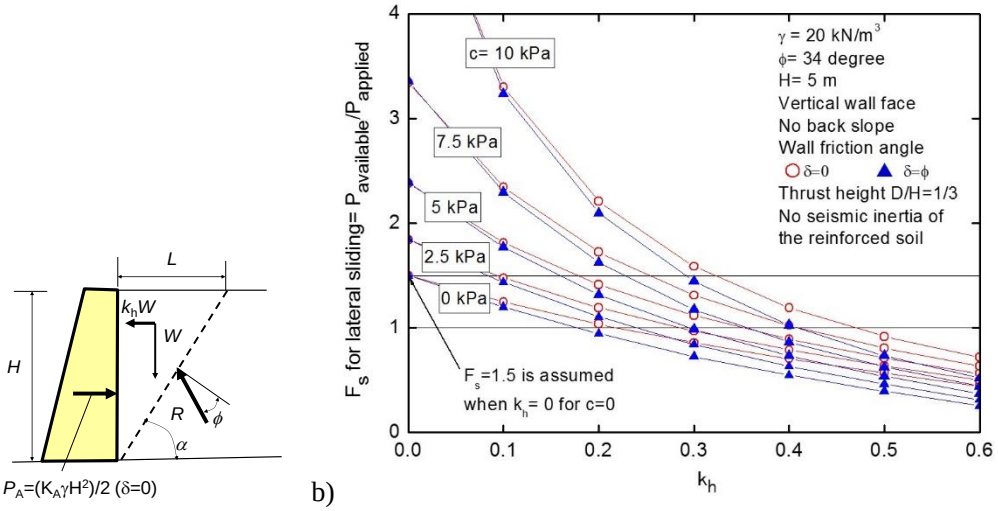

Figure 3-6. a) Vertical smooth wall with zero back slope with a linear failure plane; and b) safety factors against lateral sliding for different apparent cohesions by limit equilibrium stability analysis assuming log-spiral failure plane (modified from Vahedifard et al., 2014).

The following trends may be seen from this figure:

1) When actually c= 0, F_s is larger than 1.0 until k_h becomes about 0.2. Note that this value becomes smaller if the inertia force of RW structure is taken into account. This result does not mean that seismic design is not necessary if the design k_h value, $(k_h)_d$, is lower than about 0.2. This is because F_s= 1.5 when k_h= 0 is not introduced to ensure this seismic stability, but it is to accommodate unknown uncertainties in the other design factors (i.e. soil strength, dimensions, boundary conditions, static loads ……).
2) When actually c= 0, the F_s value becomes lower than unity if k_h becomes higher than about 0.2. This means that the wall cannot survive seismic load k_h higher than 0.2 if any uncertainty is not included in all design factors and an explicit safety margin by "F_s= 1.5 when k_h= 0" is fully available. This means that this explicit safety margin is not enough to ensure the stability of RWs for design k_h values higher than about 0.2 yet lower than 0.4 (AASHTO, 2012). In this case, if an implicit safety margin (i.e. redundancy) by apparent cohesion, c, is actually available, RWs can survive k_h higher than 0.2 while the limit increases with an increase in c. This analysis partly explains why RWs well designed and constructed against static loads could survive seismic loads below a certain level. However, it is to be emphasized again that this redundancy created by ignoring apparent cohesion in design is not controlled and is random therefore it is not reliable.
3) If the use of apparent cohesion, c, is allowed in seismic design but not in static design, for k_h values lower than a certain limit (which increases with an increase in the c value used in seismic design), the calculated seismic safety factor value, $(F_s)_{c.s}$, becomes higher than the calculated static safety factor, $(F_s)_{c.0}$. This result is indeed perplexing!

3.3.2 *Friction Angle*

Compaction control in performance construction: In the conventional field compaction control (Fig. 3-7a), all measured values of the degree of compaction, D_c (= measured dry density, ρ_d/maximum dry density, $(\rho_d)_{max}$, obtained by laboratory compaction tests using a specified compaction energy) are required to be equal to, or higher than, the specified allowable lower bound, which is typically D_c= 90 % by Standard or Modified Proctor (1Ec or 4.5Ec). Friction angles similar to the residual friction angles, ϕ_{res}, typically 40^o (well-graded sandy and gravelly soils), 35^o (ordinary sandy and gravelly soils) and 30^o (poorly-graded sandy soils) in Japan, are usually used as default design values. As seen from Figs. 2-5c & d, these standard design ϕ values correspond approximately to these allowable lower bounds of D_c. Therefore, the use of these default ϕ values in design with backfill well-compacted having D_c higher than the lower bound is conservative creating redundancy. Instead, this method does not encourage, giving no rewards to, better compaction. On the other hand, the use of both of ϕ_{peak} corresponding to the average of actual compacted

values of D_c and ϕ_{res} is more realistic with well-compacted backfill, while it encourages better compaction. This method is explained later.

Higher dry density can be obtained by improving the conventional compaction control (Tatsuoka, 2011). That is, in the conventional compaction control (Fig. 3-7a), the water content *w* is controlled to be equal to the optimum water content, w_{opt}, or a slightly higher value. However, the $(\rho_d)_{max}$ value increases and the w_{opt} value decreases with an increase in the compaction energy level (CEL). Since the introduction of this method by Proctor (1933), CEL available in the field has been increasing, while a required compacted ρ_d value has been increasing to improve performance. On the other hand, it is very difficult to accurately control and estimate CEL in the field, because, even when using the same compaction machine, the lift may vary, the compaction energy decreases with depth in respective lifts, and the number of passing may vary. To overcome this basic drawback, Tatsuoka (2013 - 2014) proposed the so-called (ρ_d & S_r) method (Fig. 3.7b) based on the following findings: a) The degree of saturation, S_r, at which a $(\rho_d)_{max}$ value is attained for a given CEL, called the optimum degree of saturation, $(S_r)_{opt}$, is independent of CEL. The effects of soil type on the $(S_r)_{opt}$ value is rather small. b) The shape of compaction curve plotted on the ρ_d and S_r plane is also rather independent of CEL, while rather insensitive to changes in the soil type. c) For a given soil type, the stress-strain properties before and after soaking and the hydraulic conductivity of saturated soil are a function of ρ_d and the S_r value during compaction not including CEL as a variable. The (ρ_d & S_r) method consists of the following steps while not referring to CEL:

1) Obtain the compaction curve on the ρ_d and S_r plane and the $(S_r)_{opt}$ value by laboratory compaction tests at a certain CEL.
2) Set the target value of S_r equal to $(S_r)_{opt}$ and determine the target value of ρ_d by which soil properties required to ensure specified performance of a given soil structure can be achieved (i.e. performance construction following performance design).
3) Determine the allowable lower bound of ρ_d for all measured values in such that the averaged value of all measured values becomes the compaction target value of ρ_d.
4) Start compaction at the water content *w* derived from the target values of ρ_d and S_r (= $(S_r)_{opt}$).
5) At relevant moments during each compaction process, find the current compaction curve from current values of ρ_d and S_r to confirm the current compaction state along the current compaction curve. Stop the compaction work if: a) S_r has reached $(S_r)_{opt}$, while not allowing S_r to become higher than $(S_r)_{opt}$; and b) ρ_d becomes equal to, or higher than, the allowable lower bound.

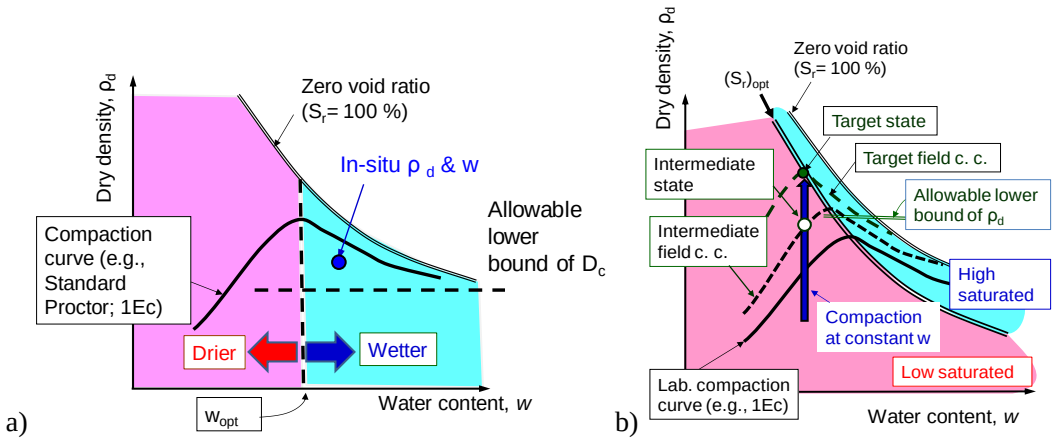

Figure 3-7. Backfill compaction control: a) conventional method; and b) (ρ_d & S_r) method (Tatsuoka, 2013-2014).

Effects of friction angle: As discussed above, the friction angle, ϕ, of well-compacted backfill can become higher than the default values usually used in routine design. Fig. 3-8a compares the safety factor F_s and k_h relations obtained by using ϕ= 34° (a typical default value in North America) and ϕ= 50° (a typical value with well-compacted well-graded drainable soil). Zero wall friction angle, δ= 0, and zero apparent cohesion are assumed. F_s is defined as $P_{available}/P_{applied}$, where:

- $P_{applied}$ is the total earth pressure activated on the RW, which increases with an increase in k_h; and
- $P_{available}$ is the fixed total earth pressure that can be resisted by the RW equal to "$P_{applied}$ when k_h= 0 determined by using ϕ= 34°" times 1.5 (as in the case illustrated in Fig. 3-6).

So, the difference in F_s between the two curves is an implicit safety margin (i.e. redundancy) created by using ϕ= 34° in design when the actual ϕ value is 50°. Fig. 3-8b shows the similar F_s and k_h relations for different ϕ values under the same conditions as Fig. 3.8a obtained by the Mononobe-Okabe seismic

earth pressure theory, which is expressed by the following equations for the simplest wall structure with a straight failure plane (Fig. 3-6a):

$$\frac{L}{H} = -\tan\phi + \frac{\sec\phi}{\sqrt{1-\frac{\tan\psi}{\tan\phi}}} \qquad (3\text{-}1a)$$

$$K_{A.S} = \frac{1}{\cos^2\psi}\left(\frac{\cos(\phi-\psi)}{1+\sqrt{\frac{\sin\phi\cdot\sin(\phi-\psi)}{\cos\psi}}}\right)^2 \qquad (3\text{-}1b)$$

where H is the wall height; and L is the width of the active wedge on the crest of backfill when the total active earth pressure becomes the maximum equal to (1/2)・γ・H^2・$K_{A.S}$ (i.e. when the global safety factor becomes the minimum) for all possible failure plane angles, α (Fig. 3-6a); γ is the soil density; and k_h= tanψ (horizontal seismic coefficient). The relations for the same ϕ value shown in Figs. 3-8a and b are very similar. It may be seen from these figures that, if the actual ϕ value is 50°, the use of ϕ=34° in design creates redundancy that increases the k_h value at which collapse takes place from about 0.2 to about 0.5. For a peak friction angle equal to 50°, this redundancy is not fully available due to post-peak strain softening in the stress-strain behavior of the backfill, as discussed later. Yet, this analysis also partly explains why "RWs well designed and constructed against static loads can survive seismic loads below a certain level". Note again that this redundancy becomes available only when the backfill is well-compacted by relevant field compaction control, as discussed above, and relevant drainage.

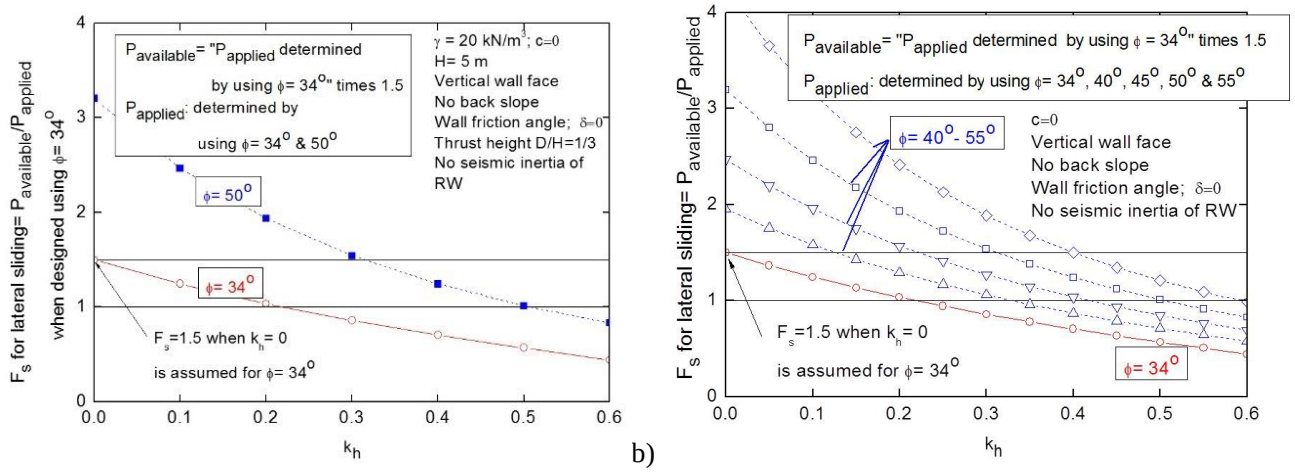

Figure 3-8. Safety factor against lateral sliding for vertical smooth walls with zero back slope (Fig. 3-6a) for different friction angles of the backfill by limit equilibrium stability analysis assuming; a) log-spiral failure plane (modified from Vahedifard et al., 2014); and b) straight failure plane (the Mononobe-Okabe theory).

3.4 *Toe Resistance*

The design codes for GRS RWs usually require the placement of the level pad of the facing at a certain depth. The minimum toe depth, D, for GRS RWs with FHR facing for railways in Japan is 0.4 m (RTRI, 2013c). Ignoring of the toe resistance in design is another source of redundancy (Leshchinsky & Vahedifard, 2012). Fig. 3-9 shows the F_s and k_h relations obtained for the active earth pressure for H= 5 m by Eq. 3-1 and the toe resistance for a depth D= 0.5 m and 1. 0 m by Eq. 3-2 (i.e., the Mononobe-Okabe seismic passive earth pressure theory when c= 0) for ϕ= 34° under otherwise the same conditions as Fig. 3.8b:

$$K_{P.S} = \frac{1}{\cos^2\psi}\left(\frac{\cos(\phi-\psi)}{1-\sqrt{\frac{\sin\phi\cdot\sin(\phi-\psi)}{\cos\psi}}}\right)^2 \qquad (3\text{-}2)$$

No wall friction was considered for the active and passive earth pressures, although the toe resistance increases with an increase in the wall friction angle. The safety factor is defined as: $F_s = P_{available}/P_{applied}$, where:

- $P_{applied}$ is the total earth pressure activated on the RW, which increases with an increase in k_h; and
- $P_{available}$ is the fixed resistance of the RW equal to "$P_{applied}$ when $k_h = 0$ determined by using $\phi = 34^o$ without toe resistance" times 1.5 (as in the cases illustrated in Figs. 3-6 and 3-8) plus "the toe resistance when D> 0".

The redundancy by ignoring toe resistance increases non-linearly with an increase in the toe depth. It may be seen that the contribution of a relatively large toe depth D= 1.0 m is smaller than that of a small value of c equal to 5 kPa (Fig. 3-6b).

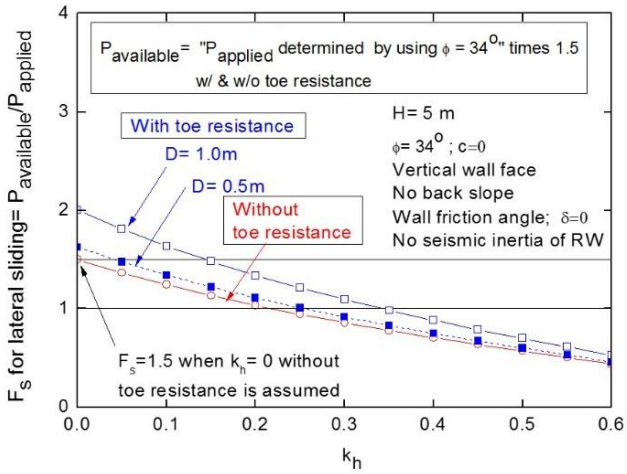

Figure 3-9. Safety factor against lateral sliding for vertical smooth walls with zero back slope (Fig. 3-6a) for $\phi = 34^o$ and c= 0 by limit equilibrium stability analysis assuming a straight failure plane (the Mononobe-Okabe theory).

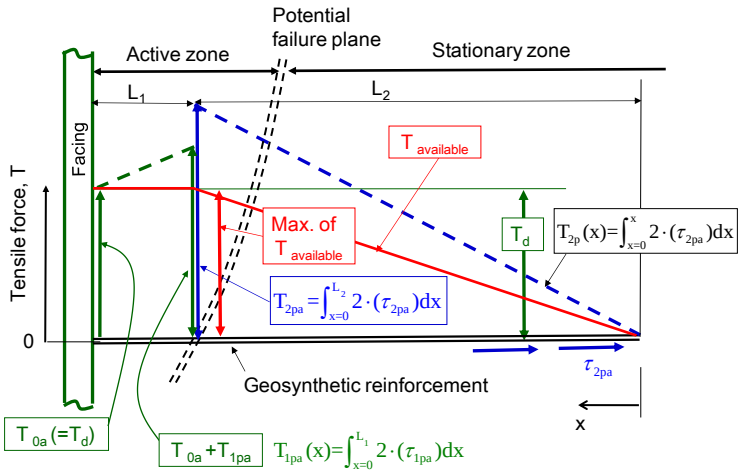

Figure 3-10. Relationship among different available strength components of geosynthetic reinforcement (when the available tensile rupture strength of reinforcement, T_d, is the minimum).

3.5 *Tensile Rupture Strength of Geosynthetic Reinforcement*

An underestimation of design (i.e. available) tensile rupture strength of a given geosynthetic reinforcement, T_d, is another redundancy component. To discuss on this issue, the distribution of available tensile force, $T_{available}$, along a geosynthetic reinforcement layer is firstly analyzed. Fig. 3-10 illustrates the case where the available connection strength at the back of the facing, T_{0a}, is equal to T_d and the facing is rigid enough to develop the earth pressure by which T_{0a} can be fully mobilized. The maximum value of $T_{available}$ along the reinforcement length is usually activated at the place where the reinforcement crosses the potential failure plane. This maximum value of $T_{available}$ is the minimum value of: 1) T_d; 2) T_{0a} (= T_d) plus available anchorage strength in the active zone, T_{1pa}; and 3) available anchorage strength in the stationary zone, T_{2pa}. Fig. 3-10 shows the case where T_d is the minimum among the three components, which is usu-

ally the case with GRS RWs having rigid facing, good connection strength and a sufficient length of reinforcement.

In current design, the value of T_d is usually determined by adjusting the strength of virgin specimens obtained by tensile loading tests at a high loading rate, T_{ult}, to account for installation damage and durability. It is further adjusted for creep reflecting field condition of sustained constant static load to obtain the unfactored design strength, $(T_d)_0$. Finally, $(T_d)_0$ is adjusted by the overall safety factor, $(F_s)_{overall}$, comprising the material safety factor and the structural safety factor to compare with the load required to maintain the stability of wall, $T_{required}$. This procedure is described by Eq. 3-3 (see Fig. 3-11).

$$T_d = \frac{(T_d)_0}{(F_s)_{overall}} \qquad (3\text{-}3a)$$

$$(T_d)_0 = \frac{T_{ult}}{RF_{ID} \cdot RF_D \cdot RF_{CR}} \qquad (3\text{-}3b)$$

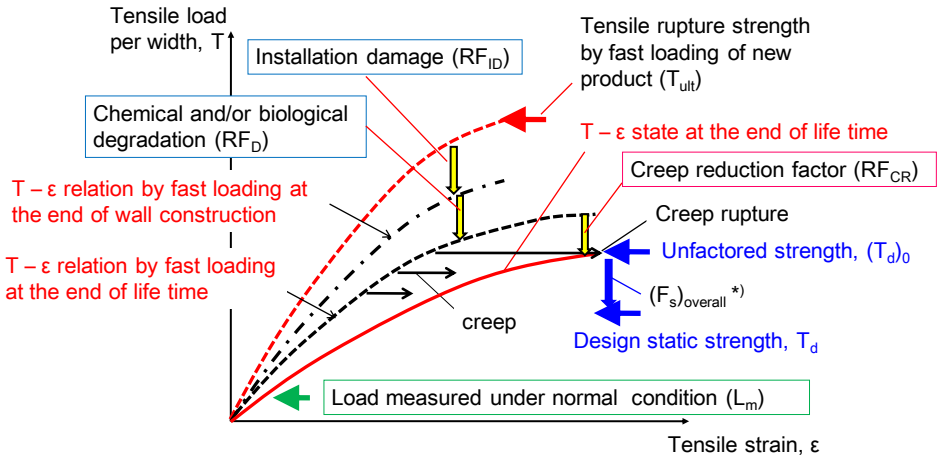

*) Overall safety factor= Material F_s times global F_s (for uncertainties with other design factors)

Figure 3-11. Procedure to obtain the design rupture strength, T_d, from the tensile rupture strength by fast loading of virgin specimens, T_{ult}.

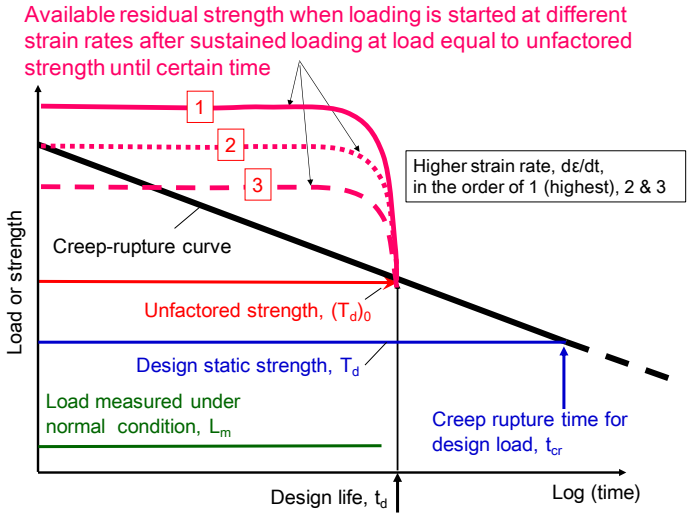

Figure 3-12. Available residual strength affected by strain rate at rupture (Greenwood et al., 2001; Tatsuoka et al., 2004, 2006b; Tatsuoka, 2008a; and Kongkitkul et al., 2007a, b).

There are two aspects of conservatism (i.e. redundancy) associated with these adjustments (Leshchinsky & Tatsuoka, 2013). Firstly, adjustments for strength due to installation damage and durability are assumed to be the same everywhere. Hence, the reduction factors, RF_{ID} and RF_D, multiply each other. This multiplication would be justified if indeed the two reductions occur at the same location where the actual long-term strength of the reinforcement is needed. It is uncertain whether this will happen at exactly the same place. This uncertainty justifies the multiplication of these two factors, creating redundancy.

Secondly and more significantly, the adjustment for creep applied so that creep rupture does not take place by the end of lifespan includes the following three redundancy factors:

1) Multiplication of reduction factors for long term durability and creep rupture, RF_D and RF_{CR}, means that creep rupture is evaluated for sustained load applied to the reinforcement that has deteriorated by chemical and/or biological effects for a considered lifespan. In actuality, the creep deformation takes place simultaneously with this degradation process, therefore, the actual creep strain is lower than in the case assumed by Eq. 3-3 (Kongkitkul et al., 2007b).

2) Due to the overall safety factor, $(F_s)_{overall}$, and the redundancy in the design load, for most of the lifespan, the actual force in the reinforcement, L_m, in the wall under normal conditions is substantially lower than the sustained load by which creep is considered to take place in design that is equal to "T_d by Eq. 3-3" times $(F_s)_{overall}$, as illustrated in Figs. 3-11 and 3-12.

3) Creep is not a degrading phenomenon, but it is merely a viscous response (Tatsuoka et al., 2004, 2006). Therefore, if chemical and/or biological degradation does not take place, the residual strength at a given strain rate does not decrease by creep deformation that has taken place until the time when the rupture takes place: i.e. the original strength is maintained until late in its service life (Fig. 3-12). Fig. 3-13 shows typical tensile loading test results showing this feature. In one of the three tests, sustained loading (SL) was applied for 30 days during otherwise monotonic loading (ML) at a constant strain rate. The load-strain relation upon the restart of ML at a constant strain rate soon rejoins the one obtained by two continuous ML loading tests not including this SL stage. The rupture strength in these three tests is a rather unique function of the strain rate at rupture and essentially the same irrespective of SL at an intermediate stage. That is, as illustrated in Fig. 3-12, when subjected to seismic loads for a limited duration during otherwise a long service period under constant load conditions, the original strength at a fast strain rate is fully activated.

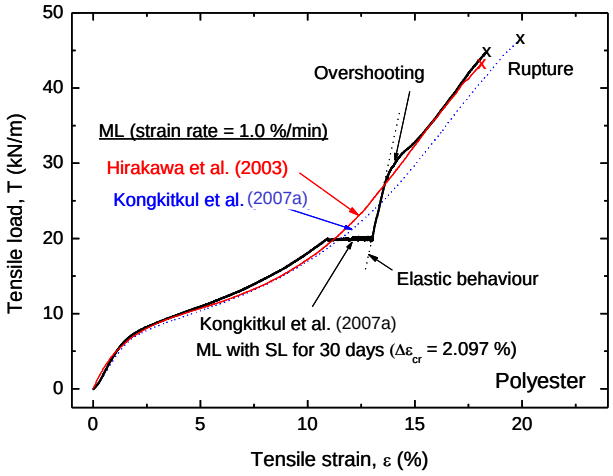

Figure 3-13. Comparison of tensile load - strain relations from three ML tests with and without sustained loading for 30 days at an intermediate load level, a PET geogrid (Hirakawa et al., 2003; Kongkitkul et al., 2007a).

Hence, usually the reduction factor for creep is not entirely relevant; in many cases, it may be close to unity (i.e. practically no reduction for creep). Particularly in setting the design tensile strength of geosynthetic reinforcement against seismic loads, the creep reduction factor is not necessary. Although no use of creep reduction factor reduces redundancy when compared to the design using a creep reduction factor, this procedure is relevant in the seismic design using realistic design seismic loads.

3.6 *Positive Dynamic Effects*

In the framework of the conventional seismic design, failure is judged to take place if the overall safety factor for wall stability calculated by the pseudo-static analysis becomes unity against a given design horizontal seismic coefficient, $(k_h)_d$, although the calculated safety factor is required to be equal to, or larger than, a given specified minimum safety factor. The value of $(k_h)_d$ is usually set to be smaller by a factor of 1/2 - 2/3 than a given "design peak horizontal acceleration, $(\alpha_{max})_d$"/"gravity acceleration, g", by taking into account so-called dynamic effects. Tatsuoka et al. (1998) argued that the dynamic effects comprise

two components: “dynamic ductility”, which decreases the ratio $(k_h)_d/[(\alpha_{max})_d/g]$; and “dynamic flexibility”, which increases this ratio.

With respect to dynamic ductility, soil structure collapses only after having exhibited unacceptable large residual deformation caused by several pulses having “horizontal acceleration, α”/g larger than the yield strength $(k_h)_y$ at which the safety factor becomes unity. Soil structures that exhibit a lower stability reduction rate with residual deformation have a higher dynamic ductility. For example, for the same input acceleration time history having a certain value of α_{max}/g, over-turning collapse can take place less easily with GRS RWs having a higher dynamic ductility due to a relatively wide reinforced zone than with conventional cantilever RWs having a lower dynamic ductility due to a relatively narrow wall structure. Therefore, for the same value of $(\alpha_{max})_d/g$, the value of $(k_h)_d$ to be used in pseudo static seismic stability analysis should be set lower with GRS RWs than with conventional cantilever RWs (Tatsuoka et al., 1998). The use of the same $(k_h)_d$ as conventional cantilever RWs creates some redundancy in the seismic design of GRS RWs. Judging of seismic stability based on calculated residual deformation can take into account such positive effects of dynamic ductility as above. Although this procedure does not create redundancy in design, it can be shown that a given wall can survive a realistic input motion having α_{max}/g significdantly higher than the yield strength, $(k_h)_y$.

With respect to dynamic flexibility, the amplification of response acceleration in GRS structures from input motion is generally much lower than in ordinary slender RC structures, such as tall bridge piers. This is due to: a) larger phase differences resulting from initial natural frequencies that are usually much higher than typical predominant frequencies of severe seismic motions; and b) higher values of material damping at large strains and dissipation damping (Tatsuoka et al., 2009, 2012d, Munoz et al., 2012). In fact, in many seismic design codes of soil structures (other than high earth/rock-fill dams), dynamic amplification is ignored. Although this simplification is un-conservative, it seems that it is usually implicitly considered that this negative effect can be compensated by other redundancy components that are large enough. In that case, the reduction in redundancy by this approximation becomes smaller with less dynamically flexible soil structures having higher natural frequencies. It is the case with GRS integral bridges (explained later) compared with conventional type bridges (Tatsuoka et al., 2009, 2012d, Munoz et al., 2012).

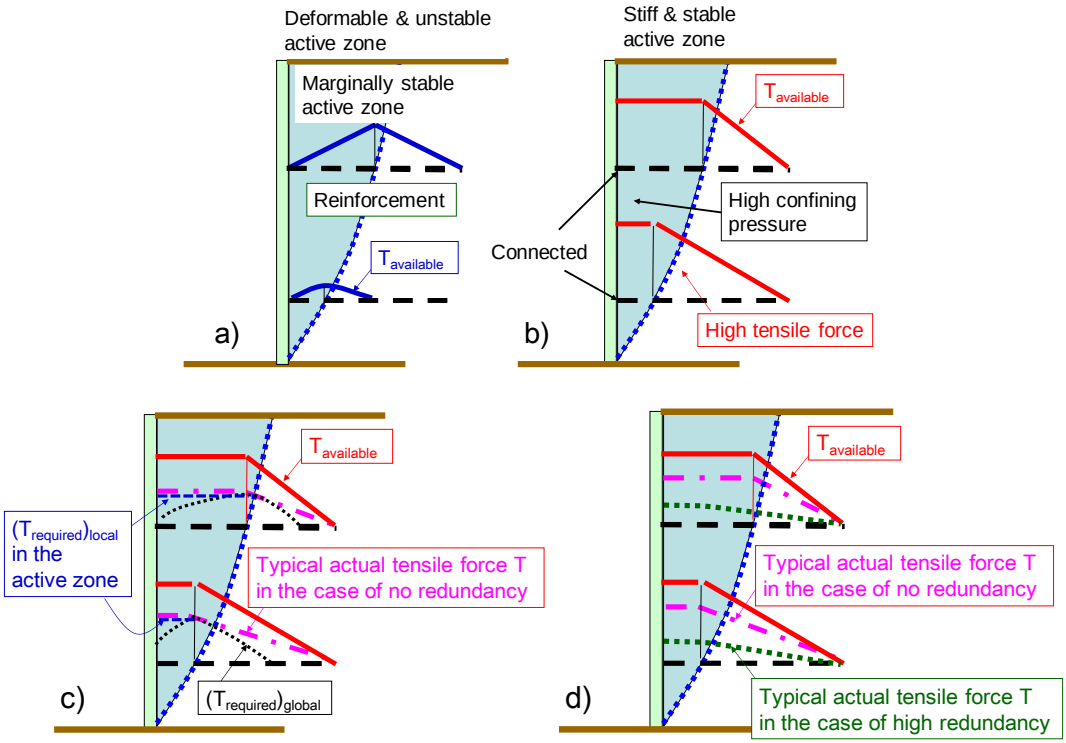

Figure 3-14. a) & b) Comparison of $T_{available}$ when the connection force is zero & high; c) comparison among available, required and actual T values when connection force is high; and d) comparison between actual T values when redundancy is zero and high in relation to $T_{available}$.

3.7 *Un-conservatism and Redundancy Related to Facing Structure*

3.7.1 *Relationship between Required and Available Strengths of Reinforcement*

The structure of facing including that of facing/reinforcement connection has large effects on the wall stability, while this factor is largely different among different MSE RW types (Tatsuoka, 1992). Over-estimation of this factor in design when it is actually insufficient is on the unsafe side reducing redundancy. On the other hand, underestimation of this factor in design when it is actually available is on the safe side creating redundancy.

To explain this issue, Figs. 3-14a & b schematically compare the available tensile forces, $T_{available}$, along the reinforcement length when the connection force is zero and when high enough. Zero connection force results from the use of very flexible facing and/or zero connection strength. High connection force results from rigid facing together with high connection strength. Fig. 3-14c compares $T_{available}$ when the connection force is high enough with the tensile force required for wall stability, $T_{required}$. As the stability of GRS RW is controlled not only by global stability but also by local stability, the distribution curve of $T_{required}$ along the reinforcement length is the envelop of the two envelops for global stability, $(T_{required})_{global}$, and local stability, $(T_{required})_{local}$. $(T_{required})_{global}$ is the envelope of the tensile forces required to prevent global failure along any potential failure plane (Leshchinsky et al., 2014). When the reinforcement is longer than required for sufficient pull-out strength, as shown in Fig. 3-14c, the maximum of $(T_{required})_{global}$ is activated at the place where the reinforcement crosses the critical failure plane. When the reinforcement is shorter than required for sufficient pull-out strength, $(T_{required})_{global}$ becomes larger than $T_{available}$ for pull-out near the rear end, and the actual tensile force is limited by $T_{available}$ (Leshchinsky et al., 2014).

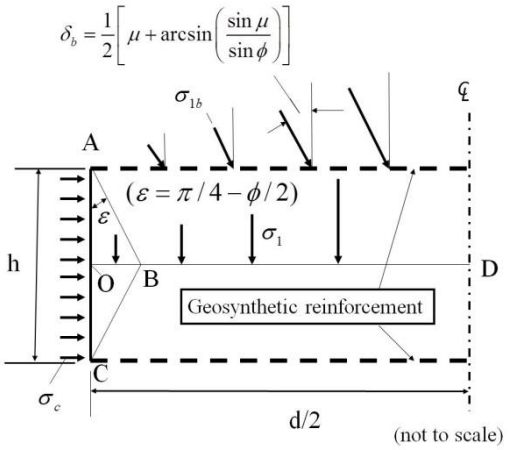

Figure 3-15. An approximate isotropic perfectly plastic solution for compressive strength of a soil layer reinforced with geosynthetic reinforcement (μ: friction angle at the interface between reinforcement and soil) (Tatsuoka, 2004).

The importance of taking into account $(T_{required})_{local}$ in design to prevent local compression collapse of backfill immediately behind the wall face at low levels of the wall is often over-looked. Fig. 3-15 shows an isotropic perfectly plastic solution for the compressive strength of a soil layer between reinforcement layers where the whole region is at failure state. The stress state in zone ABC is free from the bond stress at the interface between the reinforcement and the backfill, so free from the tensile forces in the reinforcement. When c= 0, the minimum lateral confining pressure σ_h required to keep zone ABC stable in a smooth vertical wall under static conditions is the active earth pressure when unreinforced, $\sigma_h = \sigma_v \cdot K_A$, where $K_A = (1-\sin\phi)/(1+\sin\phi)$. The minimum active earth pressure to maintain the local stability under more general conditions (such as the one illustrated in Fig. 5-1) can be evaluated by the two-wedge limit-equilibrium stability analysis. In any case, when $\sigma_h = 0$ at the wall face, the strength of soil with c= 0 becomes zero in zone ABC. The collapse of this zone is followed by progressive failure toward deeper places. With a decrease in the vertical spacing of reinforcement layer, the local stability increases associated with a decrease in the volume of zone ABC.

In Fig. 3-14c, $(T_{required})_{global}$ denotes the reinforcement tensile force required only to maintain global stability of the wall. The value of $(T_{required})_{global}$ is largest at the location where the critical failure plane crosses and becomes smaller at locations more distant from the critical failure plane (Leshchinsky et al., 2014). Then, near the wall face in the active zone, if $(T_{required})_{local}$ is larger than not only $(T_{required})_{global}$ but also $T_{available}$, (as in the case illustrated in Fig. 3-14a), the deformation of the active zone becomes too large due to local failure. That is, if the facing is very flexible (such as wall face loosely wrapped-around

with geogrid reinforcement), or if the connection strength at the back of rigid facing is zero or very low, the earth pressure that can be activated at the wall face becomes substantially lower than the active earth pressure $\sigma_v \cdot K_A$. Then, as illustrated in Fig. 3-14a, at low levels of the wall where the active zone is very narrow, only very small tensile forces can be activated along the reinforcement length, as discussed related to Fig. 3-10. If c= 0, near the wall face, $T_{available}$ becomes much lower than both $(T_{required})_{local}$ and $(T_{required})_{global}$. This situation results in low confining pressure, therefore low stiffness and strength of soil, in the active zone. If something supports the soil at the front from just flowing outwards or small apparent cohesion is available, the active zone can be marginally stable. However, if local failure takes place immediately behind the wall face, for example, by seismic load or by losing apparent cohesion due to heavy/prolonged rain, failure may progressively develop from the front towards inner locations. This is more likely to take place at low levels of the wall. Then, the global failure plane may be pushed inwards making the active zone wider, as observed in full-scale tests (Tatsuoka & Yamauchi, 1986; Tatsuoka et al., 1997a). In this case, the maximum tensile force in the reinforcement at the location crossing the failure plane may increase to maintain the global stability, but it is penalized by intolerable large deformation of the wall.

On the other hand, when the facing is rigid enough and the connection strength is high enough, the maximum value of $T_{available}$ becomes equal to the smaller of: 1) the available tensile rupture strength of reinforcement, T_d: and 2) the maximum of the available pull-out strength in the stationary zone (in the back of the failure plane), T_{2pa}. As the value of $(T_{required})_{local}$ is much lower than this maximum value of $T_{available}$, the local failure in the active zone can be easily prevented by using rigid facing firmly connected to the reinforcement. In this case, relative displacement between the backfill and the reinforcement becomes very small, therefore the shear stress mobilised at the interface becomes very low. If the shear stress is zero, the tensile force in the reinforcement becomes constant in the active zone as illustrated in Fig. 3-14b and as observed in many MSE RW having rigid facing and high connection strength (Tatsuoka, 1992). Then, the lateral earth pressure becomes constant in the active zone and the maximum value of $(T_{required})_{global}$ that develops at the place where the critical failure plane crosses becomes $\sigma_v \cdot K_A \cdot S_v$, where S_v is the vertical spacing of reinforcement layers.

3.7.2 *Effects of Facing Structure on Wall Stability*

If $T_{available}$ is actually like the one shown in Fig. 3-14a due to insufficient facing rigidity and/or insufficient connection strength and if the possibility of local failure is not taken into account in design, this design procedure reduces the redundancy created by the other components. It is likely that many of failure/collapse cases of MSE RWs reported by Koerner et al. (2013) and Valentine (2013) and others as presented in the preceding sections can be attributed to this inadequate or improper design procedure. The following is additional notions in this respect:

1) The actual tensile force, T, in back of the wall face may become higher than $T_{required}$, for example, during and immediately after good compaction. Therefore, high connection strength is essential also for good compaction. With completed MSE RWs, this situation becomes more likely at higher levels of the wall, while, at lower levels of the wall, due to vertical compression taking place by subsequent wall construction, the T value may become close to $(T_{required})_{local}$.
2) Under seismic conditions, near the wall face, both $(T_{required})_{global}$ and $(T_{required})_{local}$ increase due to an increased active earth pressure and the outward inertia of facing activated by acceleration amplified compared to the one at inner places of the wall. Therefore, high connection strength is particularly important to ensure a high seismic stability of the wall.
3) When concentrated loads, vertical and/or lateral in the outward direction, are applied to the crest near the wall face, the failure plane becomes closer to the wall face, while both $(T_{required})_{local}$ and $(T_{required})_{global}$ near the wall face increase. By using rigid facing firmly connected to sufficiently strong reinforcement layers, the value of $T_{available}$ can become higher than both $(T_{required})_{local}$ and $(T_{required})_{global}$ in such a case. By using full-height rigid (FHR) facing with high connection strength, the development of failure planes that potentially cross the wall face at mid-heights can be effectively prevented. This feature can be easily taken into account in design although not creating redundancy in this respect.

3.7.3 *Full-Height Rigid Facing*

Fig. 3-16a illustrates the staged-construction procedure of GRS RW having FHR facing. Prior to the construction of FHR facing (i.e. at stages 3 through 5 in Fig. 3-16a), the gravel bags function as a temporary stable facing resisting high earth pressure developed by good compaction. High earth pressure is subsequently transferred to the FHR facing upon its construction. After sufficient deformation takes place in

the backfill and supporting subsoil, as illustrated in Fig. 3-16c, FHR facing is constructed by casting-in-place concrete on the wall face wrapped-around with geogrid reinforcement. Fig. 3-16b shows a typical geogrid type used for this GRS RW system. As the geogrid is directly in contact with fresh concrete exhibiting strong alkaline properties, a geogrid type that has high resistance against high alkali environment, typically the one made of polyvinyl alcohol (PVA), should be used. As the completed FHR facing is firmly connected to the geogrid layers, high connection forces with high tensile forces in the reinforcement develop, therefore high confining pressure in the active zone can be realized. Then, the active zone becomes stiff and stable, then a limited amount of residual deformation of the active zone after wall completion can be realized. As of May 2014, the walls have been constructed at over 1,000 sites with a total wall length of about 160 km including those for high-speed trains (Figs. 3-16d & e). Since the first construction in 1989, there has been no problematic case during and after construction.

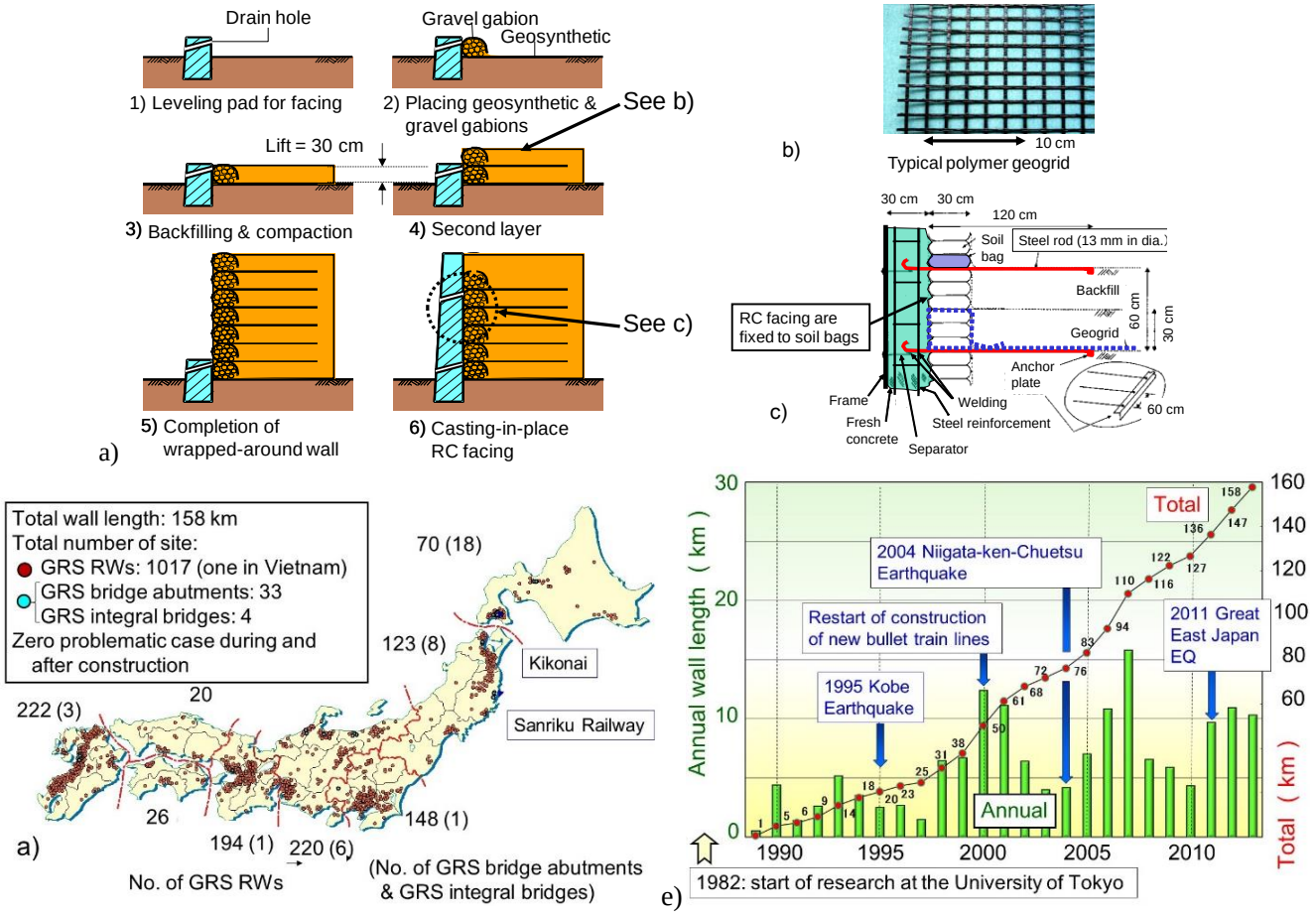

Figure 3-16. GRS RW with FHR facing (Tatsuoka et al., 1997a): a) staged construction procedure; b) a typical geogrid type; c) facing construction details; and d) locations; and e) annual & accumulated wall lengths as of May 2014 (Tatsuoka et al., 2014b; Yonezawa et al., 2014).

In summary, FHR facing can: 1) increase the available tensile strength of reinforcement, which increases the global stability along potential failure planes; 2) prevent the development of global failure plane intersecting the wall face; 3) increase the local stability near the wall face; 4) decrease the deformation (including long-term residual deformation) of wall by increasing the stiffness of the active zone; and 5) prevent the propagation of local failure, if it takes place, towards global failure of wall, unlike such cases of discrete panel facing as shown in Figs. 3-3, 3-4 and 3-5. As discussed below, factors 1), 2) and 3) are taken into account in the current design code of GRS RW having FHR facing. Although factors 4) and 5) are essential with important GRS RWs with a limited amount of allowable deformation, such as those supporting highways and railways, they are not explicitly taken into account in the current design code, thus creating redundancy relative to MSE RWs having flexible facing or discrete panel/modular block facing.

3.8 *Design based on Measured Tensile Reinforcement Forces*

The tensile force in the reinforcement measured in a GRS RW under ordinary static conditions, denoted as L_m, is usually significantly smaller than the factored design strength, T_d (Eq. 3-3a), determined by ordinary static analysis ignoring redundancy components, denoted as $[T_d]_A$ (i.e. the case illustrated in Fig. 3-2). This situation is illustrated in Figs. 3-11 and 3-12. This difference, denoted as ΔL, is created by actual apparent cohesion, actual high value of ϕ, actual toe resistance etc. That is, "additional design load created by ignoring these redundancy components that is included in $[T_d]_A$" vanish in L_m. Therefore, if the value of T_d is set to equal to the average of the values of L_m obtained from measurements in many similar GRS RWs, denoted as $[L_m]_{ave}$, the actual static safety factor, $(F_s)_{a.0}$, for the same calculated static safety factor, $(F_s)_{c.0}$, decreases significantly from the value determined by ordinary static analysis ignoring redundancy components (i.e. in the case of Fig. 3-2) as illustrated in Fig. 3-18. That is, the unfactored design strength, $(T_d)_0=T_d\cdot(F_s)_{c.0}$, decreases from $(T_d)_A\cdot(F_s)_{c.0}$ to $[L_m]_{ave}\cdot(F_s)_{c.0}=([T_d]_A-\Delta L)\cdot(F_s)_{c.0}$. Then, for the same value of L_m, the actual static safety factor, $(F_s)_{a.0}$, decreases from the value in the case of Fig. 3-2:

$$[(F_s)_{a.0}]_A = \frac{[T_d]_A \cdot (F_s)_{c.0} + \Delta T_d}{L_m} \qquad (3\text{-}4)$$

to the value in the case of Fig. 3-18:

$$[(F_s)_{a.0}]_B = \frac{\{[T_d]_A - \Delta L\} \cdot (F_s)_{c.0} + \Delta T_d}{L_m} \qquad (3\text{-}5)$$

where ΔT_d is the redundancy included in the actual unfactored strength, $(T_d)_0$.

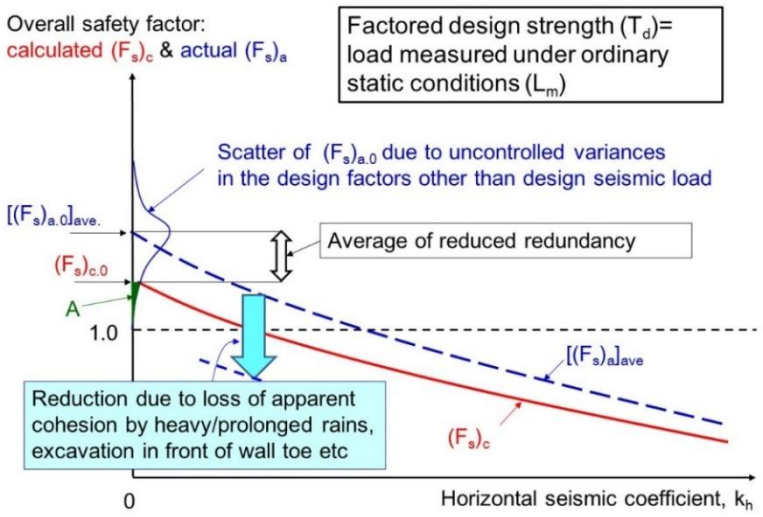

Figure 3-18. Largely reduced redundancy under ordinary static condition in $T_d=L_m$ design procedure.

Eqs. 3-4 and 3-5 imply the followings:

1) For the same values of L_m and ΔT_d, due to ΔL, the actual safety factor in this case (Fig. 3-18), $[(F_s)_{a.0}]_B$, could be substantially lower than the value obtained by ignoring the redundancy components (Fig. 3-2), $[(F_s)_{a.0}]_A$.
2) $(F_s)_{a.0}$ of a given GRS RW decreases by an increase in the actual load, L_m, which may take place in an uncontrolled and random way and differently among different GRS RWs. L_m may increase significantly by inadequate or improper design and construction: i.e. by poor drainage, poor compaction of lower-quality backfill, poor connection between reinforcement and facing, inappropriate reinforcement arrangements etc.
3) L_m also increases due to loss of apparent cohesion by heavy/prolong rains, loss in the toe resistance by scouring/excavation in front of the wall, unusual loading etc. during the lifespan.
4) The calculated static safety factor, $(F_s)_{c.0}$ in Eqs. 3-4 and 3-5 does not include seismic effects. Therefore, this value is smaller than the value when seismic design is carried out while ignoring redundancy

components (i.e. the case illustrated in Fig. 3-1).

In this case (i.e. Eq. 3-5 and Fig. 3-18), by these four factors, the value of $(F_s)_{a.0}$ may have become lower than $(F_s)_{c.0}$ (as indicated by area A) and may have become close to unity in spite of the inclusion of ΔT_d. As far as the wall is standing under ordinary static conditions, $(F_s)_{a.0}$ is kept larger than unity. However, the chance of failure/collapse by seismic loading that should be encountered during the lifespan has increased substantially. Failure/collapse may take place even by relatively small seismic loads. Furthermore, the residual deformation may increase largely corresponding to a large decrease in $(F_s)_{a.0}$, which largely increases the long-term maintenance cost. In Fig. 3-18, the relationship between the calculated safety factor, $(F_s)_{c.s}$, and k_h is schematically depicted by a solid curve considering that $(F_s)_{c.s}$ should decrease with an increase in k_h. However, it is not possible to obtain this relation by analytical stability analysis, because this method is empirical.

In summary, the design method setting the factored design strength, T_d, equal to the measured load, L_m, counts on the redundancy components that are ignored in ordinary design. As these redundancy components are uncontrolled and random while they may disappear, this design method is not reliable. Also by not including seismic effects, this design method is much more un-conservative than when seismic design is carried out based on stability analysis ignoring redundancy, as described in Fig. 3-1.

4 MANIFESTATION OF REDUNDANCY IN DESIGN

4.1 *Background*

A great number of failure/collapse cases of soil structures during earthquakes in the past, in particular those during the last 20 years in Japan, has indicated that, with soil structures, we should move from the no-seismic-design policy to relevant seismic design, or increase the design seismic load to more realistic higher values. In so doing, it is also necessary to evaluate the seismic stability more realistically by taking into account, at least partly, significant contributions of redundancy that were ignored previously, typically those created by good compaction and dynamic ductility. Fig. 4-1 illustrates this issue. Suppose that soil structure A (well drained & well compacted) survived seismic loads much severer than having been considered in the conventional seismic design. Soil structure B performed marginally, soil structure C collapsed and soil structure D (poorly drained & poorly compacted) collapsed very seriously. When following the conventional design procedure ignoring the contributions of redundancy, their calculated safety factors, $(F_s)_c$, may not be largely different while all being larger than a certain specified minimum value (e.g. 1.2 or 1.5). As redundancy is actually very different among different soil structures, the actual safety factors, $(F_s)_a$, should be largely different from each other. Over-estimation of soil strength with structure D in the conventional design is typically due to ignoring of a drastic decrease in the undrained shear strength by cyclic undrained loading with poorly drained saturated poorly compacted backfill. This strength over-estimation reduces redundancy significantly. With soil structure A, if the design seismic load is increased to a realistic high level while still ignoring the contributions of redundancy, the calculated safety factor, $(F_s)_{c.s}$, may become too low being lower than unity. This result is not consistent with the actual behaviour.

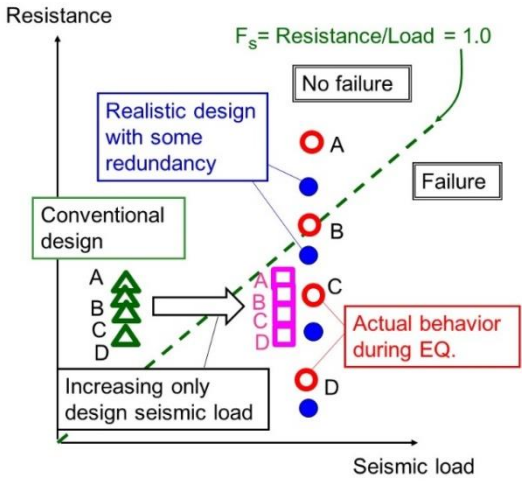

Figure 4-1. Seismic design issue of soil structures.

4.2 *Increasing Actual Stability by Manifesting Redundancy*

4.2.1 *General*

To encourage and promote the construction of soil structures that are sufficiently stable against realistic high seismic loads while exhibiting small residual deformation by good structure, good design and good construction (i.e. soil structure A in Fig. 4-1), the following three steps are necessary:

1) A relevant design seismic load is introduced if seismic design has not been performed or the design seismic load is increased to a more realistic level higher than in the conventional seismic design. This procedure increases the design load.
2) An increase in the stability realized by good structure, good design and good construction is properly manifested (i.e. specified explicitly) in design. One example is the use of realistic values of ϕ_{peak}, larger than a default value, with actually well-compacted backfill. Another is no use of a creep reduction factor to obtain design rupture strength of geosynthetic reinforcement in seismic design. Although this procedure decreases the implicit safety margin (i.e. redundancy), results of stability analysis becomes more realistic. Yet, it is still necessary to maintain some redundancy to keep as small as possible the risk of failure/collapse by unusual extreme events that may take place in the future but cannot be foreseen at the stage of design.
3) It is shown that the increase in the construction cost when following this procedure is smaller and more valuable than the cost by failure/collapse that may take place during the lifespan plus an increase in the maintenance cost when not following this procedure. If feasible, it is also shown that, for example, the LCC of a GRS RW properly designed against adequate seismic loads can become lower than the one for a conventional type RW that is not seismic-designed, as demonstrated by Tatsuoka et al. (2014b).

4.2.2 *Three Methods to Increase Stability*

GRS structures become actually more stable due to the benefits obtained by a combination of good structure, good design and good construction. By properly taking advantage of these benefits, realistic seismic design taking into account realistic high seismic loads becomes feasible.

Good structure: The factors for good structure include the following:

1) High structural strength: i.e. large load is necessary to trigger failure, as expressed by the global safety factor evaluated by the limit equilibrium analysis.
2) High structural ductility: i.e. large additional energy is necessary to reach collapse after the start of failure, as expressed by residual deformation evaluated by the Newmark method.
3) High structural integrity: i.e. restraining of local failure from its occurrence and propagation to the collapse of whole structure; and keeping the natural frequency much higher than predominant frequencies of design input motion.

These factors can be realized with GRS RWs with facing having sufficient rigidity, sufficient connection strength and relevant arrangement of reinforcement layers, such as the one described in Fig. 3-16.

Good design: The factors of good design include the following:

1) Rational design based on statics and dynamics that can be applied to broad conditions in a consistent manner, usually limit equilibrium stability analysis in practical design.
2) Relevant seismic design in seismic zones: The use of ϕ_{peak} in addition to $\phi_{residual}$ (as explained later) with actually well-compacted backfill can give reward for good compaction. Although this method reduces redundancy, soil structures actually become more stable while reducing the life cycle cost (LCC). Besides, part of the benefit by better compaction should be preserved as redundancy by determining conservatively the design value of ϕ_{peak}. No use of creep reduction factor to obtain the design rupture strength of geosynthetic reinforcement in seismic design is rational. This procedure reduces the redundancy in a consistent manner.
3) Due evaluation of the three important structural factors listed above in design.

Good construction: The factors of good construction include the following:

1) Use of as good as possible backfill (e.g. well-graded gravelly soil).
2) Good compaction, encouraged by the use of ϕ_{peak} in design.
3) Good drainage, which warrants such a design assumption that no positive pore water pressure develops even during heavy/prolonged rains in walls constructed in a water collecting place. Good

compaction with good drainage results in large apparent cohesion, which increases redundancy in the design ignoring apparent cohesion.

That is, "good performance design" is not sufficient, but "good performance construction" linked to "good performance design", such as the new field compaction control method (Fig. 3-7b), is also necessary to realize soil structures that can perform properly during the lifespan.

5 SEISMIC DESING OF JAPANESE RAILWAY SOIL STRUCTURES

5.1 *Background*

The seismic design of Japanese railway soil structures, including GRS RWs having staged-constructed FHR facing (Fig. 3-16) was revised substantially based on lessons learned from the performance of soil structures during the 1995 Great Kobe Earthquake. The design code was further revised referring to new lessons from the subsequent earthquakes. The latest version of Design Standard for Railway Soil-Retaining Structures (Railway Technical Research Institute, 2013) has the following several characteristic features that integrate the key points for design discussed in Chapters 3 and 4 (Koseki et al., 2006, 2007, 2008, 2009; Koseki, 2012; Tatsuoka et al., 2010).

5.2 *Three Required Performance Ranks and Two Design Seismic Load Levels*

According to the importance level of concerned railway soil structure, the following three ranks of required seismic performance are introduced in the same way as the other railway structures (Table 5-1):
- soil structures supporting RC slabs for ballast-less tracks of high speed trains are required rank I;
- soil structures supporting ballasted tracks for important railways are required rank II; and
- other non-critical soil structures are required rank III.

Table 5-1. Three performance ranks for two design seismic load levels

Design seismic loads / Required performance	Level 1[1]: Conventional design EQ load	Level 2[2]: Severe seismic loads as experienced during the 1995 Kobe EQ
Very important soil structures: e.g. high speed trains (rank I)	Limited deformation: expected functions can be maintained without repair works	Allowed to exhibit deformation as far as their functions can be restored by quick repair works
Important soil structures: e.g. urban trains (rank II)		Should not exhibit devastating deformation. The functions can be restored by repair works.
Other non-critical soil structures (rank III)	Should not collapse	Not specified

1) anticipated to take place at a given site several times during the design lifespan.
2) the largest seismic load anticipated at a given site during the design life time.

Level 1 design seismic load is used in the pseudo-static seismic stability analysis and represented by a horizontal seismic coefficient at the ground surface, $(k_h)_d$, equal to 0.2. This value is the same as the value that had been used before the revision of the code (i.e. before the 1995 Great Kobe Earthquake). Level 2 design seismic load was newly introduced, which is equivalent to severe seismic loads experienced during the 1995 Great Kobe Earthquake. This is assigned in terms of standard time histories of horizontal ground acceleration to be used to evaluate the residual deformation of soil structure by the modified Newmark sliding block analysis (explained below). Depending on the natural period, T_g, of the ground at a given site, different wave forms and amplitudes are assigned (Table 5-2). The peak accelerations, α_{max}, are generally very high, in a range from 500 to 920 gal (cm/sec^2), and the largest value is assigned for the G2 ground primarily consisting of Pleistocene deposits. It is assumed that the acceleration is not amplified in each soil structure. Although this assumption itself is on the unsafe side (thus reducing the redundancy in design), it is considered that this factor is covered by conservatisms in other several factors.

Table 5-2. Maximum acceleration of Level 2 design earthquake motions: the unit is gal (cm/sec^2): see Koseki et al. (2007) for the wave forms.

G0	G1	G2	G3	G4	G5	G6	G7
578	732	924	779	718	741	694	501

G0 – G7: ground classifications listed below, determined based on the natural period T_g (the unit is seconds).

G0-G2	G3	G4	G5	G6	G7
Less than 0.25	0.25-0.5	0.5-0.75	0.75-1.0	1.0-1.5	More than 1.5

G0: rock deposit; G1: firm base deposit; G2: Pleistocene deposit; G3: moderate; G4: moderate to soft; G5 & G6: soft; G7: very soft.

5.3 *No Use of Apparent Cohesion in Static and Seismic Design*

Good drainage is one of the construction keys for high performance of soil structures. With GRS RWs having FHR facing (Fig. 3-16), gravel bags, or their equivalent, wrapped-around with geogrid reinforcement are placed at the shoulder of each soil layer to help backfill compaction and to function as a vertical drain immediately behind the FHR facing during service. The water percolating into the gravel bags from the backfill is drained to the outside of the wall through small drain holes arranged for every 2 to 4 m^2 in the FHR facing. With good drainage, positive pore water pressure may not develop even during heavy/prolonged rain. Yet, with all soil types, the apparent cohesion due to matric suction is ignored (i.e. c= 0) in both static and seismic design by considering that the apparent cohesion may disappear in an uncontrolled manner with an increase in the degree of saturation, S_r, typically by heavy/prolonged rain, therefore, it is not reliable. By the same concept, the saturated unit weight of soil is used in both static and seismic design.

Table 5-3. Standard design values of density and shear strength (c= 0) for wall design (RTRI, 2013b).

Standard design values / Soil type	Soil unit weight (kN/m^3)	ϕ for seismic design against level 1 load	ϕ for seismic design against level 2 load	
			ϕ_{peak}*)	$\phi_{residual}$
Type 1: well-graded sand & gravelly soil	20	40°	55°	40°
Type 2: other ordinary types of sand & gravelly sand	20	35°	50°	35°
Type 3: poorly-graded sand	18	30°	45°	30°
Type 4: cohesive soil	18	30°	40°	30°

Type 1: SW & GW; Type 2: GP, G-M, G-C, G-V, S-M and GM & GC with fines content less than 30 %; and Type 3: other soil types with fines content less than 30 %; and Type 4: fines content more than 30 %.

*) These values can be used only when good compaction is ensured. Otherwise, $\phi_{residual}$ should be used.

5.4 *Consideration of Effects of Good Compaction on Soil Strength*

Good compaction of the backfill is also essential to ensure high stability of soil structures against heavy/prolonged rains, floods and severe earthquakes. With GRS RWs having FHR facing (Fig. 3-16), to facilitate good compaction of the backfill, the vertical spacing between geosynthetic layers is specified to be 30 cm, while the standard compacted lift of soil layer is 15 cm. It is allowed to use the ϕ_{peak} values listed in Table 5-3 in seismic design against Level 2 seismic load only when good compaction is ensured in such that: 1) all measured D_c values (Standard Proctor) $\geq$ 92 %; and the average $\geq$ 95 %; and 2) all measured values of the coefficient of vertical sub-grade reaction obtained by plate loading tests using a 30 cm-diameter plate (K_{30}) $\geq$ 70 MN/m^2; and the average $\geq$ 110 MN/m^2. The standard design values of ϕ listed in Table 5-3, as values under plane strain conditions, were determined conservatively based on results of a comprehensive series of drained triaxial compression tests on many fill samples representative of the railway soil structures in Japan. In so doing, it was considered that differences in the ϕ value between the plane strain and triaxial compression tests are balanced with effects of strength anisotropy and progressive failure (Tatsuoka, 2001).

5.5 *Seismic Design Based on Limit-Equilibrium Stability Analysis*

Static and seismic design is performed based on the limit equilibrium stability analysis. As argued in Section 3.8, the tensile geosynthetic forces in full-scale GRS RWs measured under ordinary static conditions are usually substantially lower than respective design values obtained by ignoring several redundancy components. Therefore, they are not referred to in design. The seismic stability against Level 1 load is evaluated based on the global safety factor obtained by pseudo-static limit equilibrium stability analysis. The performance against Level 2 seismic load is evaluated based on residual deformation evaluated by the modified Newmark sliding block theory based on pseudo-static limit equilibrium stability analysis by the modified two-wedge (T-W) method using both ϕ_{peak} and $\phi_{residual}$ (Tatsuoka et al., 1998). This modified T-W method is a direct extension of a modified version using both ϕ_{peak} and $\phi_{residual}$ of the Mononobe-Okabe seismic earth pressure theory (the M-O theory), as explained below.

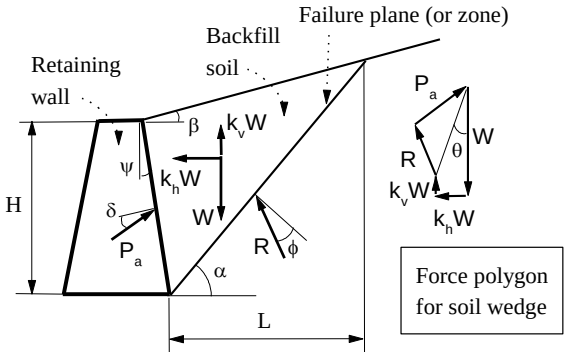

Figure 5-1. RW with unreinforced backfill with a single linear failure plane under general seismic loading conditions (Koseki et al., 1997).

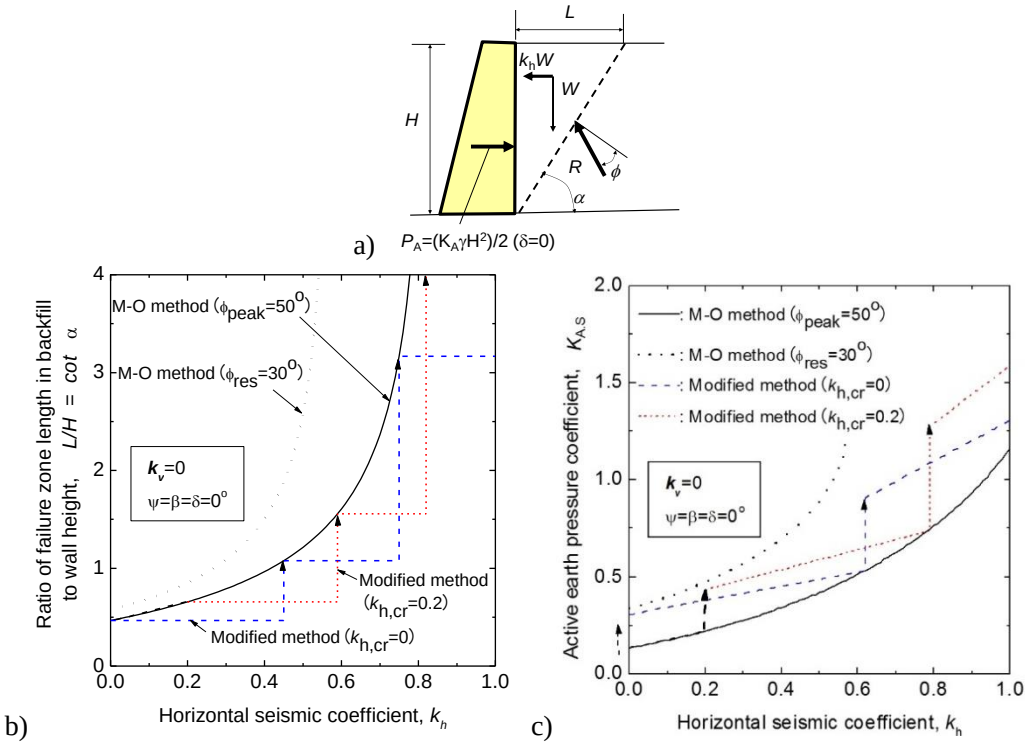

Figure 5-2. a) Simplest RW structure; and comparisons between the original and modified *Mononobe-Okabe* theories: b) the size of failure zone; and c) active earth pressure coefficient (Koseki et al., 1997).

The original M-O theory evaluates the seismic earth pressure in unreinforced backfill in the framework of Coulomb's active earth pressure theory using a single linear failure plane (Fig. 5-1). For reinforced soil RWs, two-wedge failure mechanism (explained below) is a relevant practical approximation. For homogeneous unreinforced and reinforced backfill under general boundary conditions, a log-spiral failure plane is a more relevant and consistent assumption (Leshchinsky, et al. 2014).

The simplest case (vertical smooth wall with zero back slope; Fig. 5-2a) is analyzed below. The original M-O theory assumes that always the same peak friction angle ϕ can be mobilized along any failure

plane (i.e. the isotropic perfectly plastic assumption). Therefore, the failure plane becomes deeper and shallower with an every increase and decrease in the input seismic load. If the input seismic load continuously increases, the angle α in Fig. 5-2a continuously decreases. Figs. 5-2b and 2c show the α versus k_h relations and the active earth pressure coefficient $K_{A.S}$ versus k_h relations obtained by Eqs. 3-1a & b (i.e. the original M-O theory) when ϕ is equal to either 30° or 50°. In actuality with well-compacted soil, once the peak stress state is reached then passed, the ϕ value drops from ϕ_{peak} toward $\phi_{residual}$ only inside a shear band (i.e. a failure plane), while the peak strength in terms of ϕ remains equal to ϕ_{peak} in the unfailing regions.

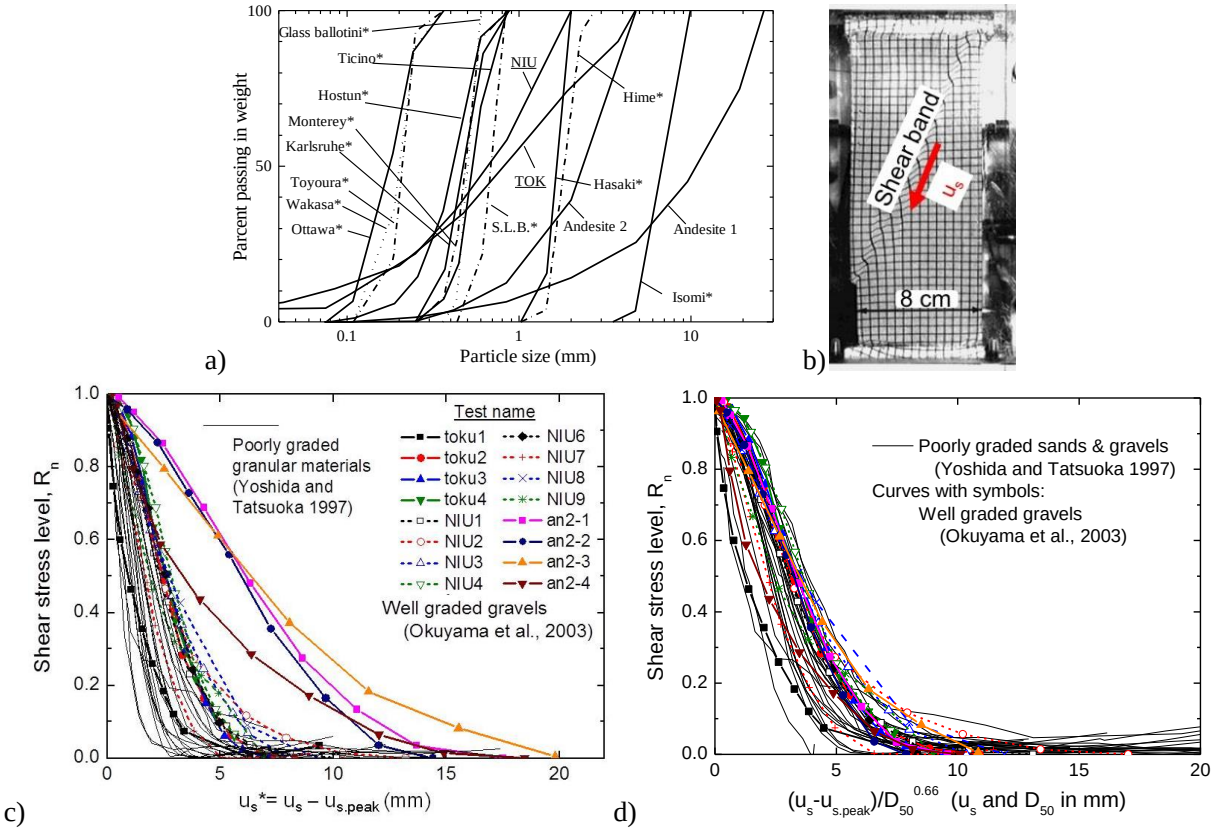

Figure 5-3. a) Grading curves of the granular materials used in drained plane strain compression tests (poorly graded granular materials* were tested by Yoshida et al., 1995; Yoshida & Tatsuoka, 1997); b) drained PSC test on dense Toyoura sand (D_{50}= 0.206 mm) , σ'$_3$= 78 kPa; axial strain= 11.8 %; c) relationships between the shear stress level R_n vs. u_s ($u_{s.peak}$: u_s at peak stress state); and d) R_n vs. normalized u_s relations (Okuyama et al., 2003; Tatsuoka, 2001; Tatsuoka et al., 1998).

Fig. 5-3c shows the relationships between the shear stress level, R_n= (R- $R_{esidual}$)/(R_{peak} – $R_{residual}$), where R= σ_1/σ_3, and the shear displacement along a shear band seen on the σ_2 plane, u_s, measured by the photogrammetric method (Fig. 5-3b) in drained plane strain compression tests on a number of granular materials (Fig. 5-3a). R_n= 1 and 0 denote the peak and residual stress states. Fig. 5-3d shows the relationships between R_n and u_s divided by $D_{50}^{0.66}$, where D_{50} is the mean diameter (mm) and a power 0.66 is the value by which the scatter in the relations becomes a minimum. The shear displacement by which the strength fully drops increases with an increase in D_{50}.

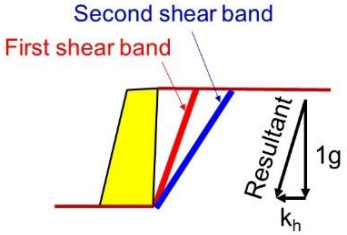

Figure 5-4. Illustration of discontinuous development of shear band in the unreinforced backfill of RW

When the input seismic load becomes higher than the level at which the development of first failure

plane has started, due to the post-peak strain-softening properties, this first failure plane develops further until the input seismic load becomes high enough to develop the second failure plane (Fig. 5-4). Therefore, during a given time history of seismic load, either no failure plane develops, or only a single failure plane develops, or a limited number of failure planes develop stepwise, in the backfill. Taking into account this process, Koseki et al. (1997) proposed the following modified M-O theory. It is assumed that the first shear band starts developing once mobilized ϕ reaches ϕ_{peak} at a certain k_h value, followed by a drop of mobilized ϕ to $\phi_{residual}$ in the shear band. It is conservatively assumed that this drop is sudden. This assumption was adopted in the design code for Japanese railway soil structures (RTRI, 2013). The limit equilibrium stability analysis is performed using ϕ_{peak} outside the shear band and $\phi_{residual}$ in the shear band. This failure plane remains the critical one despite an increase in k_h until a new critical failure plane develops in the zone outside the first critical plane. The value of $K_{A.S}$ is obtained as:

$$K_{A.S} = \frac{\sin(\alpha_{cr} + \psi - \phi_{res})}{\cos(\alpha_{cr} - \phi_{res})} \cdot \frac{\cot \alpha_{cr}}{\cos^2 \psi} \qquad (5\text{-}1)$$

where α_{cr}= arctan(L/H) is the angle of the current critical failure plane to the vertical; and $k_h = \tan\psi$ is the horizontal seismic coefficient.

Figs. 5-2c & d compare the sizes of failure zone (i.e. the angle α) and the values of $K_{A.S}$ plotted against k_h obtained by the original M-O theory (Eq. 3-1) for ϕ= 30° or 50° and the modified M-O theory (Eq. 5-1) for $\phi_{residual}$= 30° and ϕ_{peak}= 50° assuming that the first failure plane develops when k_h becomes either 0.0 or 0.2. The following trends may be seen.

1) The $K_{A.S}$ value by the original M-O theory for $\phi_{residual}$= 30° (i.e. the conventional default design ϕ value for poorly graded sand, Table 5-3) becomes extremely high when k_h becomes higher than about 0.5. In this case, the seismic design of RWs for Level 2 seismic load becomes practically infeasible. On the other hand, with a continuous increase in k_h, the $K_{A.S}$ value by the modified M-O theory increases either linearly or stepwise at several k_h values, not becoming extremely high being always smaller than the value by the original theory using $\phi_{residual}$. The difference increases as k_h increases.
2) With a continuous increase in k_h, the failure zone by the modified theory becomes larger only stepwise being consistently smaller than the one by the original theory using ϕ_{peak}. This small size failure plane was observed in model shaking table tests (Koseki et al., 2007, 2009; Watanabe et al., 2003, 2011) and in the field (typically Fig. 2-1a).

Figs. 5-5c and d show results from seismic active earth pressure analysis for a GRS RW having FHR facing with typical arrangements of geogrid (Fig. 5-5a) evaluated by the conventional and modified T-W methods (Fig. 5-5b). The response amplification inside the wall is ignored. Fig. 5-5d shows the $K_{A.S}$ values of the seismic active earth pressure acting in the wall for the failure mechanism exhibiting a minimum safety factor for either over-turning or sliding obtained by the modified T-W method using ϕ_{peak}= 45° and $\phi_{residual}$= 30°. It is assumed that the first T-W failure mechanism develops when k_h becomes 0.2 and the ϕ value inside the first failure planes suddenly drop from ϕ_{peak} to $\phi_{residual}$ and, as k_h increases, this first failure mechanism continues developing until the second one starts developing. These results are compared with those obtained by the conventional T-W method using ϕ= either 30° or 45° (Fig. 5-5b). The modified T-W method yields reasonable earth pressure, which is always between those obtained by the conventional T-W method using either ϕ_{peak} or $\phi_{residual}$.

Fig. 5-5a compares the failure planes in the reinforced backfill for which the global safety factor becomes the minimum against k_h=0.5 evaluated by different methods. The failure planes in the reinforced backfill evaluated by the conventional T-W method using either ϕ_{peak} or $\phi_{residual}$ are similar to those for the unreinforced backfill evaluated by the original M-O theory using either ϕ_{peak} or $\phi_{residual}$. On the other hand, the failure planes in the reinforced backfill evaluated by the modified T-W method using both ϕ_{peak} and $\phi_{residual}$ are noticeably smaller. Fig. 5-5c compares the size of the failure zone, where L* is the total width of two wedges on the backfill crest. The failure zone evaluated by the modified T-W method is considerably smaller, but more realistic, than those obtained by the conventional T-W method using ϕ_{peak}. This analysis shows that, when designed by the conventional T-W method using a conventional default soil friction angle (such as $\phi_{residual}$), relatively short reinforcement layers are judged to be ineffective in increasing the wall stability. On the other hand, when designed by the modified T-W method, relatively short reinforcement layers are judged to contribute significantly to the increase in the wall stability.

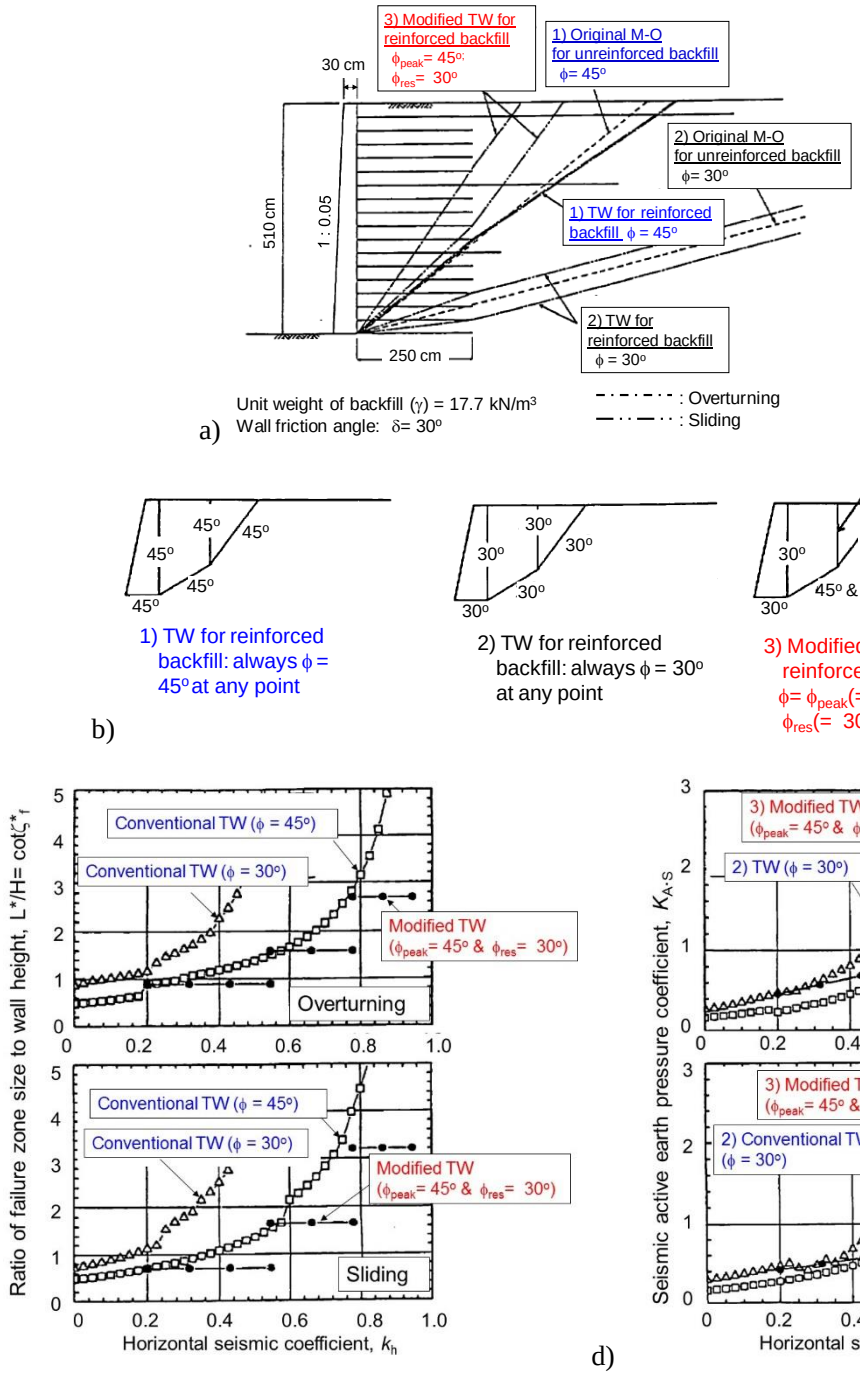

Figure 5-5. Comparison of seismic-stability analysis of reinforced soil RW between the conventional method and the modified T-W method assuming that first active failure develops when k_h= 0.2; unfactored design tensile rupture strength of reinforcement $(T_d)_0$= 30 kN/m: a) wall structures with failure planes; b) ϕ values used in the analysis (dimensions are not to scale); c) the ratio of failure zone size at the crest to the wall height; and d) active earth pressure coefficient (Tatsuoka et al., 1998).

For a typical GRS RW wall structure (Fig. 5-6a), Fig. 5-6b compares the safety factors for sliding and overturning obtained by the modified T-W method using ϕ_{peak} and $\phi_{residual}$ of type 2 soil (Table 5-3) assuming that the first failure planes develop when k_h= 0.28 with those by the conventional T-W method using either ϕ_{peak} or $\phi_{residual}$. The failure planes obtained by the modified T-W method are depicted in Fig. 5-6a. The safety factor by the modified T-W method is always in between the values by the conventional T-W method using either ϕ_{peak} or $\phi_{residual}$.

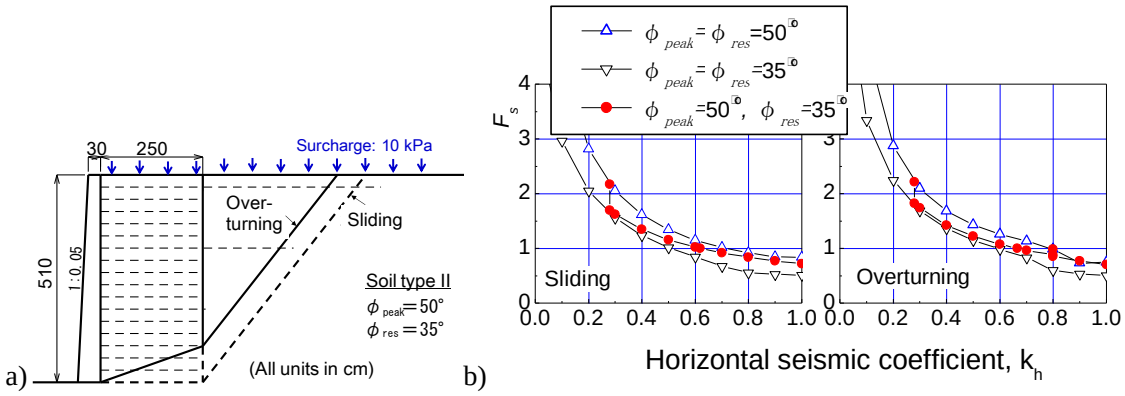

Figure 5-6. a) GRS RW with FHR facing and critical failure planes by modified T-W method; and b) results of stability analysis: unfactored design tensile rupture strength of reinforcement $(T_d)_0$= 30 kN/m; and the friction angle at the reinforcement/backfill interface (ϕ_B) and the back and bottom of facing (δ_w)= $\phi_{residual}$ of the backfill (Horii et al., 1998).

5.6 *No Creep Reduction Factor for Design Rupture Strength of Geogrid*

The unfactored design rupture strength of geosynthetic reinforcement under long-term static loading conditions, $[(T_d)_0]_{static}$, is obtained by following Eq. 3-3b. The creep reduction factor, RF_{CR}, is determined in such that the long-term rupture strength (before applying the overall safety factor, $(F_s)_{static}$) is equal to the maximum load below which the creep failure does not take place until the end of 50 years. It is postulated that the above condition is satisfied if the strain rate after 500 hours becomes smaller than 3.5 x 10^{-5}/h in all three sustained loading tests of a given geosynthetic reinforcement type. On the other hand, the unfactored design rupture strength used in seismic design, $[(T_d)_0]_{seismic}$, is obtained using RF_{CR}= 1.0 for the three reasons explained in Section 3.5.

The unfactored design strength, $[(T_d)_0]_{seismic}$, is used to calculate the stability of a given GRS RW in terms of the yield value of k_h, $(k_h)_y$, at which the calculated global safety factor evaluated by limit equilibrium stability analysis becomes unity. Seismic residual displacement/deformation is computed for seismic load pulses having k_h larger than $(k_h)_y$ by the Newmark method. Therefore, in design against Level 1 seismic load, the minimum required value of $(k_h)_y$ is 0.3, which is $(k_h)_0$= 0.2 (the design value) times $(F_s)_{overall}$ = 1.5, which is equal to a structural safety factor (= 1.25) times a material safety factor (= 1.25). As $(T_d)_0$ has not been reduced by a material safety factor, the residual displacement/deformation by Level 2 design seismic load obtained by this procedure does not include the redundancy created if using $[(T_d)_0]_{seismic}$ divided by a material safety factor to obtain $(k_h)_y$. It is considered that it is not necessary to create this redundancy in the seismic design using a very high design seismic load, Level 2.

5.7 *Residual Deformation by Level 2 Seismic Load*

The allowable residual deformation of a given soil structure is specified by the owner based on the criteria shown in Table 5-1. For example, for performance ranks II and III, the ballasted track may allow a maximum residual settlement of 20 cm and 50 cm (RTRI, 2013d). The allowable lateral displacements at the wall top are of the similar order. Residual deformation of GRS RW when subjected to Level 2 design seismic load is evaluated by three failure modes: 1) sliding; 2) overturning; and 3) shear deformation of the reinforced backfill are evaluated. The displacements by the first two modes are evaluated by the modified Newmark method based on the modified T-W stability analysis.

Referring to Fig. 5-7b, a T-W failure mechanism consisting of a set of failure planes for either sliding or over-turning failure mode when k_h= "$(k_h)_y$ for shear deformation" is sought by using ϕ_{peak}. In the current practice, "$(k_h)_y$ for shear deformation" is assumed to be equal to L/(2H), where H is the wall height, and L is the average geogrid length. "$(k_h)_y$ for shear deformation" is usually lower than those for sliding and over-turning failure modes. It is assumed that, in each of sliding and overturning modes, the T-W mechanism that has developed when k_h= "$(k_h)_y$ for shear deformation" continues developing as k_h further increases. Then, the values of $(k_h)_y$ for sliding and overturning modes are sought using ϕ_{peak} outside the failure planes and $\phi_{residual}$ inside the failure planes. In each failure mode, residual displacement takes place once k_h exceeds the respective $(k_h)_y$ values. The time history of residual sliding displacement, δ, in each mode is obtained by the double integration of $\ddot{\delta}$ obtained from Eq. 5-2 with respect to time starting

when the safety factor F_R/F_D becomes unity (i.e. when k_h becomes $(k_h)_y$) and ending when the velocity $\dot{\delta}$ becomes zero:

$$M \cdot \ddot{\delta} = F_D - F_R \qquad (5\text{-}2)$$

where M is the mass of sliding region (i.e. the facing and region OPRS in Fig. 5-7a that are assumed to be a monolith); F_D and F_R are the horizontal components of sliding force and resistance of this monolith.

Referring to Fig. 5-7c, the residual rotational angular displacement of the wall, θ, is obtained in the similar way as above by the double integrating of $\ddot{\theta}$ obtained from Eq. 5-3 with respect to time starting when the safety factor M_R/M_D becomes unity and ending when the velocity $\dot{\theta}$ becomes zero:

$$J\ddot{\theta} = M_D - M_R \qquad (5\text{-}3)$$

where M_D and M_R are the overturning moment and the resisting moment, both defined about the center of the bottom of the FHR facing.

Referring to Fig. 5-7d, the residual shear displacement at the wall crest, u_{top}, is obtained as $\gamma \cdot H$, where γ is the residual shear strain of the reinforced backfill zone, which develops only when k_h exceeds a given yield value $(k_h)_y$ for shear deformation. An equation to evaluate γ is obtained by assuming that the external work done by seismic load is equal to the internal work done by the shear deformation of the reinforced backfill zone having a length equal to L.

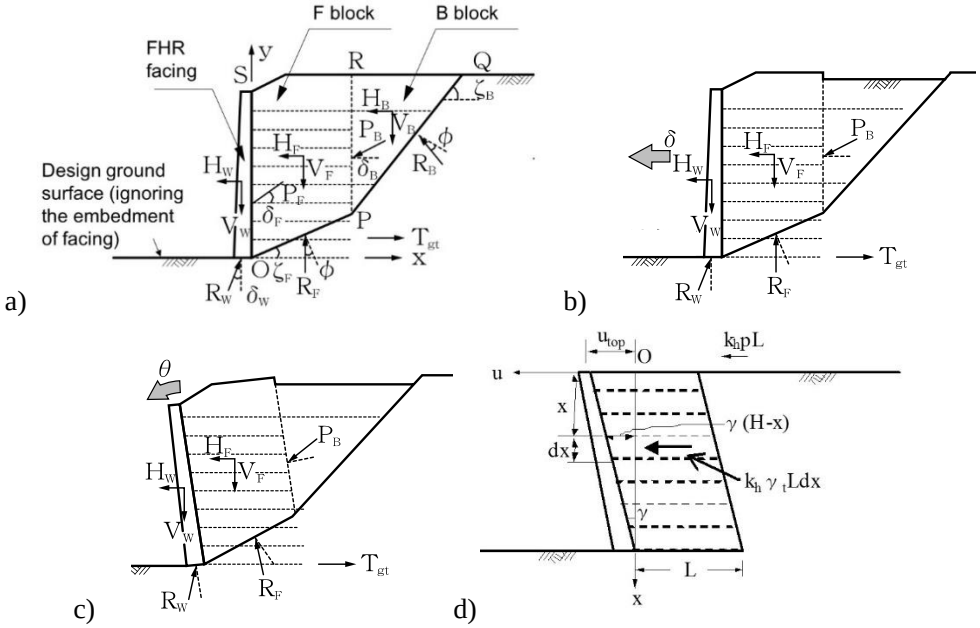

Figure 5-7. Evaluation of residual deformation of a typical GRS RW having staged constructed FHR facing: a) force components considered in the modified T-W method; b) sliding along failure planes; c) overturning about the center of the bottom of FHR facing; and d) shear deformation of reinforced backfill zone.

The residual horizontal displacements at the crest of wall due to sliding and overturning decrease by arranging a couple of long geosynthetic reinforcement layers at high levels, as shown in Fig. 5-7a. In the current practice, the tail ends of these long geogrid layers are located at a line extending from the heel of the facing at an angle equal to $\phi_{residual}$ relative to the horizontal. Therefore, these long geogrid layers become longer with a decrease in $\phi_{residual}$, which results in an increase in "$(k_h)_y$ for shear deformation".

Fig. 5-8a shows the yield k_h values, $(k_h)_y$ (i.e. k_h when the safety factor becomes unity) for a GRS RW structure shown in Fig. 5-6a having well-compacted backfill of the four different soil types listed in Table 5-3. Fig. 5-8b shows the residual lateral displacement at wall top obtained by using a typical time history of horizontal acceleration recorded on the ground surface recorded during the 1995 Great Kobe Earthquake. The residual wall deformation decreases with an increase in the quality of backfill. This result encourages not only better backfill compaction but also the use of higher quality backfill in an effort to construct GRS RWs having a high seismic stability.

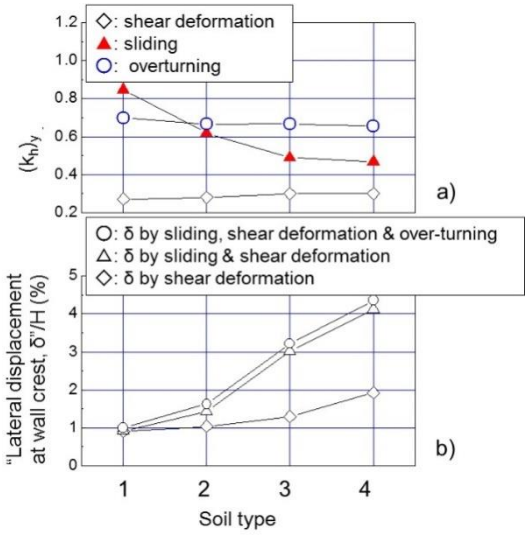

Figure 5-8. a) Critical seismic coefficient, $(k_h)_y$; and b) residual horizontal displacements at the crest of the wall, δ, for different soil types (Horii et al, 1998).

5.8 *Recommendation of GRS Structures*

As a whole, it is highly recommended to employ GRS structures when and where relevant and feasible: i.e. 1) embankments with backfill reinforced with geosynthetic in place of conventional type embankments; 2) GRS RWs with FHR facing in place of conventional cantilever RWs; 3) bridge abutments of GRS RWs with FHR facing in place of conventional bridge abutments with unreinforced backfill; and 4) GRS integral bridges (explained later) in place of conventional simple-supported bridges. In fact, it is extremely difficult to cost-effectively design conventional type soil structures against Level 2 seismic load. When the backfill is well-compacted and its effect on the design shear strength of backfill is taken into account (as described above), GRS structures become a much more cost-effectively solution.

5.9 *Analysis of Seismic Stability of Tanata Wall*

The relevance of the current seismic design described above is examined below by analyzing the seismic performance of Tanata wall, a GRS RW having FHR facing that survived the 1995 Great Kobe Earthquake (Figs. 2-2).

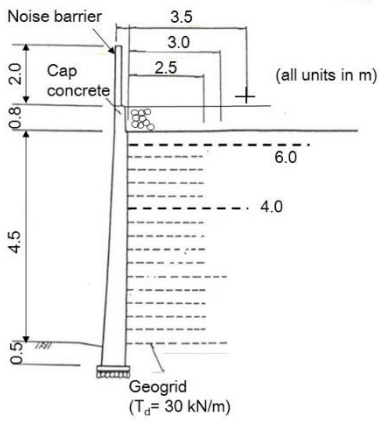

Figure 5-9. Typical section (H= 5.3 m) of Tanata wall (shown in Fig. 2-2a) if designed following the standard practice.

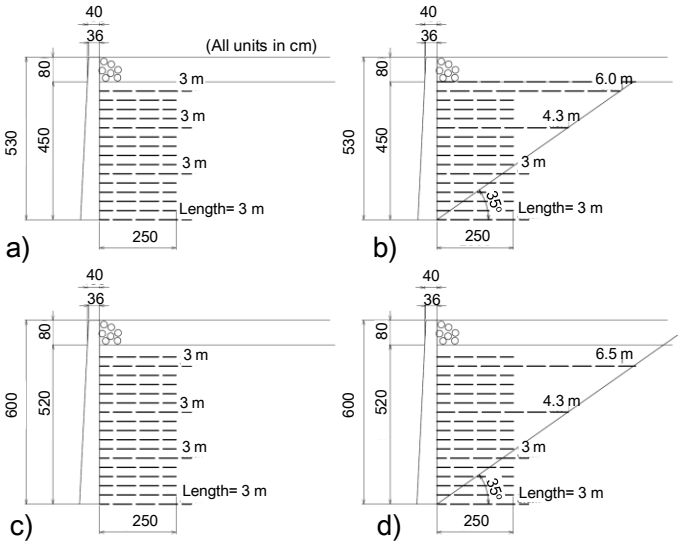

Figure 5-10. Models of Tanata wall for seismic stability analysis (in the case of D= 0 m): a) & b) H= 5.3 m without and with long reinforcement layers; and c) & d) H= 6 m without and with long reinforcement layers.

Table 5-4. Six models for seismic stability analysis of Tanata wall.

Wall model	1		2		3		4		5		6	
Soil strength & toe resistance (TR)	Old code		New code		ϕ_{peak} & ϕ_{res} with c= 5 kPa & TR		ϕ_{peak} & ϕ_{res} with c= 10 kPa & TR		New code		New code with train load	
Geogrid layers	Actual arrangement with Tanata wall (without long layers)								Standard practice with long layers			
Wall height, H (m)	5.3	6	5.3	6	5.3	6	5.3	6	5.3	6	5.3	6
Φ_{peak} (deg.)	35		50									
$\Phi_{residual}$ (deg.)	35		35									
c (kPa)	0				5		10		0			
Toe resistance	No				Yes (D= 0.5 m)				No			
Train load	No										Yes	
(Failure mode)	$(k_h)_y$: yield horizontal seismic coefficient											
Sliding	0.414	0.371	0.446	0.401	0.614	0.548	0.773	0.686	0.567	0.505	0.544	0.479
Over-turning	0.636	0.550	0.649	0.565	0.678	0.594	0.673	0.595	0.823	0.711	0.860	0.697
Shear deformation	0.248	0.219	0.248	0.219	0.248	0.219	0.248	0.219	0.275	0.260	0.275	0.260
(Failure mode)	δ (cm): residual lateral displacement at wall top by Level 2 design seismic load for ground conditions G2 / G3											
Sliding	15.5 / 13.58	24.47 / 21.93	9.77 / 7.99	16.07 / 14.22	3.54 / 1.6	5.45 / 2.94	0.83 / 0.07	2.02 / 0.63	5.01 / 2.61	7.38 / 4.4	5.25 / 2.87	7.85 / 5.24
Over-turning	3.04 / 1.25	5.89 / 3.19	2.61 / 1.03	4.81 / 2.52	1.95 / 6.4	3.81 / 1.85	2.03 / 0.69	3.79 / 1.84	0.4 / 0.0	1.78 / 0.45	0.18 / 0.0	2.06 / 0.58
Shear deformation	1.73 / 1.64	2.46 / 2.34	1.73/ 1.64	2.46 / 2.34	1.73 / 1.64	2.46 / 2.34	1.73 / 1.64	2.46 / 2.34	1.46 / 1.35	1.23 / 1.83	1.73 / 1.6	2.26 / 2.13
Total	20.27 / 16.47	32.82 / 27.46	14.11 / 10.66	23.34 / 19.08	7.22 / 3.88	8.27 / 7.13	4.59 / 2.4	8.27 / 4.81	6.87 / 3.96	10.39 / 6.68	7.16 / 4.47	12.17 / 7.95

Two sections of Tanata wall are analyzed where a total wall height H is equal to 4.5 m (reinforced backfill) + 0.8 m (ballast) = 5.3 m (Fig. 2-2a) and H= 6 m (the tallest section). In both cases, the basic geogrid length is 2.5 m. In all the analysis, an unfactored design rupture strength of geogrid, $[(T_d)_0]_{seismic}$ equal to 30 kN/m is used to obtain the value of $(k_h)_y$ of the respective models. The density of the backfill, ρ, is 19.6 kN/m^3; and the friction angle between the facing and the soil is equal to $\phi_{residual}$ of the backfill (i.e. 35^o). For each wall height, the following six wall models were analyzed (Table 5-4 and Fig. 5-10):

Model 1: This model (Figs. 5-10 a & c) has the actual wall structure (Fig. 2-2a). This model lacks long geogrid layers that would have been arranged as shown in Fig. 5-9 and Figs. 5-10 b & d to increase the wall stability if the standard practice had been followed. These long geogrid layers were not arranged in this particular wall, because the nearest railway track in operation should have been closed if they had been arranged. It was also considered at the design stage that severe earthquakes would not take place in the area where this wall was constructed. ϕ= 35^o with c= 0 is used as in the original design by following the old seismic design code. The bearing capacity at the foundation of the facing is evaluated for the ground conditions: ρ= 17.4 kN/m^3; ϕ= 33.4^o; and c= 0. The old seismic code requires only that the minimum overall safety factors for sliding and over-turning obtained by the limit equilibrium stability analysis is 1.5 against $(k_h)_d$= 0.2. Residual deformation by Level 2 seismic load of model 1 is

evaluated following the current seismic design code, although this analysis is not required by the old code.

Model 2: Under otherwise the same analysis conditions as model 1, ϕ_{peak}= 50^o and $\phi_{residual}$= 35^o (Table 5-3) are used following the current seismic design code.

Models 3 and 4: Under otherwise the same conditions as model 2, c= 5 kPa (model 3) and 10 kPa (model 4) with a toe resistance by the embedded portion of the facing with a depth D of 0.5m are introduced. The passive earth pressure at the embedded portion of the facing is calculated using a friction angle between the facing and the soil equal to ($\phi_{residual}$ of soil)/2= 17.5^o. The bearing capacity at the foundation of the facing is evaluated for the ground conditions: ρ= 17.4 kN/m^3; ϕ=33.4^o; and c= 5 kPa (model 3) or 10 kPa (model 4).

Model 5: Under otherwise the same conditions as model 2, following the standard practice, two long geogrid layers are arranged (Figs. 5-10 b & d).

Model 6: Under otherwise the same conditions as model 5, train load is applied on the backfill crest.

Two seismic waves for two ground conditions G2 (α_{max}= 924 gal) and G3 (α_{max}= 779 gal) among those listed in Table 5-2 are used. These α_{max} values are the two largest values among those for the eight different ground conditions listed in Table 5-2 while being similar to the value recorded at Higashi Nada, 2 km west from Tanata site. No amplification of response acceleration in the wall is considered.

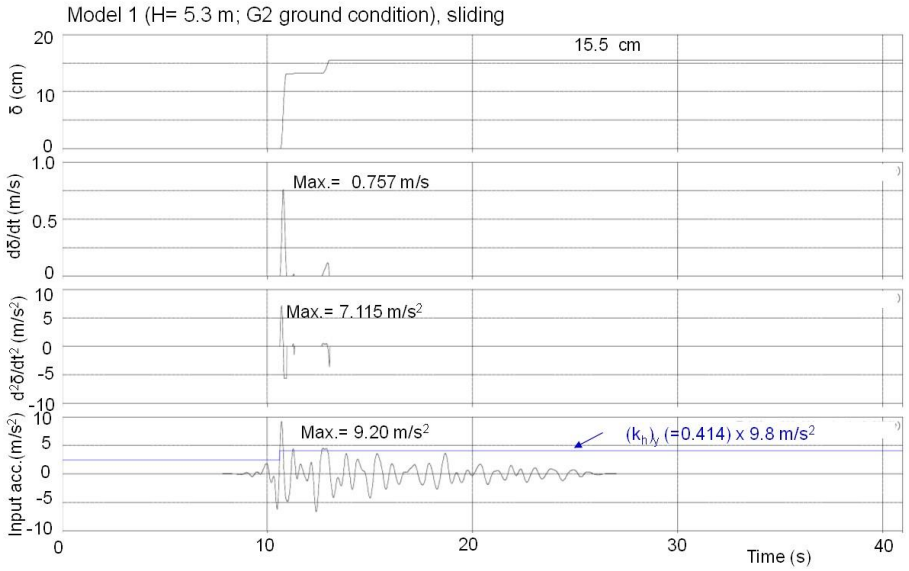

Figure 5-11. Typical Newmark analysis of sliding for model 1 (H= 5.3 m; G2 ground condition).

Fig. 5-11 shows a typical sliding analysis. In Table 5-4, $(k_h)_y$ is the yield k_h value in the respective failure modes. Figs. 5-12a and b show the $(k_h)_y$ values for the three failure models of the six wall models. "$(k_h)_y$ for shear deformation" is smallest among the three failure modes. It is assumed that the first T-W failure mechanism in each of sliding and overturning failure modes develops at this k_h value, which continues developing as k_h further increases. Figs. 5-13a and b show the lateral outward displacements at wall top, δ (cm), in the respective failure modes and their total values. Although the evaluation of δ is relevant only with models 2 through 6 (having $\phi_{peak} > \phi_{residual}$), the same procedure is applied to model 1 (having $\phi_{peak} = \phi_{residual}$). The following trends may be seen from Figs. 5-12 and 5-13:

1) With all the models, the wall becomes less stable with an increase in the wall height H and with an increase in the seismic load, as expected.
2) The values of $(k_h)_y$ are generally lower than the α_{max}/g values of Level 2 design seismic load. Yet, with models 2- 6 (H= 5.3 m) and models 3 – 6 (H= 6 m), the total δ value is lower than the allowable limit for rank 2 performance required with this wall (20 cm). Here, it is assumed that the allowable limit of settlement at the wall crest is the same as the allowable limit of lateral displacement at the wall top, δ. In the design using Level 2 seismic load, although the redundancy in respect of dynamic ductility is not included, it is more realistic therefore relevant to evaluate the seismic wall stability based on displacements in relation to an allowable limit than based on $(k_h)_y$ values in relation to the design seismic load $(k_h)_d$. In the latter method, the determination of the ratio of $(k_h)_d$ to the design value of α_{max}/g is always arguable. A too low ratio is unsafe, while a too high ratio creates too much redundancy.
3) When following the old code, model 1 (H= 6 m), using ϕ= 35^o, is judged to be stable, as both $(k_h)_y$ values for sliding and over-turning are larger than a required minimum value equal to 0.3: i.e. $(k_h)_{d.1}$

(= 0.2; Level 1 design seismic load) times a safety factor (=1.5) (Fig. 5-12). In the old code, the shear deformation failure mode is not examined. If only the seismic load is increased to Level 2, the total δ for H= 6 m becomes noticeably larger than the observed value (26 cm) (Fig. 5-13b). This result indicates that a combination of the use of a default ϕ value= 35^o following the old code and the use of Level 2 seismic load following the new code is conservative, creating some large redundancy. It is considered that this feature is unnecessary in the seismic design using such very high seismic load as Level 2.

4) Model 2 (using ϕ_{peak}= 50^o & $\phi_{residual}$= 35^o according to the new code) is more stable than model 1. Yet, when following the new code, the stability against Level 2 of the wall is judged to be insufficient, as the total δ value for H = 6 m reaches the allowable limit (20 cm), while the result for H= 5.3 m is marginal (Fig. 5-13). If the wall had been designed following the standard practice, the structure would have become that of model 5 (having two long geogrid layers). The different performances of models 2 and 5 indicate that a couple of long geogrid layers at high levels of the wall significantly increase the wall stability. It is seen that Tanata wall would have exhibited much smaller displacements than observed if it had two long geogrid layers as model 5. Model 5 is judged to be stable enough not only when following the old code, but also when following the new code as the total δ value for H= 6 m is much lower than the allowable limit.
5) The different judgments with respect to the seismic stability of model 2 obtained by following the old and new codes shown in 4) above indicate that the new code is slightly more conservative than the old code, while being more realistic than the old code. This means that the GRS RWs designed following the old code is slightly less stable than those designed by the new code. Yet, most of the walls designed following the old code had a couple of long geogrid layers as model 5, unlike Tanata wall. Therefore, the walls designed following the old code can satisfy the seismic stability required by the new code.
6) The different performances of models 1 and models 2 - 4 suggest that the fact that Tanata wall was able to survive a seismic load significantly higher than the design load used in the old code (Level 1) is due to not only an explicit safety margin by a calculated safety factor equal to 1. 5 but also several redundancy components involved in the original design following the old code (i.e. assuming c= 0, underestimating of ϕ, ignoring of toe resistance and others). In fact, the total δ value by Level 2 seismic load decreases from a value of model 1 larger than the observed value to smaller values by taking into account the redundancy components not considered with model 1: i.e. by increasing the ϕ value (model 2) and further by adding c= 5 kPa and 10 kPa and toe resistance (models 3 and 4). The total δ value for H = 6 m of model 2 is similar to the observed value (26 cm). These results suggest that the stability analysis becomes more realistic if the redundancy components ignored in the old design can be properly taken into account. However, it is hard to accurately back-calculate the actual amount of these redundancy components due to several approximations and uncertainties in the analysis. That is, ϕ_{peak}= 50^o and $\phi_{residual}$= 35^o used in this analysis are the current default design values (Table 5-3) and could be somehow different from the actual shear strength of the backfill at the time of the earthquake. It has been very difficult to evaluate the shear strength of the backfill inside the wall, as the wall has been continuously in service. Besides, the input motions used in the analysis are those specified in the new code, which must be somehow different from the actual one, while a possible amplification of response acceleration in the wall is ignored.
7) The effects of apparent cohesion, c, on the results are significant as seen from an increase in $(k_h)_y$ and a decrease in δ with an increase in c from 5 kPa (model 3) to 10 kPa (model 4). The major part of the increase in $(k_h)_y$ and the decrease in δ from model 2 (c= 0 without toe resistance) to model 2 (c= 5 kPa with toe resistance) is also due to an increase in c. These results indicate that, if the use of an apparent cohesion in seismic design is allowed, this value at the time of design earthquakes is required to be accurately evaluated. However, it is not possible. The authors consider that it is wise and relevant to ignore apparent cohesion in both static and seismic design of newly constructed walls. It is to be noted that GRS RWs designed following the current code (i.e. models 5 and 6) still have some redundancy created, at least, by ignoring apparent cohesion and toe resistance and by under-estimation of the rupture strength of geogrid.
8) The stability of model 6 (applying train loads to model 5) is only slightly lower than model 5, showing insignificant effects of train load.

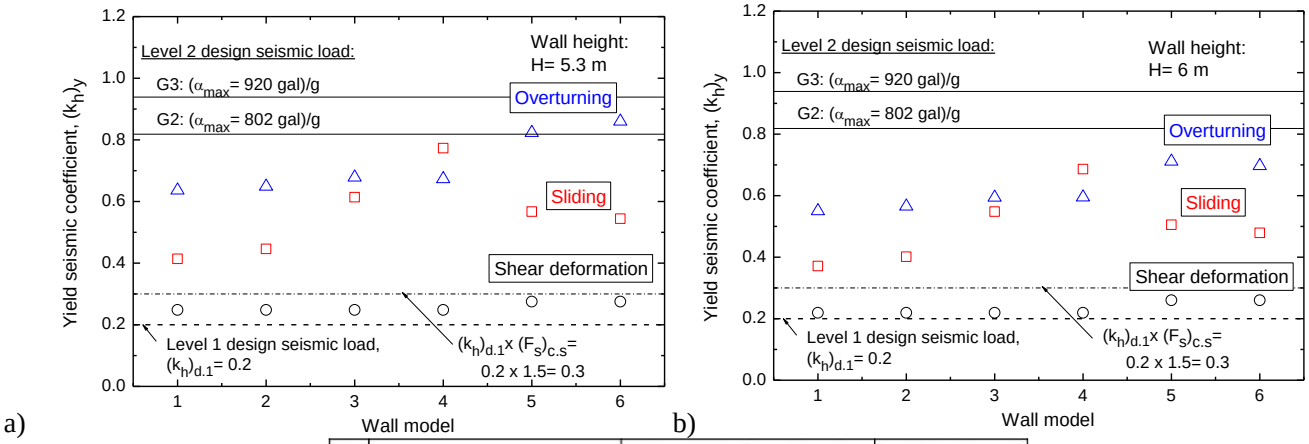

1	Actual wall structure (short geogrid layers only)	Soil model by the old code	c= 0 & no toe resistance
2		Soil model by the new code	
3		More realistic soil model	c= 5 kPa with toe resistance
4			c= 10 kPa with toe resistance
5	Wall structure following the standard practice (with two long geogrid layers)	Soil model by the new code	
6		Soil model by the new code taking into account train load	

Figure 5-12. Yield values of k_h of six models of Tanata wall (H= 5.3 m & 6 m).

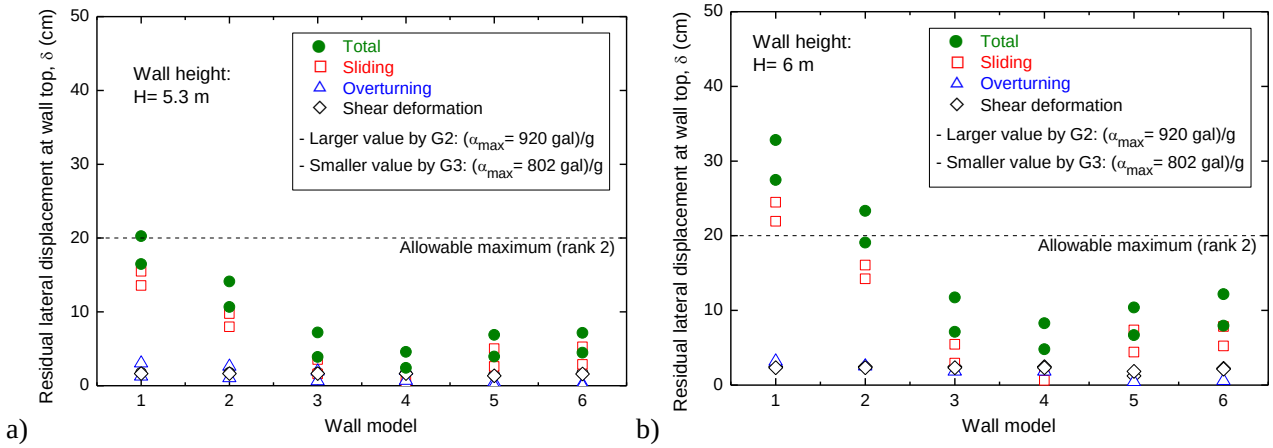

Figure 5-13. Lateral displacement at wall top, δ, of six models of Tanata wall (H= 5.3m & 6 m).

In summary, the results of the analysis presented above indicate the following:

1) Although the GRS RWs having FHR facing at Tanata and other places did not collapse during the 1995 Great Kobe Earthquake, Tanata wall exhibited deformation/displacement close to the allowable limit for rank 2 performance level to be required with this wall. If this wall had not been seismic-designed by following the old seismic design code (using Level 1 seismic load), the wall would have exhibited deformation/displacement much larger than the allowable limit. In that case, the restoration of the wall would have become much more costly and time-consuming.
2) The fact that "*actual seismic performance of the GRS RWs walls, including Tanata wall, during this very severe earthquake was better than expected based on the seismic stability evaluated in the original design"* is due likely to the redundancy that was ignored.
3) Compared with the old design code for this GRS RW type, the current seismic design code employs more realistic and higher seismic loads that are equivalent to the actual severe ones experienced during this earthquake while manifesting some redundancy components ignored in the old code by using more realistic ϕ values of backfill and evaluating the seismic stability based on deformation/displacement. The new code is more consistent with the actual seismic behavior of these GRS RWs therefore more realistic than the old code. The relevance of the new code was also demonstrated by high performance of many similar GRS RW having FHR facing designed following the new code during the 2011 Great East Japan Earthquake (Fig. 2-3). Tatsuoka et al. (1996, 1998) showed that the construction cost of the GRS RW at Tanata was much less costly (by a factor of 1/3 – 1/2 per wall length) than the one of a conventional cantilever RC wall adjacent to this wall, despite that the performances of these two walls during this earthquake were similar. No doubt, the LCC of these GRS RWs that are seismic-designed against Level 2 seismic load is much lower than the one of conven-

tional cantilever RWs that are not seismic-designed or are seismic-designed only against Level 1 seismic load.

4) When based on the above and the other facts described in this report, the authors cannot support the no-seismic-design policy.

6 RESTORATION AND DISASTOR PREVENTION

6.1 *Target Levels of Restoration and Reinforcing*

It is always strongly required to restore as soon as possible the original function of soil structures that failed/collapsed by earthquakes, as well as other natural disasters. The first issue is the level to which these soil structures are to be restored. The conventional practice has been to restore the failed/collapsed soil structures to their original structures (e.g. unreinforced embankment and cantilever RW). As most of these failed/collapsed soil structures had not been seismic-designed and constructed by using old technologies, this practice means that restored soil structures may fail/collapse again when subjected to similar seismic loads as those by which they failed/collapsed. Indeed, this restoring-to-original policy is consistent with the no-seismic-design policy.

To improve the restoration practice, it is necessary while quite feasible to restore failed/collapsed soil structures to those more seismic-resistant and less costly than before by following the up-dated seismic design methodology while using latest cost-effective technologies, such as GRS technologies. In fact, a number of conventional type embankments and cantilever RWs that collapsed by the 1995 Great Kobe Earthquake and subsequent earthquakes were reconstructed to GRS structures (Tatsuoka et al., 1977, 1998; 2007; Koseki et al., 2006, 2008, 2012; Koseki, 2012), as shown below.

In high seismicity countries including Japan, there is an enormous number of soil structures that do not satisfy the current safety standard thus do not have a sufficient seismic stability. Although the GRS technology is relatively new, many GRS structures are also so, as evident from many cases of failure/collapse by earthquakes, as shown in Section 2.3. The second issue is how to prevent failure/collapse of these existing old soil structures by relevant seismic diagnosis and necessary reinforcing works prepared for earthquakes in the future. When following the no-seismic-design policy, there are no sound reasons to perform these projects. Even when they are performed responding to requests from the society, the criterion and target of these projects cannot be specified adequately if based on the no-seismic-design policy. Relevant practice of these projects is possible only when based on relevant seismic design codes. In that case, the following points are important.

The stability under extreme conditions generally increases with an increase in the stability under ordinary static conditions. Therefore, when assessing the seismic stability of existing soil structures including GRS RWs, different from the seismic design for new construction, it is necessary to evaluate actual levels of stability under current ordinary static conditions, which should be largely different even among those designed and constructed by the same standard. More specifically, it is necessary to properly evaluate the following items under current ordinary static conditions: 1) apparent cohesion, c, controlled by the current value of S_r, which may be significant as a result of good drainage as well as good compaction; 2) friction angle of the backfill, controlled by the degree of compaction, D_c, of which the average should be higher than the allowable lower bound in compaction control while being largely different even for the same compaction criterion; 3) toe resistance, which may be largely different among different GRS RWs; 4) tensile rupture strength of reinforcement, which may have been damaged during construction and deteriorated for a long period differently among different GRS RWs even for the originally same geogrid type; and 5) facing rigidity, which may be largely different among different facing types. For example, if the current ground water level is high in the backfill therefore the current value of S_r is very high under ordinary static conditions, already the apparent cohesion may be negligible while positive water pressure may exist in the backfill. In this case, failure/collapse during earthquakes in the future becomes more likely than when no ground water level exists and S_r is low in the backfill under ordinary static conditions. In this case, the first means to be taken is usually to decrease the S_r value by installing relevant drainage.

6.2 *Some Case Histories of Restoration to More Stable Soil Structures*

A number of conventional type embankments and RWs that collapsed during the 1995 Great Kobe Earthquake were reconstructed to GRS structures, including GRS RWs having staged-constructed FHR facing (Fig. 3-16). Fig. 6-1 shows the one typical of the above.

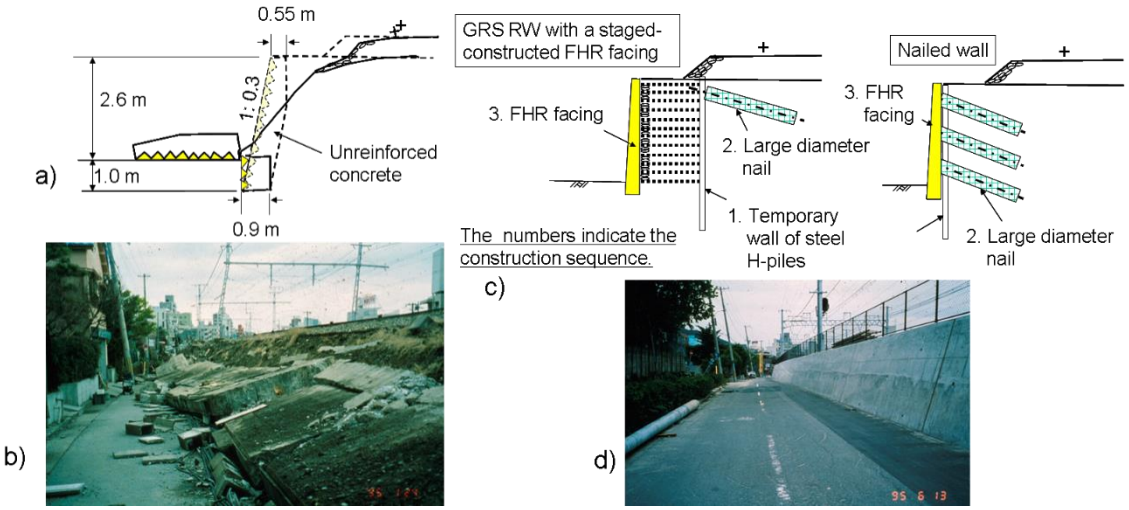

Figure 6-1. Leaning type RW of unreinforced concrete without a pile foundation between Setsu-motoyama and Sumiyoshi stations that collapsed during the 1995 Great Kobe Earthquake (Tatsuoka et al., 1997a &b); a) cross-section; and b) view of the collapsed wall; and c) cross-section; and d) view after restoration.

Fig. 6-2 shows one of the three railway embankments supported by gravity type RW on a slope that collapsed during the 2004 Niigata-ken Chuetsu Earthquake and restored to GRS RWs having FHR facing. This technology was adopted due to not only much lower construction cost and much higher stability (in particular with these soil structures on steep slopes), buy also much faster construction resulting from a significant reduction of earthwork when compared to the original gentle-sloped embankments.

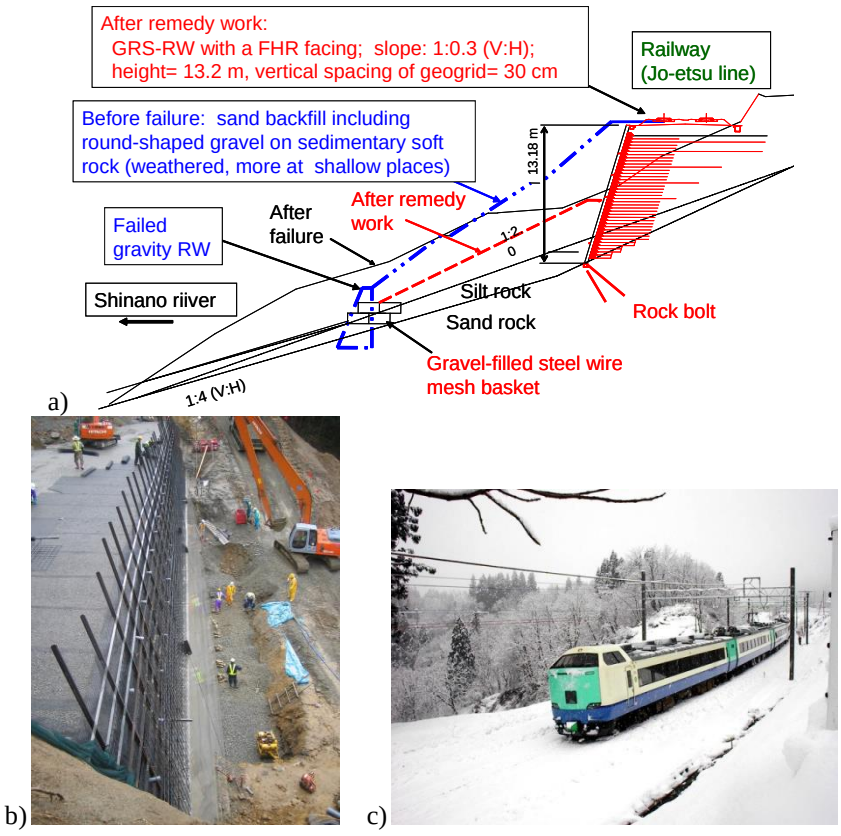

Figure 6-2. Railway embankment that collapsed during the 2004 Niigata-ken Chuetsu Earthquake and its restoration to a GRW RW having FHR facing: a) cross-sections before and after collapse compared with the one after restoration; b) view during construction; and c) the first train on the wall (Morishima et al., 2005).

During the 2011 Great East Japan Earthquake, a great number of old embankments and RWs that had not been designed and constructed following the current seismic design codes collapsed. Several of them were reconstructed to GRS RWs with FHR facing, as typically shown in Fig. 6-3. A very fast construction is one of the important advantages of this technology as in this case. In particular, the railway was reopened at a restricted speed before constructing a FHR facing (Fig. 6-3b) and this emergency restoration work was the first step of the permanent restoration work by constructing FHR facing. Fig. 6-4 shows one of the three embankments that collapsed during an earthquake induced one day after the 2011 Great East Japan Earthquake and restored to GRS RWs with FHR facing. It is now the standard practice to restore conventional type RWs and embankments for railways that collapsed by earthquakes to GRS RWs with FHR facing.

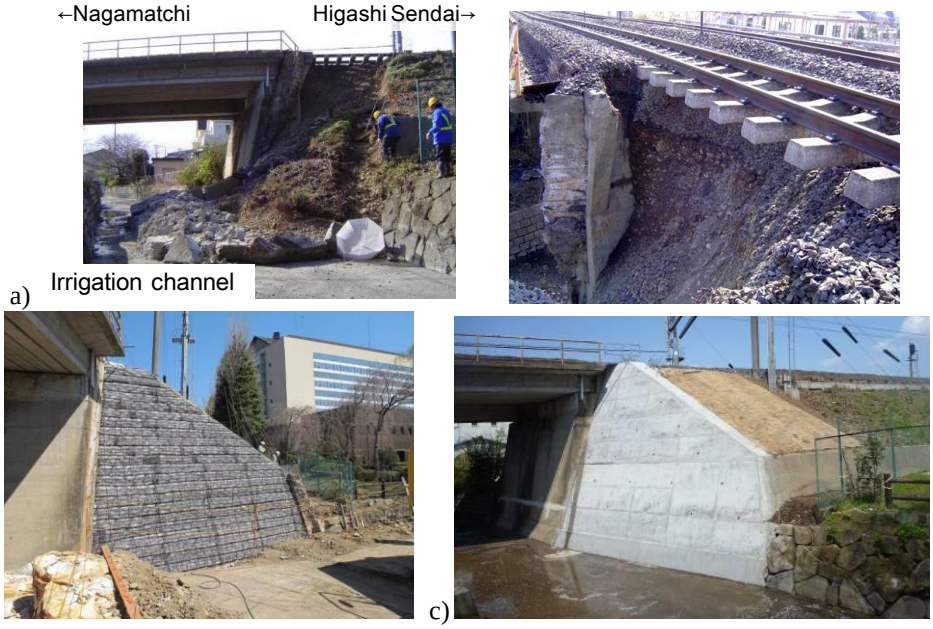

Figure 6-3. a) Collapse of a wing RW with masonry facing of a bridge abutment (Nagamachi, Sendai for Tohoku Freight line); and b) & c) restoration to a GRS RW (by the courtesy of the East Japan Railway Co.).

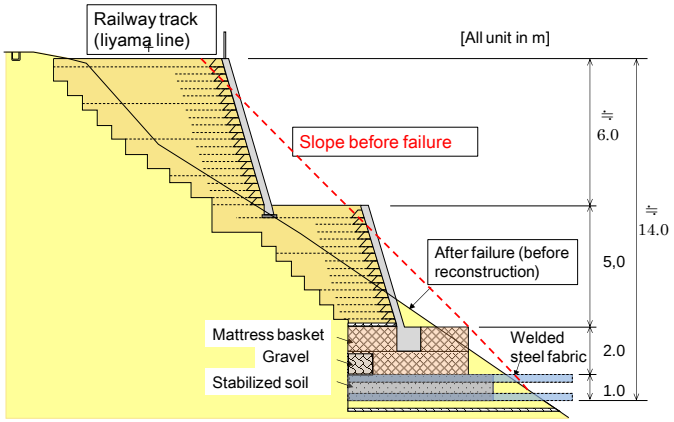

Figure 6-4. One of the three embankments between Yokokura and Morinomiya stations, Iiyama Line, that collapsed during the Nagano-Niigata Border Earthquake and restoration to GRS RWs (by the courtesy of the East Japan Railway Co.).

6.3 *Sanriku Railway*

6.3.1 *Damage by Tsunami during the 2011 Great East Japan Earthquake*

The girders and/or approach fills of a great number of conventional type bridges for roads and railways (more than 340), including those of Sanriku Railway (see Fig. 3-16d for the location), were washed away by the great tsumani during the 2011 Great East Japan Earthquake (Kosa, 2012). The girder supported by bearings exhibited very low resistance against uplift and lateral forces of tsunami current while the unreinforced backfill was quickly eroded by overtopping tsunami current. The connectors and anchors arranged to prevent dislodging of the girders from the abutments and piers by seismic loads could not prevent the flow away of the girders. These cases showed that the girder bearings and unreinforced backfill

are the two major weak points of the conventional type bridges for both seismic loads and tsunami loads. The results of small scale model tests (Kawabe et al., 2013; Yamaguchi et al., 2013) supported these features.

Sanriku Railway was opened 1984 and is running along the coastline where the tsunami damage was very serious during the 2011 Great East Japan Earthquake. The railway had been constructed at a relatively high altitude to prevent tsunami damage based on the previous tsunami disasters in 1896 and 1933 in that area. However, the tsunami this time was much higher than these previous events and the damage was very serious. In particular, three bridges located between tunnels in three narrow valleys facing the Pacific Ocean were totally washed away (Fig. 6-5). This was because, at these three sites along this railway: a) the track level was lowest (12.3 – 14.5 m); b) the track was closest to the coastline; and c) there was no coastal dyke between the railway and the coastline. In the restoration works of Sanriku Railway, the GRS technology was extensively employed. In particular, the three bridges were restored to GRS integral bridges as shown below. The railway was reopened on 6th April 2014.

Figure 6-5. Three bridges for Sanriku railway washed away by tsunami during the 2011 Great East Japan Earthquake: a) Haipe; b) Koikorobe; and c) (from inland) & d) (from seaside) Matsumae-gawa adjacent to Shimanokoshi Station: at the end of March 2011; see Fig. 3-16d for the locations of these sites (by the courtesy of Japan Railway Construction, Transport and Technology Agency).

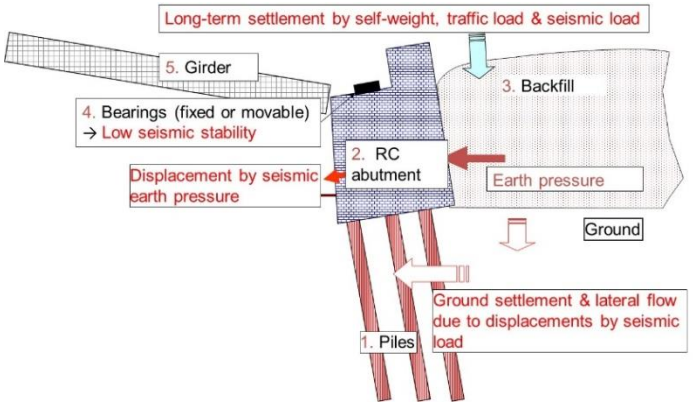

Figure 6-6. Several serious drawbacks of conventional type bridge (Tatsuoka et al., 2005, 2008a & b).

6.3.2 *GRS Integral Bridge*

A conventional type bridge comprises either a single girder simple-supported by a pair of abutments via a pair of movable and fixed bearings, or multiple girders simple-supported by a pair of abutments and a single or multiple pier(s) via multiple sets of bearings. The approach is unreinforced backfill. This bridge type has the following basic drawbacks (Fig. 6-6). Firstly, the bearings are costly in construction and long-term maintenance. Secondly, the abutments are massive and pile foundations are necessary, because the abutments are cantilever structures supported at their bottoms. This drawback becomes more serious at an increasing rate as the abutments become taller. Thirdly, the bearings and unreinforced backfill are vulnerable to seismic and tsunami loads. As a result, a great number of conventional type bridges failed/collapsed during many earthquakes in the past. Fourthly, large bumps may develop immediately behind abutments by depression of the unreinforced backfill accelerated by displacements of the wing RWs and the abutment gradually during a long period of service and suddenly during severe earthquakes.

To alleviate these drawbacks, a new bridge type, called GRS integral bridge, has been developed (Fig. 6-7; Tatsuoka et al., 2008a & b, 2009, 2012; Munoz et al., 2012). A GRS integral bridge comprises a continuous girder integrated to a pair of FHR facing (i.e. abutments) without using bearings and the backfill is reinforced with geosynthetic layers connected to the facing. Fig. 6-7c shows a two-span GRS integral bridge having a central pier. GRS integral bridges are staged-constructed basically following the method for GRS RWs having FHR facing (Fig. 3-16). 1) If the supporting ground is not sufficiently stiff and strong, the zones below the facings and their adjacent zones are improved, for example, by shallow cement-mixing in-place. 2) A pair of GRS walls with the wall face wrapped-around with geogrid reinforcement are constructed. 3) After major deformation of the subsoil and backfill has taken place, thin RC abutments (i.e. FHR facings) are constructed by casting-in-place fresh concrete on the wall face wrapped-around with geogrid reinforcement so that the reinforcement layers are firmly connected to the facings. 4) A girder is constructed structurally integrated to the top of the facings.

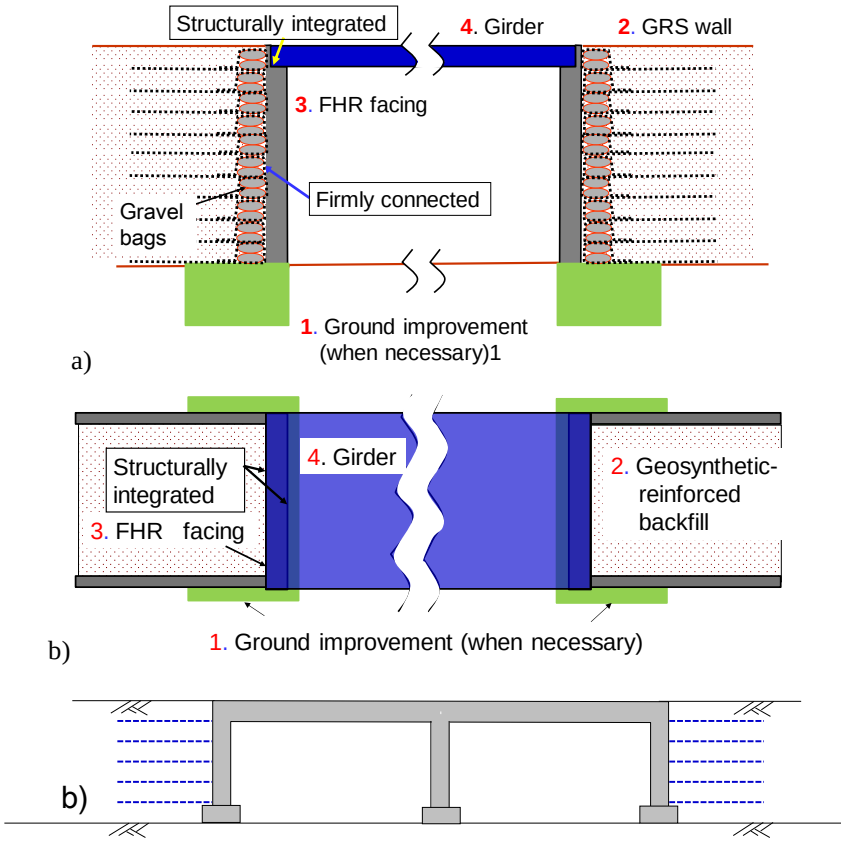

Figure 6-7. GRS integral bridge: a) elevation; and b) plan (the numbers show the construction sequence); and c) two-span GRS integral bridge

The advantages of GRS integral bridge over conventional type bridges are as follows. Firstly, the construction and maintenance of bearing becomes unnecessary. Secondly, the RC abutments (i.e. the facings) are more slender, as they are not a cantilever structure but they are supported by many reinforcement layers at the back The RC girder is also more slender due to a significant reduction (by a factor of about 0.5) of moment resulting from flexural resistance at the connection between the girder and the facing and

shorter because of direct integration to the facings. Thirdly, the settlement in the backfill immediately behind the facings and the structural damage by cyclic lateral displacements at the top of the facing caused by seasonal thermal expansion and contraction of the girder become negligible. The seismic stability also increases significantly with negligible bump immediately behind the facings due to an increased structural integrity and a reduced weight of the girder and facings. The formation of bump by traffic loads is also effectively prevented. Fourthly, due to a smaller cross-section of the girder and a high structural integrity, the resistance against tsunami loads increases significantly. These features were confirmed by various model tests and numerical analysis. A full-scale model was constructed at Railway Technical Research Institute during a period of 2011 – 2012 (Koda et al., 2013). A very high stability of GRS integral bridge was confirmed by applying design thermal deformation of the girder and Level 2 design seismic load to the girder of the model three years after its construction. The current seismic design method is described in Yazaki et al. (2013).

The first GRS integral bridge was completed in 2012 as an over-road bridge at Kikonai for a new high speed train line, Hokkaido Shinkansen (Fig. 6-8; see Fig. 3-16d for the location). As this is the first prototype and as this is for a high speed train line, its high stability is being and will be confirmed by monitoring the behavior continuously from the start of construction until the start of service (scheduled to be April 2016) (Kuriyama et al., 2012). The observations so far of strains in the steel reinforcement in the RC structures and the geogrid, the displacements of the RC structures and the backfill and earth pressures at representative places indicate that the structure is not over-stressed at all and any harmful deformation has not taken place. More details are described in Tatsuoka et al. (2014a & b).

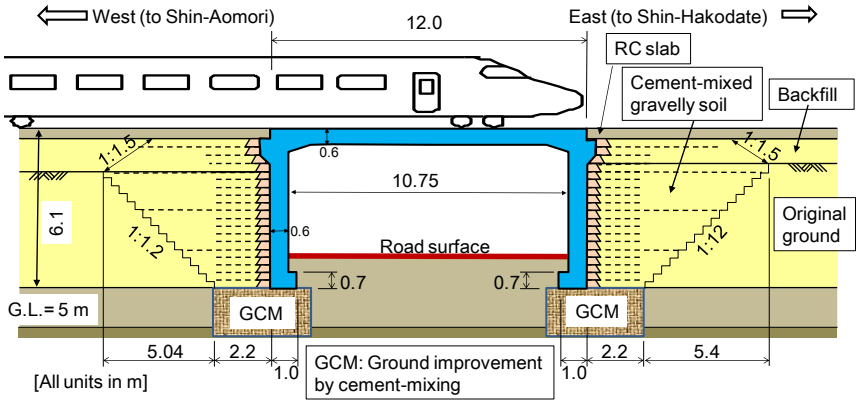

Figure 6-8. GRS integral bridge at Kikonai, Hokkaido Shinkansen (see Fig. 3-16d for location of the site).

6.3.3 *Restoration of Three Bridges for Sanriku Railway*

The railway engineers in charge of restoration of Sanriku Railway and its long-term maintenance restored the three collapsed bridges to GRS integral bridges, because GRS integral bridges are much higher resistant against both seismic and tsunami loads while less costly in construction and long-term maintenance than conventional type bridges. Figs. 6-9 and 6-10 show two GRS integral bridges with a total span length of 60 m and 40 m constructed to restore two two-span bridges having simple-supported girders that fully collapsed by tsumani. Figs. 6-11a and b show the area around the previous Shima-no-koshi Station before and immediately after the earthquake. Although the level of the railway track at the site was about 14 m from the sea level, the tsunami was much higher (22 – 23 m) and the tunnel was inundated (Fig. 6-11c). The RC framework structure totally collapsed and the station was totally washed away. On the request of the residents at the site, GRS embankment was constructed as a tsunami barrier in place of the previous RC framework structure (Figs. 6-12a, b and c). To increase the seismic stability of the embankment and to prevent erosion of backfill by over-topping tsunami current, following the results from model tests (Yamaguchi et al., 2013), both slopes of the embankment were covered with lightly steel-reinforced concrete facing firmly connected to the geogrid layers reinforcing the backfill. Fig. 6-12c shows a view of the embankment with part of the facing under construction. Figs. 6-12d and e show a GRS integral bridge, which is overlain by a backfill layer to reduce as much as possible the size of the opening. At the time of reopening (6th April 2014), part of the facing of the embankment overlying the GRS integral bridge spanning over a river was still under construction (Fig. 6-12e).

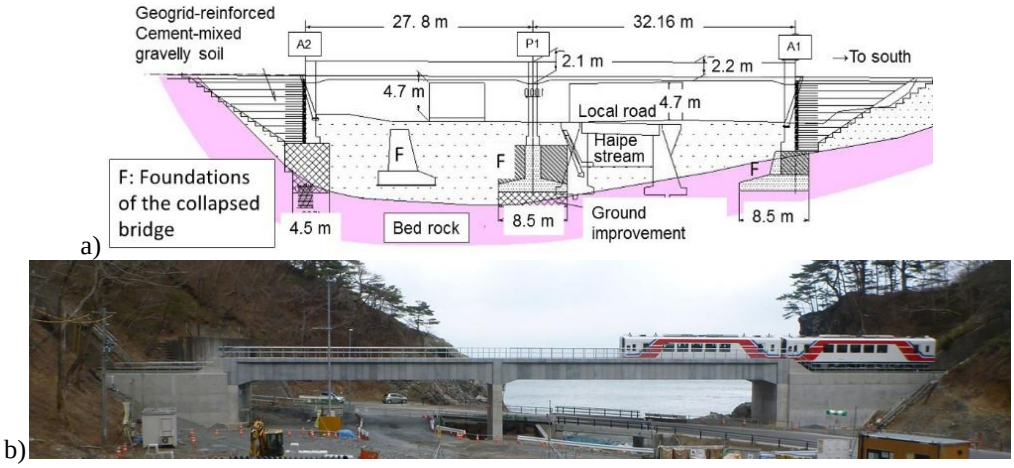

Figure 6-9. GRS integral bridge at Haipe, Sanriku Railway: a) elevation from the inland; and b) view on the day of re-opening (6th April 2014).

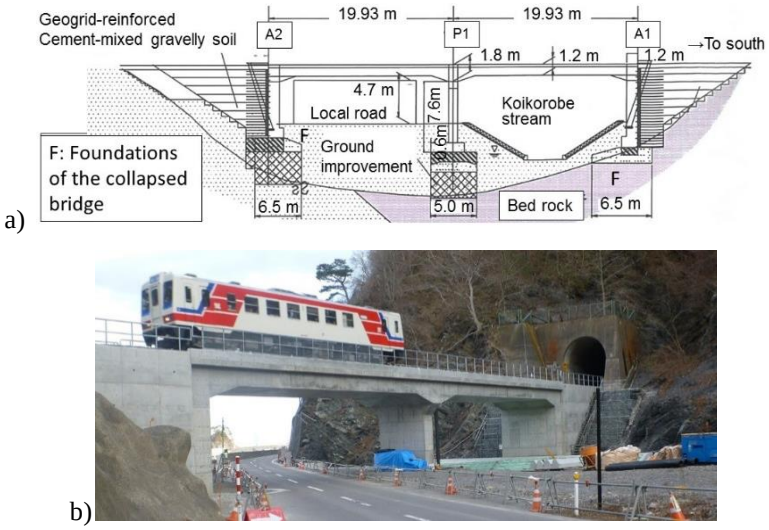

Figure 6-10. GRS integral bridge at Koikorobe, Sanriku Railway: a) elevation from the inland; and b) view on the day of re-opening (6th April 2014).

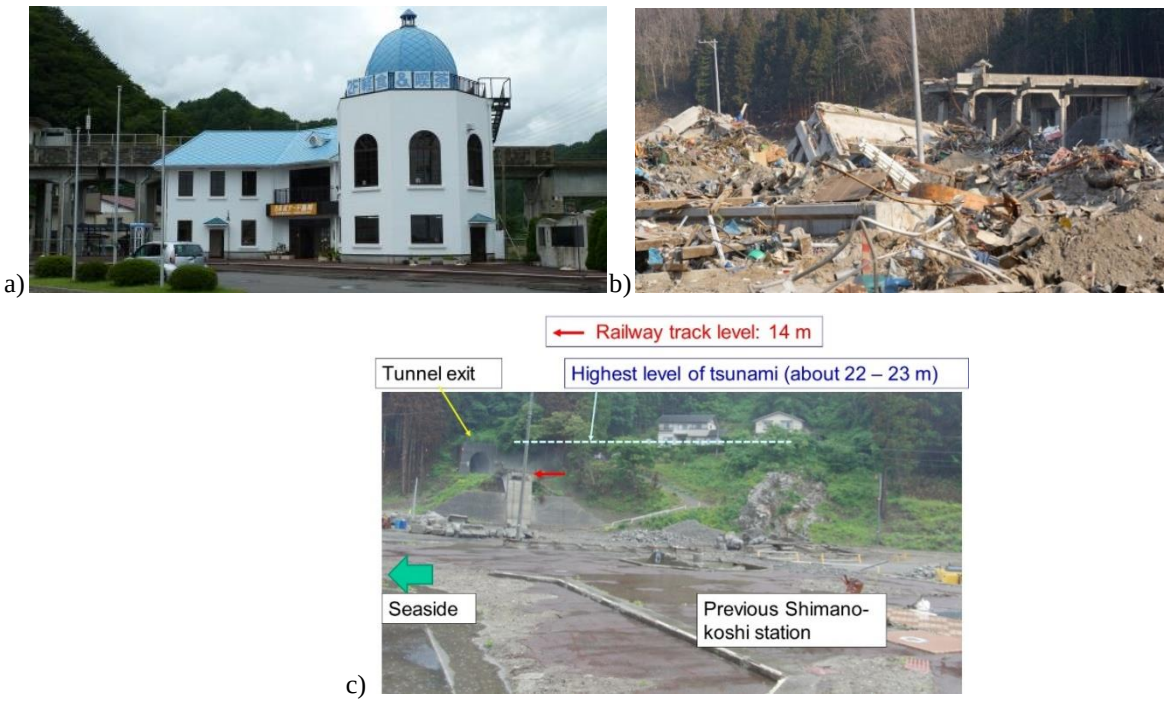

Figure 6-11. Shimano-koshi Station area, Sanriku Railway (see Fig. 3-16d for the location) seen: a) from the seaside before the earthquake; b) immediately after the earthquake seen from the inland, 30 March 2011; and c) from the seaside, 14 July 2013.

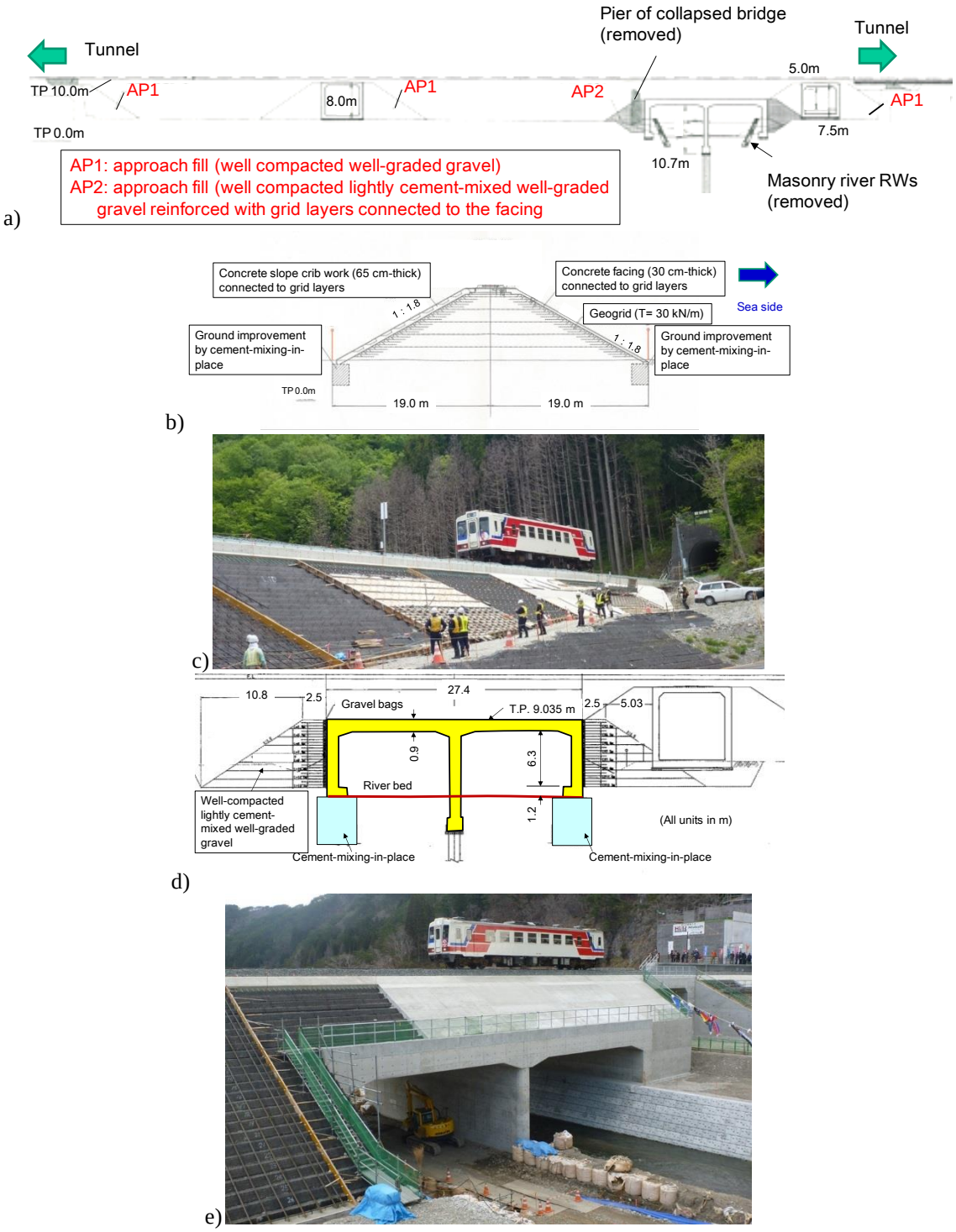

Figure 6-12. Shimano-koshi Station area, Sanriku Railway: a) overall plan of GRS structures; b) representative cross-section of GRS embankment; c) the embankment with the facing under construction seen from the inland, 20 May 2014; and d) & e) structures of GRS integral bridge over Matsumae river (e: 6th April 2014) (a, d & e: seen from the seaside).

7 CONCLUDING REMARKS

Many retaining walls (RWs) that had not been seismic-designed did not collapse during many previous earthquakes. This fact cannot be explained only by explicit safety margin (i.e. a calculated safety factor larger than unity in static design), but implicit safety margin (i.e. redundancy in design) is also necessary. With GRS RWs, significant redundancy can be created in design by: 1) ignoring apparent cohesion; 2) underestimating soil friction angle; 3) ignoring toe resistance; 4) underestimating the contribution of rigid facing; and 5) underestimating the rupture strength of geogrid. However, the redundancy components 1) – 4) are usually not controlled and are random, therefore are not reliable to be taken into account in design. Poor design and poor construction (in particular, inadequate arrangements of geosynthetic reinforcement,

poor drainage, poor compaction, inadequate facing structure with poor connection and poor treatment of weak supporting ground) may have decreased substantially the redundancy. The redundancy also decreases by losing apparent cohesion during heavy/prolonged rains and toe resistance by scoring/excavation in the ground in front of wall, by too fast deterioration of reinforcement etc. As a result, the number of failure/collapse increases. In fact, a number of mechanically stabilized earth (MSE) RWs, including GRS RWs, failed/collapsed during not only extreme but also non-extreme events.

The experience of "*performance better than expected based on the seismic stability evaluated in design*" of RWs observed under limited conditions cannot be generalized to such a no-seismic-design policy under rather broad condition as that seismic stability analysis is not required if design seismic load is lower than a certain level (e.g. $\alpha_{max}/g= 0.4$) or if RWs are lower than a certain height (e.g. H= 8 m). Such a no-seismic-design policy as above reduces the explicit safety margin, which levels down the stability of soil structures increasing the number of failure/collapse. Moreover, when seismic design is not carried out, the design and construction tends to become less careful than when seismic design is carried out, reducing redundancy. In any case, the no-seismic-design policy does not contribute to a reduction of the failure/collapse of RWs, in particular MSE RWs including GRS RWs.

If setting the design strength of geosynthetic reinforcement equal to the average of the reinforcement tensile forces measured in many similar GRS RWs under ordinary static conditions, the actual safety factor substantially decreases from the values obtained by the ordinary seismic design ignoring the redundancy components. This is because the measured forces do not include seismic effects, while they have become smaller by actual effects of apparent cohesion, high friction angle, toe resistance etc. than the ordinary design values. Therefore, this design method is much more un-conservative than the ordinary seismic design.

To construct GRS RWs that are actually sufficiently stable against seismic loads exhibiting sufficiently small residual deformation, good structure, good design and good construction are firstly required. To this end, it is necessary to properly evaluate the seismic stability by using realistic design seismic loads. At the same time, it is necessary to explicitly and properly take into account and control in seismic design the redundancy components produced by good structure, good design and good construction to resist against design seismic loads. This method encourages these good practices, although it reduces the redundancy. Some examples of this method are: 1) the use of more realistic ϕ values higher than conventional default values with actually well-compacted backfill; 2) consideration of the contributions of facing rigidity with actually rigid facings; 3) no creep reduction to obtain the design rupture strength of geogrid; and 4) evaluation of seismic stability based on residual deformation. Yet, to keep low the risk of failure/collapse of GRS RWs by unusual extreme events that may take place in the future but cannot be foreseen at the stage of design, it is relevant to maintain some redundancy by ignoring apparent cohesion and toe resistance in seismic design.

In accomplishing the above with GRS RWs, it is also important to show that the additional cost for seismic design can be lower and more valuable than the cost by failure/collapse that may take place due to no-seismic design. Besides, an increase in the actual stability by relevant seismic design improves long-term performance by decreasing residual deformations, therefore reduces the maintenance cost. Importantly, the life cycle cost for GRS RWs properly designed against realistic high seismic loads can be lower than that for conventional type RWs that are not seismic-designed.

In diagnosis of the seismic stability of existing soil structures including GRS RWs and associated reinforcing works, it is necessary to distinguish among soil structures actually having different seismic stabilities. To this end, it is necessary to assess as realistically as possible the current stability under ordinary static conditions. With a given existing soil structure, unlike the design for new construction, current available soil shear strength (which is a function of actual degree of compaction and current degree of saturation controlled by current drainage effectiveness), current available tensile strength of reinforcement together with current available connection strength, current toe resistance, current facing conditions and so on should be evaluated as accurately as possible. The no-seismic-design policy is not helpful in preparing the relevant guidelines, targets and criteria required to properly organize and execute these projects.

ACHONOLEDGEMENTS

The authors are grateful for the seismic stability analysis of Tanata wall by Mr. Yamada, Y., Integrated Geotechnology Institute, Japan and for the suggestions, comments from and review of the manuscript by Prof. Leshchinsky, D., University of Delaware, USA; Dr. Vahedifard, F., Mississippi State University,

USA; Prof. Ling, H.-I., Columbia University, USA; Dr Tateyama, M. and Dr Koda, M., Railway Technical Research Institute, Japan; and Dr. Duttine, A., Integrated Geotechnology Institute.

REFERENCES

AASHTO. 2010. AASHTO LRFD bridge design specifications, 3rd Ed., American Association of State Highway and Transportation Officials, Washington DC.

AASHTO. 2012. AASHTO LRFD bridge design specifications, 6th Ed., American Association of State Highway and Transportation Officials, Washington DC.

Committee for Double-Facing GRS RW. 2010. Design and construction manual, *Hokuriku Kensetsu Kousaikai*, September (in Japanese).

Express Highway Research Foundation. 2014. Report on disaster prevention of slopes along highways, *Road-Traffic Engineering Research Division* (in Japanese).

Greenwood, J.H., Jones, C.J.F.P. and Tatsuoka, F. 2001. Residual strength and its application to design of reinforced soil in seismic areas, *Proceedings of IS Kyushu* (Ochia et al. eds.), Balkema, Vol.1, pp.37-42.

Hirakawa, D., Kongkitkul, W., Tatsuoka, F. and Uchimura, T. 2003. Time-dependent stress-strain behaviour due to viscous properties of geogrid reinforcement, *Geosynthetics International*, Vol.10, No.6, pp.176-199.

Horii, K., Kishida, H. Tateyama, M., and Tatsuoka. F. 1994. Computerized design method for geosynthetic-reinforced soil retaining walls for railway embankments, *Proc. of Int. Symposium Recent Case Histories of Permanent Geosynthetic-Reinforced Soil Retaining Walls* (Tatsuoka and Leshchinsky eds.), Balkema, pp.205-218.

Horii, K., Tateyama, M., Koseki, J., and Tatsuoka, F. 1998. Stability and residual deformation analyses of geosynthetic reinforced earth retaining wall with rigid facing due to large earthquakes, *Journal of Geosynthetics Engineering*, IGS Japanese Chapter, Vol.13: pp.260-269 (in Japanese).

Ikehara, T. 1970. Damage to railway embankments due to the Tokachioki Earthquake, *Soils and Foundations*, Vol.10, No.2, pp.52–71.

Japan Road Association (2010): 4-1-4. Performance examination, *Design Guidelines for Embankments in Road Earthworks* (2010 version), page 87-88 (in Japanese).

Japan Road Association. 2012. Section 4-3. Design properties of backfill, *Design Guidelines for Retaining Walls in Road Earthworks* (2012 version), pp.65-66 (in Japanese).

Japan Terre Armée Association (JTAA). 1995. Report on the behavior of Terre Armée walls during the 1995 Hyogoken-Nanbu Earthquake (in Japanese).

Japan Terre Armée Association (JTAA). 2011. Report on the behavior of Terre Armée walls during the 2011 Great East Japan Earthquake (in Japanese).

Kaneko, K. and Kumagai, K. 2011. Damages of reinforced earth walls in Iwate area in the 2011 off the Pacific coast of Tohoku Earthquake and tsunami, *Geosynthetics Technical Information*, JC-IGS, Vol.27, No.2, pp.16-23 (in Japanese).

Kawabe, S., Tatsuoka, F., Kuroda, T., Yamaguchi, S., Matsumaru, T., Watananbe, K. and Koda, M. 2013. Seismic stability of geosynthetic-reinforced soil integral bridge evaluated by shaking table test, *Proc. International Symposium on Design and Practice of Geosynthetic-Reinforced Soil Structures, Oct. 2013, Bologna* (Ling et al., eds.), pp.126-141.

Kitamura, Y., Nagao, K., Matsuzawa, K. and Nagakura, H. 2006. Field investigation of a Terre Armée wall subjected to a strong earthquake motion (first report) - investigation on the inside of the backfill and structure soundness -, *Proc. 40th Japan National Conf. on Geotechnical Engineering*, JGS, paper No. C-08, pp.1959-1960 (in Japanese).

Koerner, R. M., Naei, P. E. and Koerner, G. R. 2013. Failed geosynthetic-reinforced mechanically stabilized earth (MSE) walls, *Geosynthetics and Geomembranes*, Vol.40, October, pp.20-27.

Kosa, K. 2012. Damage analysis of bridges affected by tsunami due to Great East Japan Earthquake, *Proc. International Sym. on Engineering Lessons Learned from the 2011 Great East Japan Earthquake*, March, Tokyo, Japan, pp.1386-1397.

Koda, M., Nonaka, T., Suga, M., Kuriyama, R, Tateyama, M. and Tatsuoka, F. 2013. Lateral cyclic loading tests of a full-scale GRS integral bridge model, *Proc. International Symposium on Design and Practice of Geosynthetic-Reinforced Soil Structures, Oct. 2013, Bologna* (Ling et al., eds.), pp.157-174.

Kongkitkul, W., Hirakawa, D. and Tatsuoka, F. 2007a. Viscous behaviour of geogrids; experiment and simulation, *Soils and Foundations*, Vol.47, No.2, pp.265-283.

Kongkitkul, W., Tatsuoka, F. and Hirakawa, D. 2007b. Creep rupture curve for simultaneous creep deformation and degradation of geosynthetic reinforcement, *Geosynthetics International*, Vol.14, No.4, pp.189-200.

Koseki, J., Tatsuoka, F., Munaf, Y., Tateyama, M. and Kojima, K. 1997. A modified procedure to evaluate active earth pressure at high seismic loads, *Soils and Foundations, Special Issue*, pp.209-216.

Koseki, J. and Hayano, K. 2000. Preliminary report on damage to retaining walls caused by the 1999 Chi-Chi earthquake, *Bulletin of ERS, Institute of Industrial Science, Univ. of Tokyo*, Vol.33, pp.23-34.

Koseki, J., Bathurst, R.J., Guler, E., Kuwano, J. and Maugeri, M. 2006 .Seismic stability of reinforced soil walls, *Proc. 8th International Conference on Geosynthetics, Yokohama*, 1: pp.51-77.

Koseki, J., Tateyama, M. and Shinoda, M. 2007. Seismic design of geosynthetic reinforced soils for railway structures in Japan, *Proc. of 5th Int. Sym. on Earth Reinforcement*, Fukuoka, pp.113-119.

Koseki, J., Tateyama, M., Watanabe, K. and Nakajima, S. 2008. Stability of earth structures against high seismic loads, Keynote Lecture, *Proc. 13th ARC on SMGE*, Kolkata, Vol. 2, pp.222-241.

Koseki, J., Nakajima, S., Tateyama, M., Watanabe, K. and Shinoda, M. 2009. Seismic performance of geosynthetic-reinforced soil retaining walls and their performance-based design in Japan, Theme Lecture, *Proc. of Int. Conf. on Performance-Based Design in Earthquake Geotechnical Engineering – from case history to practice* -, Tsukuba, pp.149-161.

Koseki, J. 2012. Use of geosynthetics to improve seismic performance of earth structure". Mercer Lecture 2011, *Geosynthetics*

and Geomembranes, Vol.34, pp.51-68.
Koseki, J., Koda, M., Matsuo, S., Takahashi, H. and Fujiwara, T. 2012. Damage to railway earth structure and foundations caused by the 2011off Pacific Coast of Tohoku Earthquake", Soils and Foundations, Vol.52, No.5, pp.872-889.
Kuwano, J., Koseki, J. and Miyata, Y. 2012. Performance of reinforced soil walls in the 2011 Tohoku Earthquake", Keynote lecture, Proc. *5th Asian Regional Conference on Geosynthetics*, Bangkok, Thailand, pp.85-94.
Kuwano, J., Koseki, J. and Miyata, Y. 2014. Performance of reinforced soil walls during the 2011 Tohoku earthquake, *Geosythetics International*, Vol.21, No.3, pp.1-18.
Lee, K., Jones, C. J. F. P., Sullivan, W. R. and Trollinger, W. 1994. Failure and deformation of four reinforced soil walls in Eastern Tennessee, *Géotechnique*, Vol.44, No.3, pp.397-426.
Leshchinsky, D. 2010. Geosynthetic reinforced walls and steep slopes: Is it magic? *Geosynthetics*, Vol.28, No.3, pp.17–24.
Leshchinsky, D. and Vahedifard, F. 2012. Impact of toe resistance in reinforced masonry block walls: design dilemma, *Journal of Geotechnical and Geoenvironmental Engineering*, ASCE, Vol.138, No.2, pp.236-240.
Leshchinsky, D. and Tatsuoka, F. 2013. Geosynthetic reinforced walls in the public sector: Performance, design, and redundancy, *Geosynthetics Magazine (formerly GFR)*, Vol.31, No.3, pp.12-21.
Leshchinsky, D., Beongjoon Kang, B.-G., Han, J. and Ling, H.-I., 2014. Framework for limit state design of geosynthetic- reinforced walls and slopes, *Transportation Infrastructure Geotechnology*, Springer, Vol.1, No.2, pp.129-164.
Ling, H. I., Leshchinsky, D., Mohri, Y., and Wang, J.-P. 2012. Earthquake response of reinforced segmental retaining walls backfilled with substantial percentage of fines, J. Geotech. Geoenviron. Eng., 10.1061/(ASCE)GT.1943-5606.0000669, 934–944.
Miyata, Y. 2014. Reinforced soil walls during recent great earthquakes in Japan and geo-risk-based design", *Earthquake Geotechnical Engineering Design* (Maugeri & Soccodato eds.), Springer, pp.343-362.
Morishima, H., Saruya, K. and Aizawa, F. 2005. Damage to soils structures of railway and their reconstruction. *Special Issue on Lessons from the 2004 Niigata-ken Chu-Etsu Earthquake and Reconstruction, Foundation Engineering and Equipment (Kiso-ko)*, Oct., 78-83 (in Japanese).
Munoz, H., Tatsuoka, F., Hirakawa, D., Nishikiori, H., Soma, R., Tateyama, M. and Watanabe, K. 2012. Dynamic stability of geosynthetic-reinforced soil integral bridge", *Geosynthetics International*, Vol.19, No.1, pp.11-38.
Okuyama, Y., Yoshida, T., Tatsuoka, F., Koseki, J., Uchimura, T., Sato, N,. and Oie, M. 2003. Shear banding characteristics of granular materials and particle size effects on the seismic stability of earth structures, *Proc. 3rd Int. Sym. on Deformation Characteristics of Geomaterials*, IS Lyon 03 (Di Benedetto et al. eds.), Balkema, September, 2003, pp.607-616.
Proctor, R. R. 1933. Fundamental principles of soil compaction, *Engineering News-Record*, New York, Vol.111, No.9, August 31, pp.55-58.
Railway Technical Research Institute. 2013a. *Design Standard for Railway Earth Structures (2013 version), Maruzen*, pp.56-57 (in Japanese).
Railway Technical Research Institute. 2013b. Section 2.8: Design values of backfill, *Design Standard for Railway Earth Structures (2013 version), Maruzen*, pp.56-57 (in Japanese).
Railway Technical Research Institute. 2013c. Section 8.3.7: Structural details of GRS RW, *Design Standard for Railway Earth Structures (2013 version), Maruzen*, pp.157-158 (in Japanese).
Railway Technical Research Institute. 2013d. Appendix 12-6: Damage level of embankment and allowable settlement, *Seismic Design Standard for Railway Earth Structures (2013 version), Maruzen*, p.401 (in Japanese).
Shibuya, S., Kawaguchi, T. and Chae, J. 2007. Failure of reinforced earth as attacked by typhoon No. 23 in 2004, *Soils and Foundations*, Vol.47, No.1, pp.153-160.
Tatsuoka, F. and Yamauchi, H. 1986. A reinforcing method for steep clay slopes with a non-woven fabric, *Geotextiles and Geomembranes*, Vol.4, No.3/4, pp.241-268.
Tatsuoka, F. 1992. Roles of facing rigidity in soil reinforcing, *Keynote Lecture, Proc. Earth Reinforcement Practice, IS-Kyushu '92 (Ochiai et al. eds.)*, 2: pp.831-870.
Tatsuoka, F., Tateyama, M. and Koseki, J. 1996. Performance of soil retaining walls for railway embankments, *Soils and Foundations*, Special Issue for the 1995 Hyogoken-Nambu Earthquake, pp.311-324.
Tatsuoka, F., Tateyama, M., Uchimura, T. and Koseki, J. 1997a. Geosynthetic-reinforced soil retaining walls as important permanent structures, *Mercer Lecture, Geosynthetic International*, Vol.4, No.2, pp.81-136.
Tatsuoka, F., Koseki, J., and Tateyama, M. 1997b. Performance of reinforced soil structures during the 1995 Hyogo-ken Nanbu Earthquake, Special Lecture, *International Symposium on Earth Reinforcement (IS Kyushu '96),* Balkema, Vol.2, pp.973-1008.
Tatsuoka, F., Koseki, J., Tateyama, M., Munaf, Y. and Horii, N. 1998. Seismic stability against high seismic loads of geosynthetic-reinforced soil retaining structures, *Keynote Lecture, Proc. 6th Int. Conf. on Geosynthetics, Atlanta*, 1: pp.103-142.
Tatsuoka, F. 2001. Impacts on Geotechnical Engineering of several recent findings from laboratory stress-strain tests on geomaterials, *2000 Burmister Lecture at Columbia University, Geotechnics for Roads, Rail Tracks and Earth Structures* (Correia & Brandle eds.), Balkema, pp. 69-140.
Tatsuoka, F., Hirakawa, D., Shinoda, M., Kongkitkul, W. and Uchimura, T. 2004. An old but new issue; viscous properties of polymer geosynthetic reinforcement and geosynthetic-reinforced soil structures, Keynote Lecture, *Proc. of the 3rd Asian Regional Conference on Geosynthetics (GeoAsia 2004)*, Seoul, Vol.2, pp.29-77.
Tatsuoka, F. 2004. An approximate isotropic perfectly plastic solution for compressive strength of geosynthetic-reinforced soil, *Geosynthetics International*, 2004, Vol.11, No. 5, pp.390-405.
Tatsuoka, F., Tateyama, M., Aoki, H. and Watanabe, K. 2005. Bridge abutment made of cement-mixed gravel backfill, *Ground Improvement, Case Histories, Elsevier Geo-Engineering Book Series, Vol. 3* (Indradratna & Chu eds.), pp.829-873.
Tatsuoka, F., Konagai, K., Kokusho, T., Koseki, J., and Miyajima, M. 2006. Special session on the 2004 Niigata-ken Chuetsu Earthquake, *Proc., 16th Int. Conf. on Soil Mechanics and Geotechnical Engineering*, Vol. II, IOS, Amsterdam, Netherlands.
Tatsuoka, F., Kongkitkul, W. and Hirakawa, D. 2006. Viscous property and time-dependent degradation of geosynthetic reinforcement, *Proc. of the 8th International Conference on Geosynthetics, Yokohama, Japan* (Kuwano & Koseki, eds.), Vol.4,

pp.1587-1590.
Tatsuoka, F., Tateyama, M., Mohri, Y. and Matsushima, K. 2007. Remedial treatment of soil structures using geosynthetic-reinforcing technology, *Geotextiles and Geomembranes*, Vol.25, Nos.4&5, pp.204-220.
Tatsuoka, F. 2008. Geosynthetics Engineering, combining two engineering disciplines, Special Lecture, *Proc. GeoSyntheticsAsia*, Shanghai, Vol.2, pp.1-35.
Tatsuoka, F., Hirakawa, D., Nojiri, M., Aizawa, H., Tateyama, M. and Watanabe, K. 2008a. Integral bridge with geosynthetic-reinforced backfill, *Proc. First Pan American Geosynthetics Conference & Exhibition, Cancun, Mexico*, pp.1199-1208.
Tatsuoka, F., Hirakawa, D., Aizawa, H., Nishikiori, H. Soma, R and Sonoda, Y. 2008b. Importance of strong connection between geosynthetic reinforcement and facing for GRS integral bridge, *Proc. 4th GeoSyntheticsAsia (4th Asian Regional Conference on Geosynthetics)*, Shanghai, pp.205-210.
Tatsuoka, F., Hirakawa, D., Nojiri, M., Aizawa, H., Nishikiori, H., Soma, R., Tateyama, M. and Watanabe, K. 2009. A new type integral bridge comprising geosynthetic-reinforced soil walls", *Gesynthtetics International, IS Kyushu 2007 Special Issue*, Vol.16, No.4, pp.301-326.
Tatsuoka, F., Koseki, J. and Tateyama, M. 2010. Introduction to Japanese codes for reinforced soil design, Panel Discussion on Reinforced Soil Design Standards, *Proc. 9th International Conference on Geosynthetics, Brazil*, pp.245-255.
Tatsuoka, F. 2011. Laboratory stress-strain tests for the development of geotechnical theories and practice, *First Bishop Lecture, Proc. 5th International Conference on Deformation Characteristics of Geomaterials*, Seoul, Korea, Sept., pp.3-50.
Tatsuoka, F. and Tateyama, M. 2012a. Geosynthetic-reinforced soil structures for railways in Japan, Keynote Lecture, *Proc. International Conference on Ground Improvement and Ground Control (ICGI 2012)* (Indraratna et al., eds.), pp.43-56.
Tatsuoka, F., Tateyama, M. and Koseki, J. 2012b. GRS structures recently developed and constructed for railways and roads in Japan, Keynote lecture, *Proc. 2nd International Conference on Transportation Geotechnics (IS-Hokkaido 2012)* (Miura et al., eds.), pp.63-84.
Tatsuoka, F., Kuroda, T. and Tateyama, M. 2012c. Research and practice of GRS integral bridges, *Proc. EuroGeo 5, Valencia*, September, pp.177-181.
Tatsuoka, F., Tateyama, M., Koseki, J. and Yonezawa, T. 2014a. Geosynthetic-reinforced soil structures for railways in Japan, *Transportation Infrastructure Geotechnology*, Springer, Vol.1, No,1, pp.3-53.
Tatsuoka, F., Tateyama, M., Koda, M., Watanabe, K., Koseki, J., Aoki, H. and Yonezawa, T. 2014b. Design, construction and performance of GRS structures for railways in Japan, Prof. 10th ICG, Berlin (this conference).
Tatsuoka, F. 2013 - 2014. A series of articles on soil compaction, *Foundation Engineering and Equipment (Kiso-ko)*, monthly from July 2013 through September 2014 (in Japanese).
Vahedifard, F., Leshchinsky, B., Sehat, S., and Leshchinsky, D. 2014. Impact of cohesion on seismic design of geosynthetic-reinforced earth structures, *Journal of Geotechnical and Geoenvironmental Engineering, ASCE*, DOI: 10.1061/(ASCE) GT.1943-5606.0001099 , 04014016.
Valentine, R. J. 2013. An assessment of the factors that contribute to the poor performance of geosynthetic-reinforced earth retaining walls, *Proc. International Symposium on Design and Practice of Geosynthetic-Reinforced Soil Structures, Oct. 2013, Bologna* (Ling et al., eds.), pp.318-330.
Wang, Z.-J., Tatta, N., Hattori, H., Tsuji, S. and Ota, H. 2011. Damage to a reinforced soil retaining wall having a double facing during the 2008 Iwate-Miyagi Nairiku Earthquake and its repair work, *Foundation Engineering and Equipment (Kiso-ko)*, April, pp.80-82 (in Japanese).
Watanabe, K., Munaf, Y., Koseki, J., Tateyama, M. and Kojima, K. 2003. Behaviours of several types of model retaining walls subjected to irregular excitations, *Soils and Foundations*, Vol.43, No.5, pp.13-27.
Watanabe, K., Koseki, J. and Tateyama, M. 2011. Seismic earth pressure exerted on retaining walls under a large seismic load, *Soils and Foundations*, Vol.51, No.3, pp.379-394.
Yamaguchi, S., Yanagisawa, M., Kawabe, S., Tatsuoka, F. and Nihei, Y. 2013. Evaluation of the stability of various types of coastal dyke against over-flowing tsunami current, *Proc. International Symposium on Design and Practice of Geosynthetic-Reinforced Soil Structures, Oct. 2013, Bologna* (Ling et al., eds.), pp.572-581.
Yazaki, S., Tatsuoka, F., Tateyama, M., Koda, M., Watanabe, K. and Duttine, A. 2013. Seismic design of GRS integral bridge, *Proc. International Symposium on Design and Practice of Geosynthetic-Reinforced Soil Structures, Oct. 2013, Bologna* (Ling et al., eds.), pp.142-156.
Yonezawa, T., Yamazaki, T., Tateyama, M. and Tatsuoka, F. 2014. Design and construction of geosynthetic-reinforced soil structures for Hokkaido high-speed train line", *Transportation Geotechnics*, Elsevier, Vol.1, No.1 pp.3-20.
Yoshida, T., Tatsuoka, F., Siddiquee ,M. S. A. and Kamegai, Y. 1995. Shear banding in sands observed in plane strain compression", *Localisation and Bifurcation Theory for Soils and Rocks* (Chambon et al., eds.), Balkema, pp.165-179.
Yoshida, T. and Tatsuoka, F. 1997. Deformation property of shear band in sand subjected to plane strain compression and its relation to particle characteristics, *Proc. 14th ICSMFE, Hamburg*, Vol.1, pp.237-240.
Yoshimi, Y. 1970. An outline of damage during the Tokachioki Earthquake, *Soils and Foundations*, Vol.10, No.2, pp.1–14.